SEGREGATION AND INITIAL STAGES OF OXIDATION ON NI-CO ALLOYS

THE SURFACE SEGREGATION AND INITIAL STAGES
OF OXIDATION ON NI-CO ALLOYS

by

ERNEST E. HAJCSAR, B.SC.

A Thesis
Submitted to the School of Graduate Studies
in Partial Fulfilment of the Requirements
for the degree
Doctor of Philosophy
McMaster University
September 1988

DOCTOR OF PHILOSOPHY (1988)
(Materials Science)

MCMASTER UNIVERSITY
Hamilton, Ontario.

TITLE: The Surface Segregation and Initial Stages of Oxidation on
Ni-Co Alloys

AUTHOR: Ernest E. Hajcsar, B.Sc. (McMaster University)

SUPERVISORS: Professor P.T. Dawson
Professor W.W. Smeltzer
Dr. P.R. Underhill

NUMBER OF PAGES: viii, 192

Abstract

This thesis consists of studies carried out on the Nickel-Cobalt alloy system. The surface segregation behaviour has been studied over the range of composition from 14 to 90 atomic percent Nickel using Auger Electron Spectroscopy (AES). An analysis procedure has been developed that is based on computer simulation of observed spectra using pure metal standard spectra and has resulted in excellent matches. Nickel has been observed to segregate over the entire range of compositions studied and the driving force for segregation has been investigated by monitoring the equilibrium surface composition over a range of temperatures from 813 to 1100 K. The enthalpy and entropy of segregation has been determined on single grains of orientations (111) and (210) in a sample of composition 56.0 atomic percent Nickel as well as on the (111), (100) and (110) faces of a 50.0 atomic percent Nickel single crystal.

The initial stage of oxidation has also been studied here using Scanning Auger Mapping and digital image processing. The initial stage of oxidation carried out in-situ has been shown to proceed via an island nucleation and growth mechanism which has been confirmed by imaging islands based on the oxygen Auger signal. A preliminary study of the effects of temperature and pressure on the island growth stage of oxidation has been completed and results are reported.

(iii)

Acknowledgements

The author wishes to express his deepest gratitude to my supervisors

Dr. P.T. Dawson, Dr. W.W. Smeltzer and Dr. P.R. Underhill whose guidance and support has proved to be invaluable.

I would also like to express my deep thanks to the people of IMR whose kind help have made my years as a graduate student happy ones. I would especially like to thank Mr. Frank Szostak for being a great friend and help above and beyond the call, Mrs. Heather Halabourda who has also excelled in kindness and warmth, Mrs. Shirley Williams who has aided me greatly and last but not least Mr. Jim Garrett whose knowledge and expertise in sample preparation and crystal growth facilitated the pursuit of this study.

...so long and thanks for all the fish.

TABLE OF CONTENTS

LIST OF FIGURES

(vii)

Chapter 1

INTRODUCTION

The study of the chemistry and physics of solid material surfaces is of increasing importance in today's rapidly advancing technology. The activity of solid state catalysts is usually defined by the nature of the surface of the catalyst, but only rarely is there an understanding of the processes involved. Investigations into the surface compositions of materials such as metals and alloys (common catalyst materials) at elevated temperatures would be useful in the pursuit of understanding catalytic processes. The prevention of corrosion on metals and alloys is also of major importance. Protection from corrosion is usually achieved by having a compact oxide on the surface of the material that slows the corrosion process enough to provide a useable lifetime for the material, but the entire process of oxidation from clean surface to compact oxide is still not completely understood.

The surface of a solid substance can be a complex regime to investigate because that surface rarely, if ever, resembles the bulk in composition or structure. A common phenomenon in the surface behavior of materials is surface segregation. Surface segregation, generally, is the process of enriching the surface region of a solid in one component in order to reduce the free energy of the system. Very often impurities (eg. Carbon and Sulfur) will segregate to surfaces but,

since catalytic activity and oxidation are mostly dependant on the behavior of major substituents, the emphasis in this field has been concentrated on the segregation of one element in binary alloys.

There is a large body of theory in the literature today that attempts to predict which element will segregate and quantify the extent of enrichment in the surface region but, there is some disagreement as to the nature of the actual driving force and considerable disagreement about predicting the extent.

The initial stages of the oxidation of clean alloy surfaces may affect greatly the nature of a compact oxide grown to protect the underlying metal. The composition of the surface region may affect these early stages of oxidation as well as the conditions of temperature and pressure used to oxidize a sample. An understanding of this stage of oxide growth may lead to the development of better oxide coatings to resist corrosion.

This thesis reports the results of investigations into segregation in a binary alloy system consisting of Nickel and Cobalt (Ni-Co) and into the very early stages of oxidation on those alloys using Auger Electron Spectroscopy (AES).

CHAPTER 2

Theoretical Considerations of Segregation

2-I Classical Thermodynamics

In order to discuss the thermodynamics of a surface phenomenon it is necessary to first define what is meant by a surface since, different definitions of a surface can seriously alter the interpretation of experimental findings. Here, in a classical approach, we shall define the surface as being the region where atoms are affected by the fact that they are not in an infinite continuum[1]. What this effectively means is that, for the purposes of developing theories at least, the segregation is usually confined to a layer of material known as the surface. The remainder of the material in the system is therefore defined as bulk. Classically we may treat the surface and the bulk as being two separate components of the overall system[2,3] and can therefore describe each via a free energy G_{bulk} and $G_{surface}$ (Note here that the Helmholtz energy is not used since a real segregation process will not involve a mechanical work term if there is no change in volume and the process proceeds under conditions of constant temperature and pressure.). Each of the bulk and surface free energy terms for an alloy must also contain a term which describes the free energy of mixing such that;

$$G_{mix} = H_{mix} - TS_{mix} \qquad 2.1)$$

3

In order to preserve simplicity, the assumption is made that the alloy in question (AB) is an ideal solution and hence[4] $H_{mix} \simeq 0$, which leaves the entropic component given below, using Stirling's approximation, as:

$$S_{mix} = -R[X_A \ln X_A + X_B \ln X_B] \qquad 2.2)$$

It is therefore possible to write the free energy expressions as

$$G_{bulk} = \{G_b^* - RT[X_A^b \ln X_A^b + X_B^b \ln X_B^b]\} \qquad 2.3)$$

$$G_{surface} = \{G_s^* - RT[X_A^s \ln X_A^s + X_B^s \ln X_B^s]\} \qquad 2.4)$$

where the superscripts s and b refer to surface and bulk respectively, and the G_b^* and G_s^* terms describe all other contributions to the free energy. We assume that for any change in arrangement due to segregation, that the atoms enriching the surface come from the bulk and that atoms expelled from the surface (because of unfavourable energetics) return to the bulk. Therefore at equilibrium, the molar free energy of the two phases must be equal.

$$G_b^* - RT[X_A^b \ln X_A^b - X_B^b \ln X_B^b] = G_s^* - RT[X_A^s \ln X_A^s - X_B^s \ln X_B^s] \qquad 2.5)$$

which may be re-written

$$X_A^s / X_B^s = X_A^b / X_B^b \exp^{(-\Delta G_{seg.}/RT)} \qquad 2.6)$$

This equation is therefore the most general, model independent, expression describing surface segregation. Models to predict and/or explain the physical origins of segregation seek to evaluate the free energy term and apply other assumptions. Here the only assumptions used to derive the general segregation equation are; there is no mechanical work done, the alloy is an ideal solution and conservation of mass is assumed.

a) Bond-Breaking Model

Since atoms in the surface region experience a different environment than those in the bulk, the total energy of bonds holding an atom at the surface is different than the total energy of bonds holding an atom in the bulk. Individual types of atoms say A and B, will have different bond energies and hence the atom type which has the lowest amount of binding energy missing, will be preferentially positioned at surface sites. The driving force for segregation in this model is therefore determined by the difference in bond energies between the two alloy components, and the number of missing bonds at the surface.

The observation is made that the energy of breaking all 12 bonds in an FCC metal may be replaced[1,2,7-11] by the vaporization energy $\Delta G_{vap.}$. The assumption that $T\Delta S_{vap.} << \Delta H_{vap.}$ is then made, and the resulting expression is;

$$\frac{X_s^A}{(1-X_s^A)} = \frac{X_b^A}{(1-X_b^A)} \exp^{[-k\Delta H_{vap.} / RT]} \qquad 2.7)$$

here k is the fraction of bonds missing for a surface atom eg. 3/12 for a (111) FCC surface.

This equation therefore forms the basis for a large class of theories describing surface segregation called "the bond-breaking models" where the driving force for segregation is related to the energy of bonds missing at the surface and entropy is strictly configurational. In this simplest of bond-breaking models, where only atoms missing bonds are considered to be in the surface and the enriched layer would be confined to these atoms. Modifications and elaborations have been made to this basic model and the interested reader is referred to Appendix 1 where some of the more successful models are presented. The next section deals with the underlying ideas behind the second major class of segregation theories collectively referred to as "the surface tension approaches".

b) Surface Free Energy Model

Gibbs[3] addressed the problem of segregation in a slightly different way, but achieved a similar result to the preceeding section. He began by defining a two phase system where α is the metal alloy and β is a vacuum adjacent to the alloy. The interface region is called the Gibbs dividing plane, and the positioning of the plane will greatly affect the interpretation of any experimental results using this model. The difference between an interface where the bulk composition of both phases is unaltered up to the dividing plane, and an interface where the surface of the α phase has been changed relative to the bulk, is defined as the surface excess (Γ) of the enriched component.

The total number of A atoms in the system is therefore the total of atoms in both phases and the interface;

$$N_A = \Gamma_A \Lambda + c_A^\alpha v_\alpha + c_A^\beta v_\beta \qquad 2.8)$$

where Λ is the area of the interface. Since we have defined phase β as being a vacuum, the last term will be zero. Surface tension was then defined as the reversible work to increase the interface area Λ when T,V and the N_A are constant. Since such a process involves work, the process was described by the absolute Helmholtz free energy (f) and the total change given as;

$$df_{tot.} = df_\alpha + df_\beta + df_s = \gamma \Lambda \qquad 2.9)$$

where

$$df_{\alpha,\beta} = -SdT - PdV + \Sigma \mu_A dN_A \qquad 2.10)$$

with df_s is the per atom change in free energy due to the surface and γ is the surface tension. But we have defined the process as occurring at constant T and V so that;

$$\gamma d\Lambda = df_s + \Sigma \mu_A d(N_A^\alpha + N_A^\beta) \qquad 2.11)$$

Since this model system is closed, any change in the surface of phase α must come from the bulk of phase α and

$$\Sigma \mu_A d(N_A^\alpha + N_A^\beta) = -\Sigma \Gamma_A \mu_A d\Lambda \qquad 2.12)$$

converting now to a per unit area and molar basis, and realizing that β phase is a vacuum here, we may get;

$$\gamma = F_s - \Sigma\Gamma_A\mu_A \qquad 2.13)$$

and since at equilibrium dF = 0, we may perform the total differential to arrive at the Gibbs adsorption isotherm 2.14). The Gibbs adsorption isotherm is also intuitively satisfying since segregation of an atom from the bulk of a material could be considered the same as adsorbing that atom onto a surface. Therefore;

$$\Gamma_A = -d\gamma/d\mu_A \qquad 2.14)$$

where Γ_A is the surface excess of A (the solute), γ is the surface tension and μ_A is the chemical potential of A. If the chemical potential obeys Henry's law for dilute binary solutions then we may have[4];

$$\Gamma_A = -X_B X_A (KT - 2X_B X_A \Delta H_m)^{-1} (d\gamma/dX_A)_T \qquad 2.15)$$

The new term ΔH arises from the following;

$$\Delta H_m = 2H_{AB} - (H_{AA} + H_{BB}) \qquad 2.16)$$

where H_{AB} is the interaction energy between an A atom and a B atom etc.. If the solution is dilute enough that A atoms are completely engulfed in a matrix of B atoms and there are no A-A interactions in the alloy then;

$$H_{AB} = \frac{1}{2} (H_{AA} + H_{BB}) \quad 2.17)$$

and hence $\Delta H_m = 0$ and eqn 2.15) becomes;

$$\Gamma_A = - (\frac{X_A}{RT}) \frac{d\gamma}{dX_A} \quad 2.18)$$

The end result of this equation is that the component that reduces sur-
face tension will be enriched at the surface. Eqn. 2.18) is a very
important relation to the theorist but it's practical application is
seriously restricted by the lack of knowledge concerning the variation of
surface tension with composition on solid surfaces. It is therefore
necessary to obtain a more convenient equation with more accessible
quantities. What is arrived at[5] is;

$$\gamma = \gamma_A + \frac{RT}{\Lambda} \ln X_A^s/X_A^b \quad 2.19)$$

where γ_A is the surface tension of pure A, Λ is the surface area oc-
cupied by the component (it is assumed that neither component takes up
more or less space at the surface--a potentially serious restriction).
It is then possible to write the similar expression for component B, and
taking a ratio of the two expressions eliminates γ, which yields;

$$X_A^s/X_B^s = X_A^b/X_B^b \exp^{[-(\gamma_B - \gamma_A)\Lambda/RT]} \quad 2.20)$$

Equation 2.20) can also be expressed in a more general form such that ideality and equal atomic surface areas[6,7] are not required if it is recognized that surface tension is a surface free energy term expressed on a per unit area basis[2]. If G_s and G_b are the free energies of a system with a solute atom on the surface and in the bulk respectively, and G_s° and G_b° are free energies for pure solvent. We now have;

$$X_A^s/X_B^s = (X_A^b/X_B^b) \, \exp^{\{-(G_s - G_s^\circ)-(G_b - G_b^\circ)\}/RT} \qquad 2.21)$$

and we may define

$$\Delta G_a = (G_s - G_s^\circ) - (G_b - G_b^\circ) \qquad 2.22).$$

Here ΔG_a ,the Gibbs free energy of adsorption, again represents the "driving force" for segregation instead of the Helmholtz free energy since no mechanical work is done in a real system, and;

$$X_A^s/X_B^s = X_A^b/X_B^b \, \exp^{(-\Delta G_a/RT)} \qquad 2.23)$$

which is very similar to eqn 2.7).

Here the exact interpretation of what is meant by X_A^s must be addressed. Clearly X_A^s is the composition of material on the vacuum side of the Gibbs dividing surface. The results of experimental determinations are most easily interpreted if the Gibbs surface is positioned such that segregation is confined to the first monolayer only and this is

often used. It should be noted therefore that in a real system, this assumption may not be valid and interpretation of data complicated.

Most theories therefore strive to evaluate the energy term of eqn. 2.23 or more often just one component of the total energy term, and the following sections deal with some of the important points to consider when developing theories. Also presented in appendix 1 are some of the more successful models[2,6-9,16,17,23,30-33] proposed in the literature (success based on the model's ability to predict segregation) which generally take into account some or all of the important considerations presented in the following sections.

2-II Quasichemical Models:Considerations of The Classical Approaches

a) Surface Energy

The surface energy can be thought of as the energy required to create the surface whether it be by removing a plane of atoms or by adsorbing the surface atoms. No matter what approach is taken, several points must be kept in mind:

1) The surface energy will be greatly affected by how the surface is defined. This may seem very simple and not worth mentioning except that some models define the surface as a monolayer of atoms while others take

into account several atomic layers. The exact definition of the boundaries of the surface region will be critical to the success of any model or theory and the interpretation of experimental results.

2) The simplistic frameworks assume ideality and therefore no mixing enthalpy, but real systems rarely have $\Delta H_{mix} = 0$ and any comprehensive model or calculation scheme will have to make an accounting of mixing energy.

i) Mixing Energy

Mixing energy arises from the free energy change associated with changing the environment of both the alloying elements. When mixing energy is large and negative a well ordered alloy is formed, while if it is positive, mixing is usually not complete and clustering ensues. In the first case above, a segregation phenomenon would be energetically unfavourable and in the second, segregation might be favoured. Thus the mixing energy can be of vital importance in surface segregation studies. The simplest case occurs when the mixing enthalpy is zero, this is the ideal solution case. In this case only the mixing entropy is important and it is configurational so we may have for ideal binary solutions;[2]

$$G_m = -TS_m = -RT[X \ln X - (1-X)\ln(1-X)] \quad 2.24)$$

where X may be for the surface or the bulk and the difference between surface and bulk would be the driving force for segregation. Eqn. 2.24) is very simple but extremely limited since very few binary alloys may be considered to be ideal and have only configurational entropy. It has

therefore been necessary to develop extensive theory for both mixing enthalpy and entropy.

ii) Mixing Enthalpy

Mixing enthalpy treatments involve a possibly variable bond enthalpy term but, bond enthalpies for unlike atoms H_{AB} are assigned fixed values for the sake of simplicity. The mixing enthalpy would therefore be defined as;

$$H_m = \frac{Z}{2} (H_{AB} - \frac{H_{AA} + H_{BB}}{2}) X_A X_B \qquad 2.25)$$

where Z is the coordination number. To simplify matters, the regular solution parameter Ω is defined as;

$$\Omega = \frac{Z}{2}(H_{AB} - \frac{H_{AA} + H_{BB}}{2}) \qquad 2.26).$$

At the end what is desired however, is a ΔH_m for surface segregation and that would involve differing co-ordination numbers. Another simplified parameter might therefore be;

$$W = \Omega/Z \qquad 2.27)$$

and equation 2.25) would then be;

$$H_m = ZWX_AX_B \quad 2.28).$$

Miedema[8,15] arrives at a slightly different equation, but that is dealt with separately in appendix 1.

3) Surface energy is made up of at least two components in the simplest plausible framework. One component is enthalpy and the other is of course entropy. Most models deal exclusively with enthalpy and assume any non-mixing entropy component is insignificant. This approach is convenient but, not necessarily valid.

i) Surface Entropy

It is normal to think that the re-arrangement of a surface has associated with it some change in entropy in addition to enthalpy changes. The questions are; is the entropy contribution significant and how do we evaluate it if it is?

Firstly we may consider that if an unsegregated surface exists, those atoms populating the surface region have certain additional vibrational modes different than those in the bulk because of the lack of atoms on one side. One might say that any atom coming from the bulk to the surface in a segregation process would also experience the different environment and also receive the additional vibrational modes and hence the entropy change will be essentially zero. Most of the pure bond-breaking models in fact make this assumption[1,2,7-11]. In ref. 2 there is actually a proposed proof of this assumption;

$$\Delta S_a = (S_s - S_s^{\circ}) - (S_b - S_b^{\circ}) \quad 2.29)$$

where ΔS_a is the entropy of adsorption and S is the vibrational entropy given by

$$S = k \ln(RT/h\nu_E) \quad 2.30)$$

where ν_E is the Einstein vibrational frequency. Then the surface vibrational frequency would be

$$\nu_{E,s} = (z_s/z_b)^{1/2}\nu_{E,b} \quad 2.31)$$

where z_s and z_b are the surface and bulk coordination numbers respectively. Making appropriate substitutions into 2.29) we can get;

$$\Delta S_a = 3k \ln[(\nu_{E,s}^{\circ}/\nu_{E,s})(\nu_{E,b}/\nu_{E,b}^{\circ})] \quad 2.32)$$

and since we assume in eqn. 2.31) that

$$\nu_{E,s}/\nu_{E,b} = \nu_{E,s}^{\circ}/\nu_{E,b}^{\circ} = (z_s/z_b)^{1/2} \quad 2.33$$

then

$$\Delta S_a = 3 \ln(1) = 0 \quad 2.34).$$

Hence the vibrational entropy contribution (independent of mixing entropy) is zero. The critical assumption of this proof is the relation linking the coordination number to vibrational frequencies in eqn 2.31) of the surface and bulk. This relation seems unlikely since vibrational modes perpendicular to the surface plane will be greatly changed by the absence of an overlayer and modes parallel to the surface plane will be only moderately affected by being at the surface. The net result of these changes to the vibrational frequencies are therefore not likely to follow the rule of eqn. 2.31, especially in the case of an atom of type A populating a surface on top of a randomly mixed AB subsurface layer. Reverting for a moment to the extremely simplistic balls and spring type model for an oscillator, it is unreasonable to assume that the frequency of a vibration at a segregated surface is some easy fraction of the bulk value because for alloys where the elements have different mass the reduced mass at one end of the spring will be very different depending on which element is at the surface.

Overbury et.al.[12] utilized the empirical observation that surface tensions (which are surface free energies for pure elements) are approximately 1/6 of atomization enthalpies (in many cases this is true, but not always, and this is an important point for this thesis in particular), a simple rule of thumb measurement is as follows;

$$G_s = H_s = \frac{1}{4} H_{atom.} \quad - \text{from bond breaking model} \quad 2.35)$$

$$S = \frac{1}{T_{meas.}} (H_s - G_s) \quad \text{from 2nd law} \quad 2.36)$$

therefore substituting 2.35) into 2.36) yields

$$S = \frac{1}{T_{meas.}} \left(\frac{H_{atom}}{4} - \frac{H_{atom}}{6} \right) = \frac{H_{atom.}}{12T_{meas.}} \qquad 2.37).$$

But H_{atom} is usually measured at the melting temperature T_m and solids would be at some fraction of this, so we may easily see

$$\Delta G_s = 0.25(H^B_{atom.} - H^A_{atom.}) - \frac{T_x}{12T^A_m T^B_m} (T^A_m H^B_{atom.} - T^B_m H^A_{atom.}) \qquad 2.38)$$

where T_x is the temperature of interest, less than T_m.

This is interesting and appears to be valuable except that when an evaluation of ΔS is made, the uncertainties are larger than the value obtained and very little is accomplished.

There are other[13,14] theories for estimating the surface entropy but they suffer from depending on hard to measure parameters like the Einstein temperature and very few direct measurements of surface entropy have been done. As mentioned before however, bond-breaking models assume that any additional entropy component is zero and use vaporization enthalpies as free energies of segregation.

b) Surface Enthalpy;The Approximation Using Vaporization Enthalpies

The estimation of differences in surface enthalpy via vaporization enthalpies commonly used in the bond breaking models, must be considered in light of some important limitations.

1) If the surface enthalpy is thought to be related to the energy of bonds missing at a surface, a knowledge of the energy of one bond is thought to be of value in predicting segregation. One of the problems associated with this approach is that the appropriate term for evaluating the average energy of bonds is the atomization enthalpy. Unfortunately atomization enthalpies are not usually reported, but rather vaporization enthalpies are. This may seem to be an acceptable substitution except in the cases where gas phase di or multi-atomic species are formed upon vaporization.

2) Since a fraction of the difference between vaporization enthalpies is used, experimental errors associated with the determination of those values will become especially critical, even in cases where it is clear that the substitution is valid.

3) Differing atomic size is not accounted for. If one type of atom is much larger than the other type of atom in a binary alloy, and has a higher $\Delta H_{vap.}$ it may be preferred at the surface over smaller atoms with lower $\Delta H_{vap.}$ since the total surface energy may be lowest with fewer large atoms of higher $\Delta H_{vap.}$ rather than a higher number of atoms with

lower enthalpy of vaporization. There are also other considerations to differing atom size and the next sub-section deals with this aspect of the overall problem.

c) Strain Effects[1,2,8,16,17]

If one imagines a very large solute atom in a solvent matrix made up of relatively small atoms, it is easy to envision the distortion of the solvent matrix to accomodate the solute (fig 1a). Any distortion of the solvent matrix would of course involve the input of energy and a re-arrangement of atoms to minimize distortion and hence the total energy of the system would be favoured. One such re-arrangement would be to have the solute migrate to the surface and remove distortion in one direction (fig 1b). A further energy savings would be realized if the solute were relaxed out into the vacuum so as to reduce the distortion into the bulk and laterally along the surface (fig 1c).

There would therefore seem to be a driving force for segregation of large solute atoms to a surface. After a time, the surface may become saturated with solute atoms and the situation may be as in fig 1d where the surface is all solute and a series of edge dislocations accomodate the mismatch between the different layers. The strain energy associated with fig 1a was defined by Friedel[18] as;

$$E = \frac{24\pi k_s G_m r_s r_m (r_s - r_m)^2}{3k_s r_s + 4G_m r_m} \quad 2.39)$$

where k is the bulk modulus, G the shear modulus, r are radii and the subscripts are; s for solute and m for matrix. The equation came about as a result of considering the energy required to expand a solvent sized hole in a matrix to solute size. Eqn. 2.39) would seem to be very straight forward except that the estimation of the final radius is crude due to the fact the hole is probably distorted. In light of this limitation, Eshelby[19] put forth a simpler version based on atomic volume of the pure solute and solvent atoms;

$$E = \frac{2}{3} \frac{G_m K_s}{3K_s + 4G_m} \frac{(V_s - V_m)^2}{V_m} \qquad 2.40).$$

Figure 1
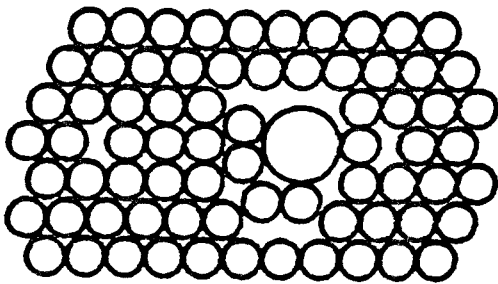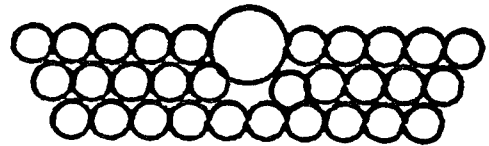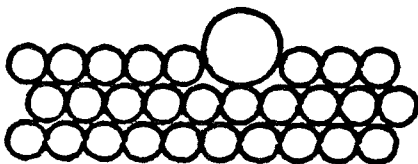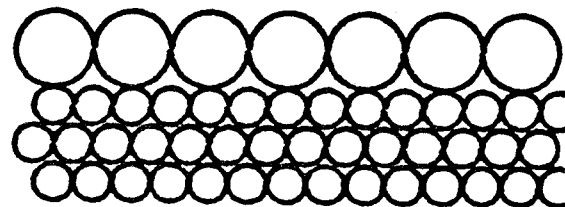
Possible accomodation arrangements for an oversized solute. a) distorted and strained bulk, b)deeply set solute at the surface, c) solute relaxed slightly into vacuum and d) a monolayer of solute with edge dislocations to accomodate mismatch.

This expression was later revised[20] to;

$$E_{el} \doteq \frac{16}{3} \pi \mu_m r_m^3 (\sigma^* - 1)^2 \qquad 2.41)$$

where σ^* is the ratio of atomic sizes r_s/r_m , μ_m is the sheer modulus of the matrix and can be evaluated using the expressions given by Fuchs[21] considering only nearest neighbour interactions of the Leonard-Jones m:n form;

$$\mu = (4/\sqrt{2})r(m-n)(m/n)^{(n+3)/(n-m)}\varepsilon\sigma^3 \qquad 2.42).$$

In order to calculate E_{el} one must then make another assumption. The assumption is that $E_{el} = \Delta Q_{el}$, where ΔQ_{el} is the energy recovered by segregating the solute to the surface. This assumption needs to be examined more closely:

1) Implicitly the assumption says that all the strain energy of the bulk is recovered by atoms segregating to the surface. Figs. 1b and c showed solitary atoms at the surface and it is quite clear that some distortion remains unless the atom is positioned out of the plane of atoms entirely, which is not likely if the atom is alone. The solution to this dilemma would seem to be the situation pictured in fig 1d where a monolayer of solute atoms removes all strain from the bulk. As mentioned before this is quite well within the realm of possibilities but there must be edge dislocations present to account for the misfit between the solute surface layer and the bulk matrix. These dislocations had to be

formed and energy had to be expended to form them, so the assumption that $E_{el} = \Delta Q_{el}$ appears to be a poor one.

2) The original composition of the material is totally ignored. This is equivalent to stating that there are no solute-solute interactions and that means this model is useful only for very dilute solutions. The correction, or at least partial correction, for this and point number **1)** is given in eqn. 2.43)

$$E_d = \frac{A_s - A_b}{b} \times \frac{Gb^2}{2} \quad 2.43).$$

Here E_d is the energy of the dislocations needed to accomodate a pure solute overlayer. A_s and A_b are the molar areas of the surface and bulk compositions, G is the shear modulus and b is the burgers vector of the dislocations (assuming all the dislocations are the same and hence have the same burgers vector). Using eqn. 2.43) and including composition we may now arrive at;

$$E_{strain} = E_{el} - E_d = E_{el}(X_b) - \frac{Gb}{2}[A(X_s) - A(X_b)] \quad 2.44).$$

It has been suggested[22] that when the solution is no longer dilute the strain contribution may become insignificant and even when dilute eqn. 2.44) can only estimate the upper boundary for the elastic contribution. The second term in eqn. 2.44) always opposes segregation and in most systems very nearly cancels the first term. The outcome of

this observation is given by Abraham et.al.[23] and supported by Seah[24] and it is that, when a solute is smaller than the solvent no segregation occurs and only dilute systems of large solute in small solvent have significant strain energy terms. The system most often quoted as an example of segregation due to size mismatch is Ni(Au) where Au segregates[17] at both extremes of composition. It is difficult however to say that the segregation is due only to strain or even that strain is important since the bond breaking models also predict Au segregation. It is therefore quite reasonable to say that except in extreme cases (and no one is sure of those) the strain contribution is small and indeed when the ratio of atomic radii is between 0.95 and 1.05 the strain contribution is virtually zero[25].

The preceeding sections have sought to point out some of the considerations used to develop overall models which are routinely used by researchers when studying the segregation phenomenon. The most common and successful of these models, based on classical ideas, are presented in Appendix 1 for the interested reader and will be referred to in later sections when quantitative predictions are made regarding the system under study here.

Not all of the theories proposed to predict segregation are based on classical ideas. There have been several other models proposed and the following sections give a brief overview of three of these models.

2-III Other Models For Surface Segregation:Non-Classical Approaches

a) Correlation of Segregation to Bulk Diffusion

It has been pointed out that one could easily compare an atom at a surface to an atom bordering a vacancy in the bulk of a material. In terms of energy, it takes a certain amount of energy to create a vacancy, Swartzfager and Kelley[34] proposed that the energy required to exchange a bulk atom with a surface atom is some fraction of that vacancy creation energy i.e.

$$G_{AS} - G_{BS} = k(G_{AV} - G_{BV}) \qquad 2.45)$$

In eqn 2.45) G_{AS} and G_{BS} are the surface energies of atoms A and B respectively and G_{AV} and G_{BV} are the energies of atoms A and B beside vacancies. k is some proportionality constant and requires some specific model to predict it. Le Claire[35] related G_{AV} and G_{BV} to tracer diffusion coefficients,

$$D_A/D_B = \frac{f_A W_A}{f_B W_B} \exp^{[-(G_{BV} - G_{AV})/RT]} \qquad 2.46$$

Here the new factors f and W are correlation factors and jump frequencies. We can now utilize the normal equation relating surface composition to a change in free energy;

$$\frac{X_s}{(1-X_s)} = \frac{X_b}{(1-X_b)} \exp^{(-\Delta G/RT)} \qquad 2.47)$$

where $\Delta G = G_{AS} - G_{BS}$ and we can thus get the very simple expression;

$$\frac{X_s/(1-X_s)}{X_b/(1-X_b)} = k^{\cdot}\frac{D_A(X_b)}{D_B(X_b)} \qquad 2.48)$$

where D_A and D_B are the tracer diffusion coefficients at composition X_b, and $k^{\cdot}$ has all the previous constants included.

This very simple theory is very attractive since it requires only the knowledge of diffusion constants and the factor $k^{\cdot}$. The diffusion constants are readily available[36] and the limited work to date assumes $k^{\cdot}=1$ and yields some quite remarkable correlations, not only qualitatively but quantitatively. Another very promising feature is the ease of including the temperature dependence;

$$\frac{X_s/(1-X_s)}{X_b/(1-X_b)} = k^{\cdot}\frac{D_A^{\circ}}{D_B^{\circ}} \exp^{[-(Q_B- Q_A)/RT]} \qquad 2.49)$$

where the Q's are the activation energies.

Not mentioned in this model however is its dependence on the assumption that diffusion occurs strictly via a vacancy mechanism and the theory does not apply when interstitial mechanisms are operating. The theory therefore is quite useful in metal alloys but not particularly useful in the prediction of small non-metal impurity segregation.

b) Electronic Theories

These theories are very complex sets of equations which describe the internal energy of a system using some equations like;

$$E_{int} = N_{//} \sum_i \int_{-\infty}^{E_f} E \, N_i(E, X_1, X_2, \ldots) dE \qquad 2.50)$$

where $N_{//}$ is the number of atoms in a layer parallel to the surface and,

$$N_i(E) = -(1/\pi) \mathrm{Im} G_i(E) \qquad 2.51)$$

"is the average electronic density of states"[37] for the crystal plane layer i. The calculation of eqn 2.51) is achieved by using the average electronic Green 's functions. Taken into account in the individual Greene's functions are hopping integrals and the Wannier-State electron energy which together determine the energy an individual electron is likely to have depending on it's position in the electronic structure of the metal and the position of the atom in question in relation to the crystal and the surface. In short the electronic theories provide an electronic rationale behind the actual surface tensions in metals. Several recent reviews[1,2,16] note this fact and mention that the results of these electronic density of states calculations would suffer from the same sort of assumptions as conventional theories while being much more difficult to handle. In the future however these theories (when sufficiently developed) should provide direct calculation of solid state surface tensions, but for now they simply conclude that segregation in

transition metal alloys is favoured for the component with most d-electrons over 5 (when both atoms have more than 5 d electrons). Quantification of the segregation phenomenon using these approaches is well beyond the scope of this thesis but it is clear that a complex modelling approach is more likely to generate a realistic driving force than correlations to bulk phenomenon which may have been extrapolated from liquid or vaporization data. A somewhat less demanding approach is outlined in the following section.

c) Monte Carlo and Embedded Atom Calculations

Monte Carlo calculations have come to be in very common use by theoreticians seeking to calculate properties of solids that depend on the arrangement of atoms in a bulk. The details of the procedure will not be covered in this thesis as they would not serve to clarify the underlying approach. Instead, it will serve to simply give an overview of the general approach.

In order to find the configuration of atoms that defines a bulk system's minimum energy state, an imaginary slab of atoms is created in computer memory. The positions of the atoms are re-arranged in a fashion dictated by a random number generator, hence the name. The configuration of the atoms that produces the lowest total energy for the slab is then found after a very large number of iterations. Sundaram and Wynblatt[38] used cubo-octahedral particles with either 38 or 201 atoms, in a calculation of total energy based on sublimation energies only, and is the basis for other calculation attempts which seek to modify the energy

equations[2,6,23,39-41]. Since the positions of all the component atoms can be varied without restriction, the positions of atoms at the surface are allowed to relax if that relaxation reduces the total energy of the system. This feature of the Monte-Carlo method therefore allows lattice strain considerations to be intrinsic to the calculation and hence no "add on" terms of questionable applicability need be relied upon.

When the minimum total energy of the slab has been found, the difference between that energy and the known energy of some reference state, can then be thought of as the driving force behind the change in the subject state from the reference state. For surface segregation studies, the difference in total energy between a hypothetical alloy that has not been allowed to segregate and an alloy whose atoms have been allowed to move freely to a minimum energy condition, is considered the driving force for segregation.

The general procedure behind Monte-Carlo methods is very versatile but it's accuracy is in fact determined by the accuracy of the equations used to determine the energy of the system. For the study of surface segregation, one of the newest and apparently most accurate methods is the "Embedded Atom Method" (EAM)[40,41]. In the embedded atom method the total energy $E_{tot.}$, is assumed to consist of two parts, one which depends only on electron densiy at an atom site and a second pairwise interaction. This can be written as;

$$E_{tot.} = \sum_{i}^{atoms} (F_i(\rho_{h,i}) + \frac{1}{2} \sum_{i \neq j} \phi_{ij}(R_{ij})) \quad 2.52)$$

where the first term can be thought of as the energy required to embed an atom i into the electron gas of density $\rho_{h,i}$ and the second term can be viewed as representing the core-core repulsion between atoms i and j separated by a distance R_{ij}. The approximation is made such that the electron density is given by superimposing atomic densities,

$$\rho_{h,i} = \sum_{j \neq i} \rho_j^a (R_{ij}) \qquad 2.53)$$

where $\rho_j^a (R_{ij})$ represents the atomic electron density for atom j. $\phi_{ij}(R)$ is assumed to be the geometric mean of the interactions between atoms of the same kind;

$$\phi_{ij}(R) = [Z_i(R_{ij})Z_j(R_{ij})]/ R_{ij} \qquad 2.54)$$

where $Z_i(R_{ij})$ is the effective core charge of atom i at distance R_{ij} from the atom. Theoretical predictions from first principles are not immediately forthcoming for either $F_i(\rho_{h,i})$ or $\phi_{ii}(R)$ but since values of sublimation energy, lattice constant, elastic constant and vacancy formation energy are well known, one can use these constants to empirically evaluate these functions for use in determining different properties of the model bulk slab[41] and $\rho^a(R)$ have been calculated from the Hartree-Foch wave functions by

$$\rho^a(R) = N_s\rho_s(R) + N_d\rho_d(R) \qquad 2.55)$$

where N_s and N_d are the number of outer s and d electrons and ρ_s and ρ_d are the densities associated with s and d wavefunctions respectively. where the effective charge $Z(R)$ is given by;

$$Z(R) = Z_\circ \exp^{-\alpha R} \qquad 2.57)$$

where $Z_\circ$ is given by the number of outer electrons and α can be determined by fitting the bulk pure element and alloy parameters. It is clear therefore that the embedded atom method must satisfy many electronic and bulk thermodynamic parameters and hence would be the most all encompassing approach to date. The negative side of this approach is the fact that the calculation procedures are extremely long and this is very much a specialty field, thus restricting their general applicability in the scientific community.

This chapter has now covered the major points of theory and the most successful models currently in print to predict the composition of segregated surfaces. It was with these theories in mind that an alloy system was sought that would provide a useful insight into which (if any) of the models are most appropriate. It can be said that all the theories agree that the driving force for segregation is the difference in surface free energy between an unsegregated and a segregated surface. The major differences lie in the evaluation of that segregation energy, and hence the real surface composition, from readily available bulk thermodynamic quantities. In the next chapter the rationale for the choice of the

alloy system finally decided upon will be revealed, as well as, what the
models presented in this chapter and in appendix 1 would predict.

Chapter 3

Rationale For The Selection of The Co-Ni Alloy System

3-I Criteria for Selection

The selection of the alloy system to be studied in this thesis was a very carefully considered decision. The theoretical predictions outlined in the previous chapter are consistent with each other as to qualitative predictions in many cases but there is disagreement as to extent in most cases. The reason there is often qualitative agreement between the simple bond-breaking models and the surface free energy (surface tension) models is that, very often the differences in surface tension are mirrored by differences in enthalpy of vaporization and indeed, Overbury et.al.[12] stated that the surface tensions of metals are fractions of their vaporization enthalpies. This however is not the case in all systems and Chelikowsky[42] has compiled a comprehensive table predicting the segregating element for 702 possible binary alloys via the equation of Miedema[8,31,32] given here as eqn A.29) and compared these predictions to those of a surface enthalpy approach eqn 2.25). Chelikowsky pointed out that there are a number of cases where the two models predict opposite segregation. From the point of view of these models (the two most widely used models) it would then be useful to study an alloy where they predict opposite results.

If an alloy system is found that has the bond breaking and surface free energy approaches predicting opposite segregation trends, it is most desirable that there are no other possible driving forces for segregation such as; bulk strain or enthalpy of mixing. Systems where bulk strain is thought to play a role are best avoided since the strain contribution terms of eqns. 2.47) and 2.48) at best represent an upper boundary to the extent of segregation, and the empirically determined effect is much smaller than theory would predict[22]. In fact if the ratio of radii of the two types of atoms in the alloy is $.95 < r_A/r_B < 1.05$ the contribution of strain to the driving force for segregation is essentially zero[25].

The best alloy system to study would be an ideal solution. That is to say that the phase diagram would have only a continuous series of solid solutions with low heat of mixing. If the alloy system were ideal then one can safely make the assumption in the bond-breaking models that $H_{AB} = 1/2(H_{AA} + H_{BB})$ and hence that segregation is confined to the first monolayer only. The ability to make this assumption is extremely important if one considers the complexity of equations A.1), A.2) and the multi-layer solutions of eqns. A.16) and A.17) . A non-ideal solution would require the determination of compositions for up to 4 monolayers and this represents a major barrier to the experimentalist.

3-II Satisfaction of The Criteria and Qualitative Predictions

There are now three criteria to be satisfied in the process of selecting an appropriate alloy system: 1) opposite predictions based on the bond breaking and surface free energy models, 2) both elements should be very nearly the same size and 3) the alloy system should be ideal with a continuous series of solid solutions.

The Co-Ni alloy system satisfies all three of these criteria. Treating point 3) first, we may see in figure 2 that the phase diagram is a continuous series of solid solutions with only a magnetic transformation at relatively high temperatures and an $\varepsilon \rightleftharpoons \alpha$ transformation at temperatures below our range of interest. The heat of solution is given as -1 kJ/mole[8] (extremely small). The Atomic Radii are 1.25 and 1.24 Å for Co and Ni resectively, or a ratio of 0.992. Therefore effects of differing atomic size can be completely ignored. The Enthalpy of Vaporizations are; 428.4 kJ/mol and 430.1 kJ/mol for Co and Ni respectively[43]. This qualitatively predicts slight segregation of Co in the bond-breaking models although the difference in $\Delta H_{vap.}$ is very small. The surface energies at 0° K are listed[8] as 2550 and 2450 $mJmol^{-1} m^{-2}$ for Co and Ni respectively. The surface free energy approaches would then qualitatively predict that Ni would segregate.

Additionally it should also be noted that electronic theories would predict that Ni would segregate since it has configuration $[Ar]3d^8 4s^2$ while Co has configuration $[Ar]3d^7 4s^2$ i.e. Ni has more d-electrons.
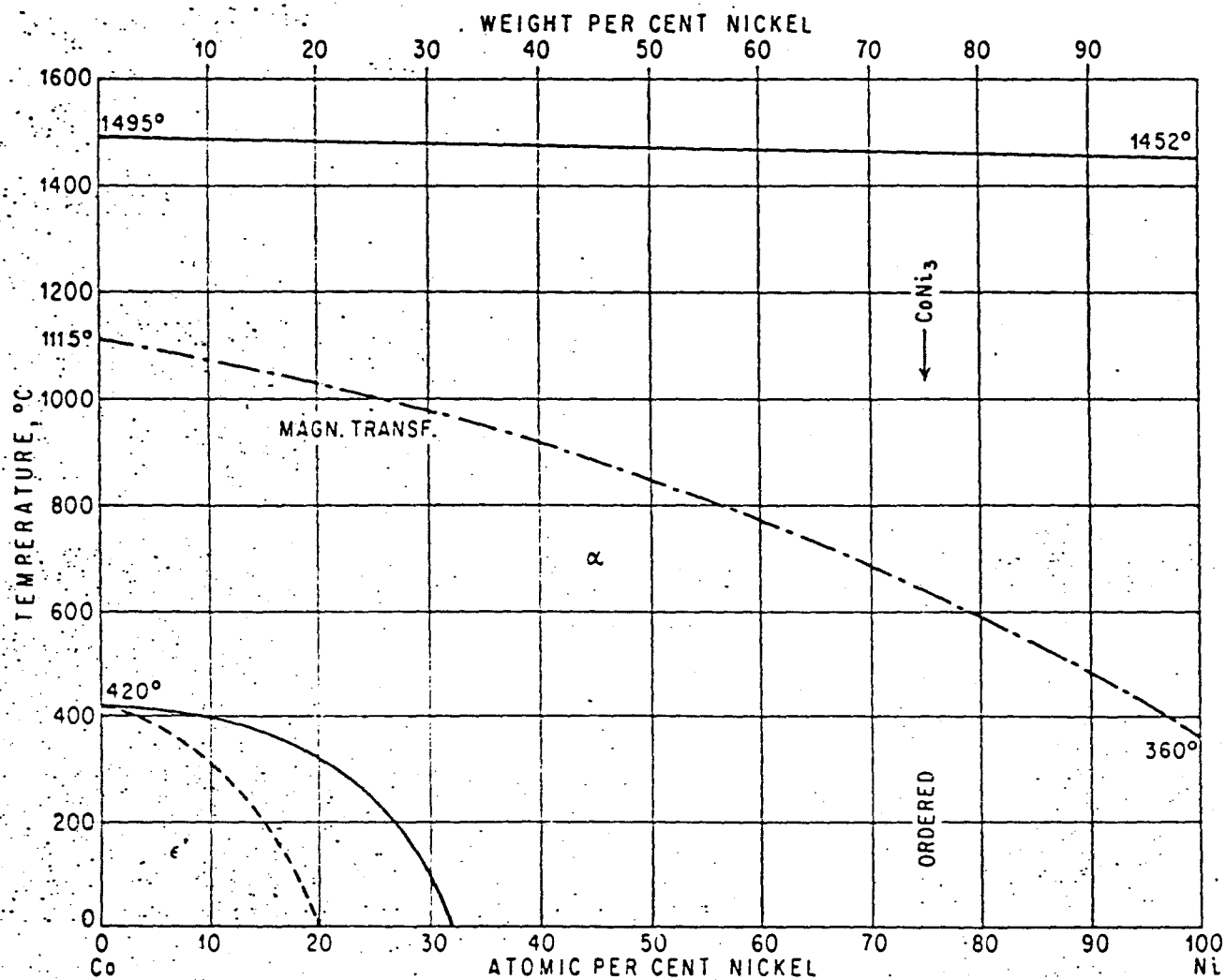
Phase diagram of Ni-Co system Figure 2

3-III Previous Work on Segregation in the Co-Ni System

Because this system represents a test case for bond-breaking vs. surface free energy theory, it would be logical to assume that it has been examined before. In fact the segregation behaviour of Ni-Co alloys has been the subject of four other investigations to date. The continued interest in this system stems from the fact that the four previous studies arrive at three different conclusions and as such there was no definite determination of which element segregates, let alone any reliable estimate as to the extent, at the outset of this investigation. A brief review of the previous work is presented here merely to acquaint the reader with an additional reason for doing the work presented in this thesis. A further discussion of the previous results will be given in a later section.

The first reported study was by Goretzki et.al.[45] in 1977. That study used a Scanning Auger Microprobe to analyze a 30 a/o (a/o = atomic percent) Ni alloy. Only one sample was quenched from a ten minute anneal at 350 $\overset{\circ}{C}$ and the cold surface analyzed, using the Auger peaks in the energy range 650-850 eV. The authors claimed that equlilibrium, as determined by constancy in the Ni peak height, was established after 8 min.. Without stating the exact quantification method, they claimed that Ni segregated to enrich the surface by approx. 10%

In 1979 Cherepin et. al.[46] did an Appearance Potential/Auger Spectroscopy study of a range of alloys from 20 to 80 a/o. They used peak to peak height analysis vs. pure element standards and found slight enrichment of Ni but did not offer quantitative results.

Shpiro et.al.[47] did an XPS/AES study of the Co-Ni system and found Co enhancement of the surface upon annealing in vacuum and re-establishment of the bulk Ni content upon annealing in $H_2(g)$. The calibration method used was peak height in N(E) mode adjusted by a sensitivity factor determined from ionization cross sections and inelastic mean free paths.

Most recently Tanaka et.al[48] used computer simulation of Auger spectra using pure element standards on the high energy peaks (650-850eV). This study reported that excellent simulation matches were possible if the highest energy peak (pure Ni signal) were omitted. The compositions from the simulations showed essentially no segregation of either component.

We then have all three of the possible observations reported in the literature i.e. Ni segregation, Co segregation and no segregation. This study reports not only the qualitative observation of segregation in this alloy system but also determines to a high degree of accuracy (for surface determinations) the quantitative extent of that segregation. To compare experiment to theory it would then be useful to have the quantitative predictions for the alloys investigated in this thesis.

3-IV Quantitative Predictions

There were a number of relations proposed in chapter 2 that claimed to predict the extent of segregation but, Co-Ni alloys were selected to eliminate a number of these equations. Basically no strain contribution need be considered in any equation and the assumption that

segregation is confined to the first monolayer only is held as valid and at worst one would need to consider only 2 monolayers. The equations used for quantitative predictions would then be;

i) simplistic bond-breaking with configurational entropy
($X_1 \neq X_2 = X_3 = X_b$) eqn. 2.39). Data from refs. 31 and 9

ii) multi-layer bond-breaking (up to 2 monolayers only)
($X_1 \neq X_2 \neq X_3 = X_b$) eqns. A.10) with A.11) and A.12).Data from ref. 31 and 9

iii) Bond-breaking and enthalpy of mixing eqn A.22). Data from ref. 31 and 9

iv) Combined surface free energy and heat of solution. eqn A.24) Data from ref. 8

v) Correlation to bulk diffusion eqn. 2.56) Data from ref. 49)

TABLE 3-1 Quantitative Predictions for 580 °C

Sample Comp. a/o Ni	i)	ii)	iii)	iv)	v)
14.1 ± .04	13.6	13.3	13.4	20.2	25.4
22.6 ± .01	22.1	21.7	21.6	31.1	37.8
43.1 ± .1	42.4	41.8	41.1	53.9	61.2
56.0 ± .06	55.3	54.6	53.4	66.3	72.6
78.7 ± .01	78.2	76.1	75.1	85.1	88.5
89.6 ± .01	89.3	89.1	85.5	95.7	94.7

Predictions of various models (see text) for the surface composition of alloys investigated here in % Ni.

The reader should note from Table 3-1 that contributions from a second layer and heat of mixing to bond-breaking models, do not alter the resulting prediction significantly. Also there is a caveat that must go along with the predictions of column v): the diffusion coefficients used were those that ref. 49 labelled as being most trustworthy, other values also listed gave radically different results.

The bulk compositions listed, correspond to samples made for this thesis and predictions are set for 580 $^{\circ}$C which is the temperature studied in the first phase of this study. The next chapter deals with the details of the preparation of those samples and subsequent chapters deal with determinations of thermodynamic quantities associated with segregation in this system.

Chapter 4

Sample Preparation

4-I Polycrystalline Boules

The preparation of samples with known composition and low con-
taminant level is a critical requirement in any investigation into
surface phenomena. Starting materials were necessarily of the highest
purity available on the commercial market, 99.999% from Johnson Mathey
Chemicals Co. Ltd.. The supplier's analysis claimed the major bulk
contaminant detected was Fe at 3 ppm and 4 ppm for Ni and Co
respectively. Non-metallic bulk impurities were not analyzed for, and
since both Ni and Co are mined from sulfide ores, it is expected that the
major non-metallic impurity was Sulfur.

Alloy preparation was carried out in an arc-melt apparatus built
in house with a rotating water cooled OFHC Copper hearth. The sample
preparation chamber was evacuated via rotary pumping to a start pressure
of approximately 10^{-3} torr and backfilled to approx. 380 torr (0.5 atm)
dynamic pressure (continuous pumping) of research grade Argon. Pure
element rods were sliced to lengths appropriate to the target composition
using a high speed saw and Alumina blades. Each element was separately
liquified under Ar and, allowed to de-gas and eventually cool to form a

pure element boule. Pure element boules were them weighed to ± 0.05 mg accuracy and placed side by side in the arc-melt chamber. The pure elements were allowed to mix as liquids for several minutes and allowed to re-solidify. Each sample boule was then turned and re-melted at least 7 times to ensure complete homogeneity. Sample boules were then annealed just below the melting temperature for ten minutes and allowed to cool slowly in order to remove stress. The solid boules were then re-weighed and the composition was calculated from the ratio of the starting number of moles of each element. Errors on bulk compositions were estimated by assuming that all mass loss due to evaporation came from the solute (a worst case scenario) and were at most 0.1 % and at best < 0.01 %.

Prepared boules were then mounted on metal blocks with epoxy glue and sliced into ˜ 3 mm wafers. Wafers were then mounted in a parallel surface polishing jig with mounting wax. The surface was then polished with increasingly fine abrasive until a smooth mirror-like surface was achieved after the final 1 μm diamond polish stage. EDAX line scans were used to check for homogeneity in some of the early samples and no in-homogeneity was detected.

One of the polycrystalline samples that was annealed in vacuum for great lengths of time (56.0 a/o Ni) displayed two very large crystals visible under low magnification light microscope. These crystals were visibly continuous from front to back in this, now 0.5mm thick sample. The Transmission Laue method[50] was employed, using a 50 kV 12mA Mo Kα collimated (˜ 1 mm diameter beam) X-ray source, to determine that the two grains had orientations within 2° of the (111) and (210) planes. These grains were then the subjects of a study to determine the temperature and

crystallographic dependence of the surface segregation phenomenon and the results are presented later.

4-II Single Crystal Samples

From the results of the temperature and crystallographic dependence study, a need to perform more experiments on well oriented single crystal samples was indicated. A facility exists in the Institute For Materials Research where single crystals can be grown from pure elements by Mr. J.D. Garrett. The Czochralski procedure used, involved the liquification of starting materials in a water-cooled rotating (80 rpm) OFHC Copper hearth, under Ar atmosphere, by a Reed type Tri-arc^{TM} welding furnace. A liquid cooled rotating (20 rpm) seed crystal was then dipped into the liquid alloy by a crystal pulling rod and slowly withdrawn at a rate of 1.3 to 2.3 mm/hr.. The alloy solidified as a single crystal with orientation the same as the seed crystal. In this particular case there was no single crystal of Co-Ni available to act as a seed, instead an oriented single crystal of pure Ni was used since the melting temperature and lattice parameter would be very close to those of the alloy. This arrangement yielded a single crystal of the desired composition on the first attempt. The exact composition required was 50 a/o Ni for reasons which will be explained later and the final sample composition was 50.02 ± 0.005 a/o Ni.

The single crystal was then mounted on a goniometer, an end was sliced off, and polished in the previously mentioned fashion in order to facilitate the determination of the orientation of the single crystal by

Laue Back Reflection[51] again using the collimated 50 kV 12 mA Mo Kα source. The crystal was then rotated, wafered to ~ 1.5 mm thickness and polished in the previously mentioned fashion, to yield samples with surfaces of the three principle faces: (111), (100), and (110) to ± 1° or less. Uniform 7 mm diameter sample discs were cut from the single crystal wafers with a spark cutter courtesy of A.J. Slavin of Trent University. Again the results of this study are presented later.

4-III Sample Cleaning In Vacuum

Even in the ultra-high vacuum conditions ($< 1 \times 10^{-9}$ torr) maintained in an Auger Electron Spectrometer, the surface of a sample which has been de-greased with Acetone and rinsed with Methanol, as all samples were in this work, will be slightly oxidized and covered in contaminants like Carbon, Chlorine and Sulfur. Removal of contaminants of this nature is routinely done by ion beam sputtering. In this procedure, gas atoms are ionized by a filament in an ion gun and accelerated towards the sample with energies from 500 eV up to 5 kV in most commercial instruments. The ions impinge on the surface, "sputtering" substrate atoms and molecular fractions off into the vacuum. Noble gases are most commonly used for this purpose and Ar was used exclusively during this entire project. No spectra was ever accepted for quantitative analysis if there was any detectable level of any contaminant. A study of the effects of ion beam sputtering on these alloys is presented in a later chapter.

4-IV Mounting and Heating: Method 1

The analyses reported in this thesis were performed in two different Auger Electron Spectrometers that had two very different configurations and ways of holding and heating samples. The first instrument had samples mounted by thin Tungsten wires spot-welded onto flat Tantalum plates. The sample holder was then screwed onto a 12 position sample carousel which could be rotated into a position suitable for sample analysis.(see fig. 3). Heating was achieved by electron bombardment from a stationary filament inside the carousel and thus behind the sample. The analysis chamber was back-filled to 5×10^{-5} torr of high purity Ar in order to facilitate simultaneous 3 keV Ar^+ ion sputtering while annealing or alternating sputtering and non-sputtering while annealing. The ion beam and sample were held at a fixed angle to each other of ~ 71° from sample surface normal.

Due to the position of the heating filament and the interference of escaping heating electrons in Auger spectra, only quenched segregation experiments could be performed in this instrument. Samples were heated to the desired temperature and sputter cleaned by on/off cycles of the ion gun until the surface could be maintained contaminant free for up to 2 hrs. The now temperature equilibrated samples were then sputtered quickly to remove any trace level contaminants, allowed to segregate for 10 mins. (the time mentioned in ref. 45 as being sufficient to allow the sample to reach equilibrium) and quenched to room temperature. The temperature of the sample was monitored via a W/Re thermocouple spot welded directly to the sample. All the quenching experiments were done

at 580 ± 20 C$^{\circ}$, and this is the reason that all the predictions listed in table 2 of chapter 3 are for that temperature.

Fig. 3a
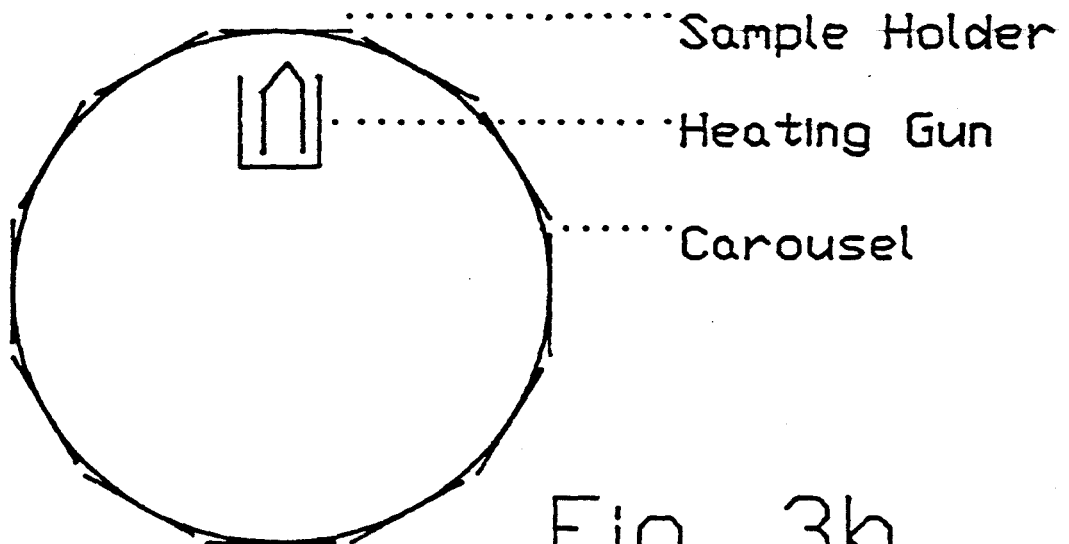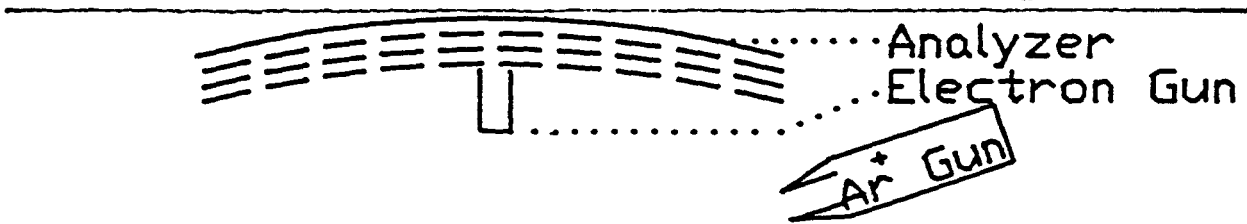
sample

W mounting wire

Ta sample holder

Mounting Screw

Analyzer

Electron Gun

Ar⁺ Gun
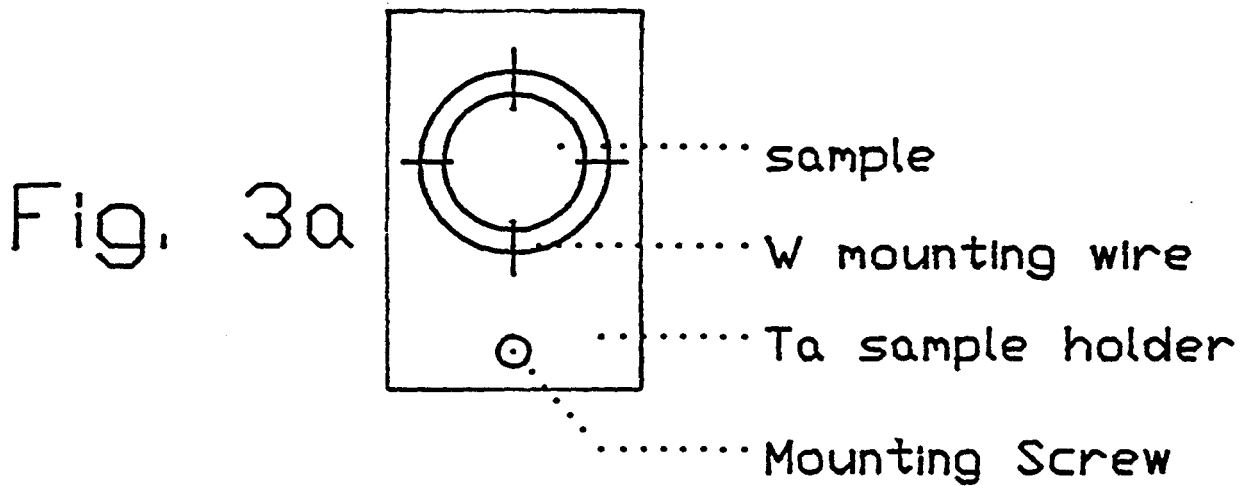
Sample Holder

Heating Gun

Carousel

Fig. 3b

Figure 3a) Ta sample holder set up. Figure 3b) Experimental arrangement
for static Auger analysis chamber.

4-V Mounting and Heating: Method 2

The second instrument used in this experiment (a PHI 600 Scanning Auger Multiprobe) was equipped with a more sophisticated hot stage that allowed analyses to be performed while the sample was held at a temperature of interest. The hot stage is described fully in ref. 52 and a reproduction graphic is presented in figure 4. The sample was heated by electron bombardment from behind as in the previous instrument but the sample edges are now covered with a Mo foil skirt that effectively traps electrons from the heating filament thus eliminating this interference in Auger spectra. Sample temperature was monitored using a Chromel-Alumel thermocouple welded directly to the sample. Calibration of this thermocouple via melting points of pure elements proved it to be accurate to within 5 K. The maximum stable temperature achieved was ~ 1200 K, but this could not be maintained for long since flexing of the sample mounting wires caused occasionally increased contact with the Mo skirt which then cooled the sample. Below 1000 K temperatures were stable enough ($\pm$ 5 K) to permit long term experiments for all samples up to 4 hrs. in length and for the single crystal samples up to 1150 K and 4 hrs..

Cleaning of the sample in this case was again done via an Ar^+ ion beam, but here a 4 keV accelerating potential was used and the angle of incidence was 60° from the surface normal. Also, in this instrument there was no need to back fill the entire chamber with Ar as the gun where the ions are generated is differentially pumped. The same on/off cyclic approach to cleaning, mentioned above, was used in this instrument and this procedure could greatly expand the time a surface could be

maintained in a clean state.

Copper

Steel (304SS)

Macor

copper braiding to
cooling reservoir

thermocouple
wire

alumina
wafer
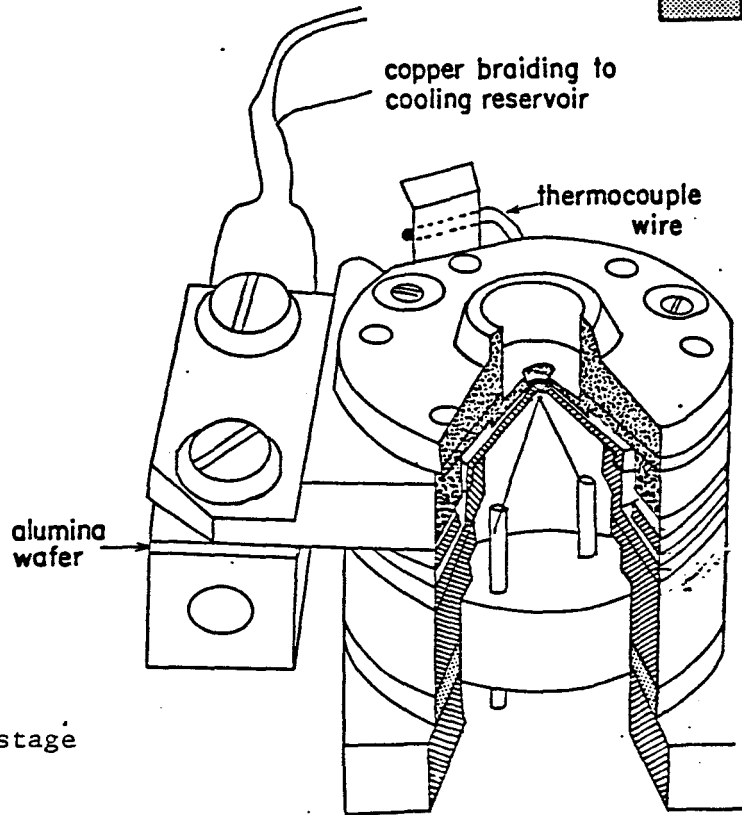
UHV compatible hot stage

Macor

Sample

Steel (304 S.S.)

Molybdenum
foil

thermocouple
posts and wires

Hot stage sample holder

thermocouple
wire rim
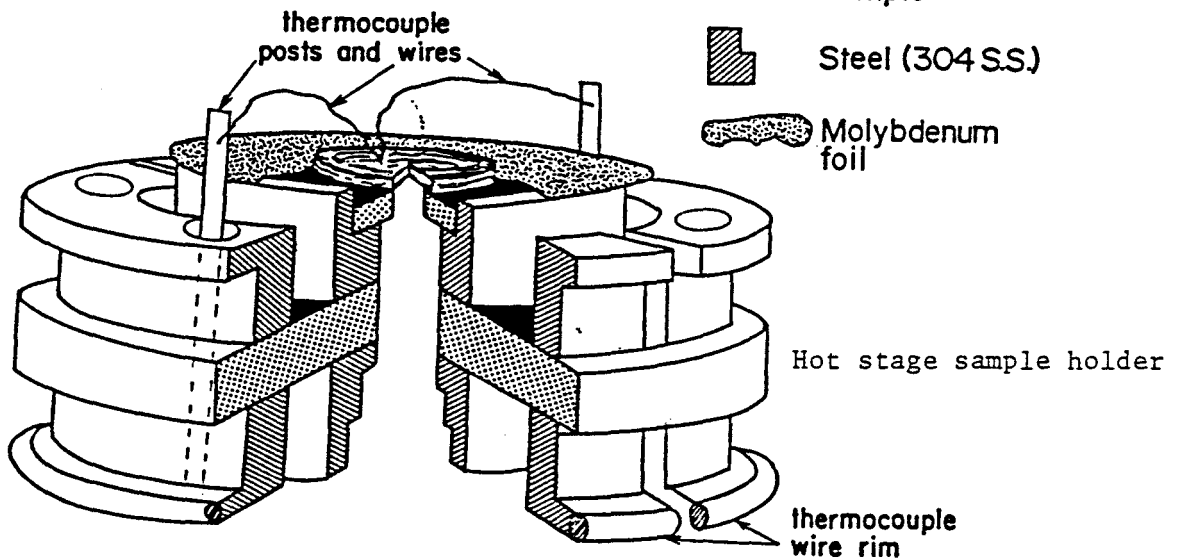
Figure 4

Chapter 5

Surface Analysis: Auger Electron Spectroscopy (AES)

5-I General Description

Auger Electron Sprectroscopy (AES) is today one of the main surface science investigation tools. It's general features are; analysis depth from a few Å up to approx. 2nm, sensitivity to all elements except Hydrogen and Helium, can be combined with ion beam milling to produce depth profiles of thin films up to 1 μ thick and can be made quantitative if standards are available and semi-quantitative if they are not. Since AES is an electron spectroscopy, the sample must be analyzed under high vacuum conditions ($\sim$ 1 x 10^{-6} torr) at least and more usually under ultra-high vacuum conditions (< 1 x 10^{-9} torr) in order to have the cleanest possible surfaces for the greatest length of time.

In order to initiate the Auger process, a beam of electrons is directed at the sample and an electron is removed (fig 5a). The removal of this electron leaves the atom in an excited ionized state which rapidly decays to an unexcited ionized state by an electron, from a valence level L_1, "relaxing" into the core level hole. This relaxation to a lower level requires the atom to emit energy, equivalent to the transition energy of the "relaxing" electron, of one form or another. In the Auger process the emission of energy is via the ejection of another valence electron L_2 with energy equivalent to the de-excitation transi-tion (fig 5b).

Fig 5a

Vacuum

Electron Beam

Vacuum

Φ

L_2
L_1

L_2
L_1

Ionization

K

K

Auger Electron

Vacuum

emission

L_2
L_1

Fig 5b

decay

K
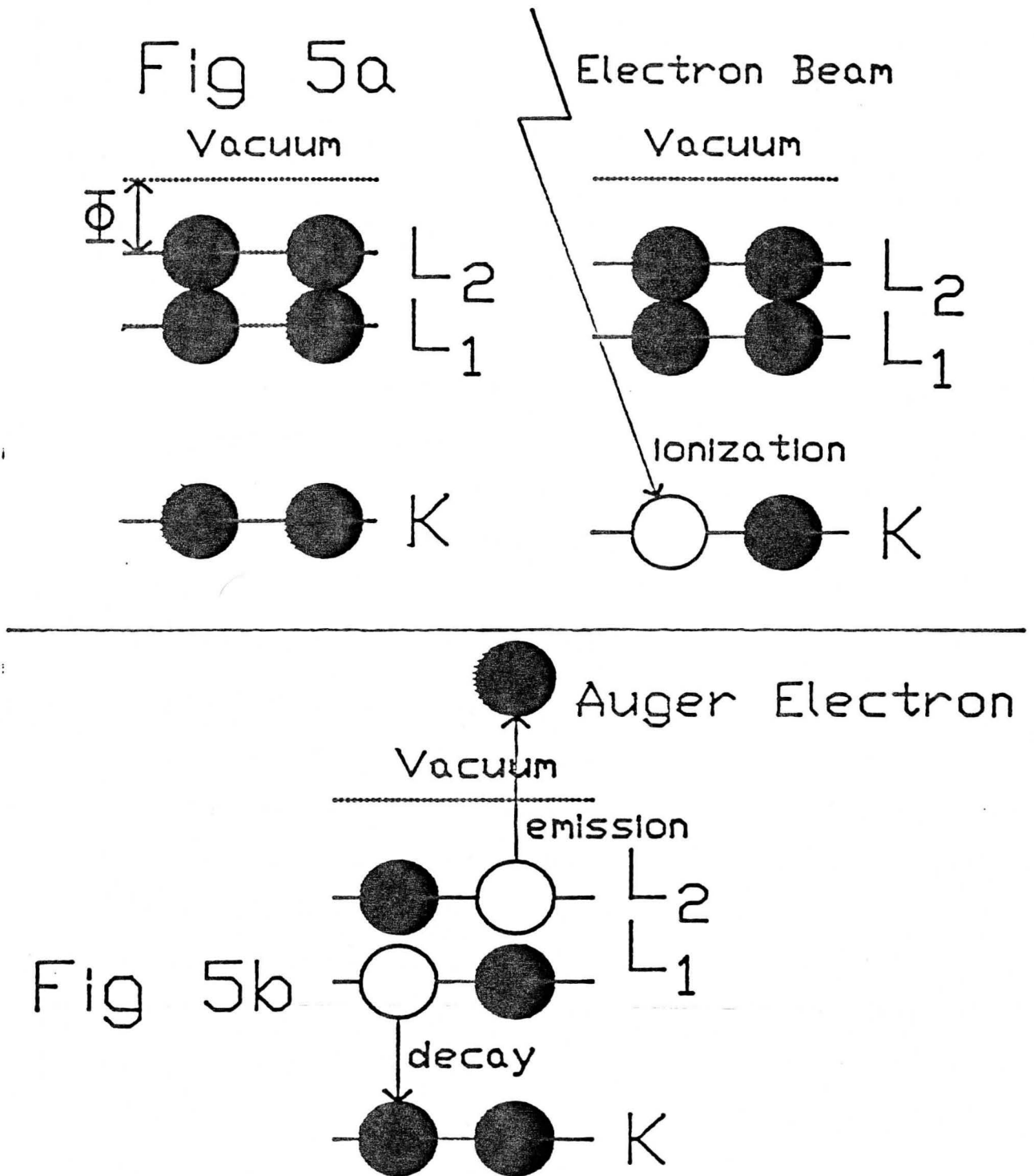
Schematic representation of the Auger process.
a) The initial ionization event by an incoming high energy electron.
b) Internal decay to fill core electron hole followed by emission
   of an Auger electron to release energy from the decay.
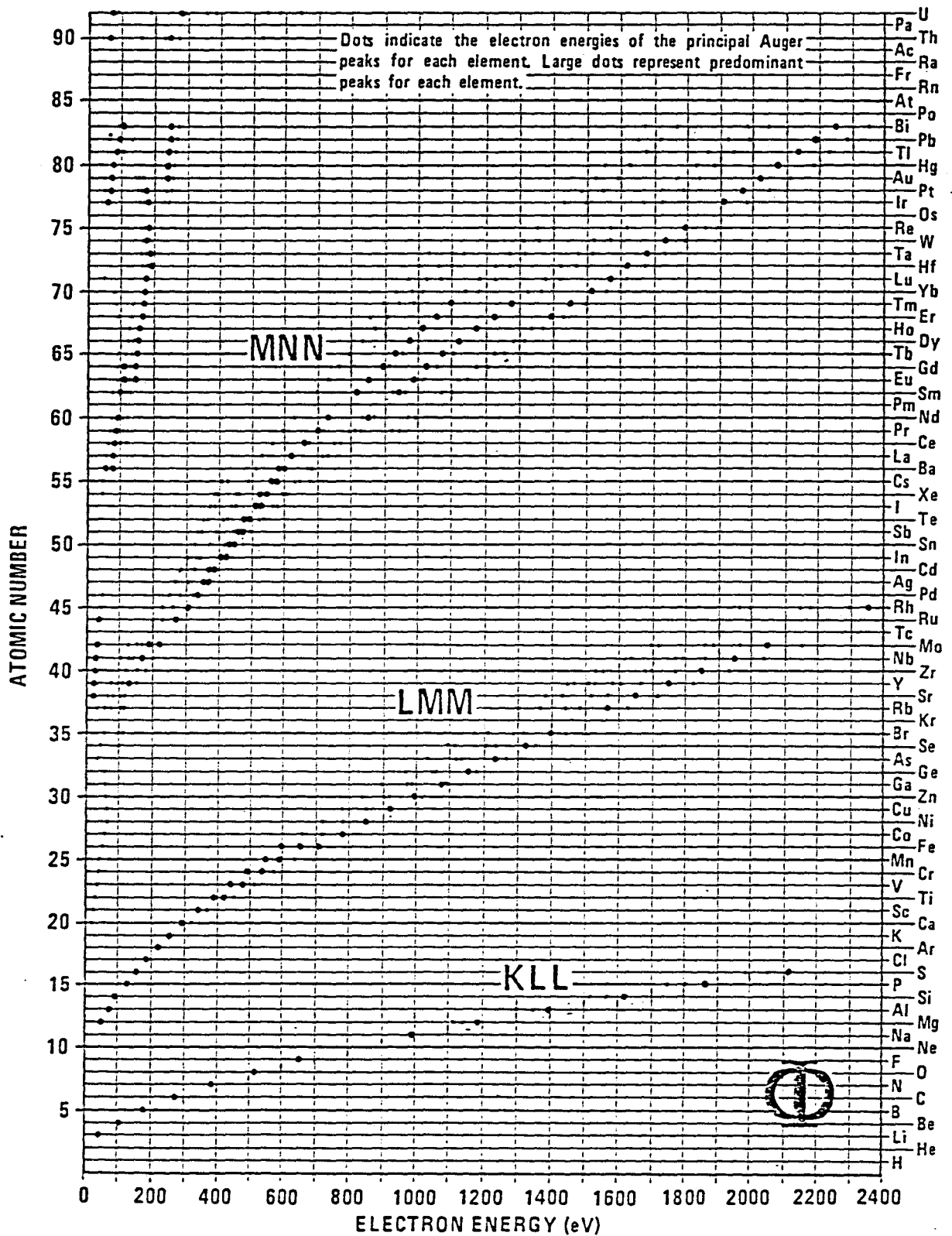
Figure 6
From the Perkin Elmer Handbook of Auger Transitions

This general transition is given the label KL_1L_2 and other transitions such as MNN and LMM are also possible. A graphic depicting the known Auger transitions for the elements is given in figure 6. Because the final state is essentially doubly ionized, there must be a mechanism to re-supply the sample with electrons, or a charge will build up on the surface. The re-supply of electrons is usually facilitated via a ground connection to the sample, this places the restriction of conductivity on samples to be analyzed. Another major restriction on AES is the fact that it is a three electron process and thus eliminates elements with less than three electrons i.e. Hydrogen and Helium.

The energy of the electron as it enters the vacuum is reduced by the work function (Φ_A) and a small relaxation term, thus the final energy is given by;

$$E_{Auger\ electron} = E_K - E_{L_1} - E_{L_2} - \Phi_A - E_{rel.} \qquad 5.1)$$

The energy of Auger electrons therefore provides the basis for unambiguous qualitative analysis. It is to be noted that the energy of the emitted electron is independent of the energy of the incident beam, as long as the primary beam has energy sufficient to cause the initial ionization event. It should also be noted however, that the yield of electrons for any transition is a function of the ionization energy required and the energy of the primary beam since the ionization cross-section varies with primary beam energy.

Spectra are recorded by sweeping an energy analyzer through an energy range of interest and are usually collected in one of two forms: $dN(E)/dE$ (differential mode) or $N(E)$ mode, where auger signal as counts

of electrons is differentiated or plotted directly vs the energy of the electrons respectively. Example spectra are given in figs. 7a (N(E)) and b (dN(E)/dE). Quantitation is usually done by relating signal intensity to concentration but more details are given in subsequent sections.

Figure 7a
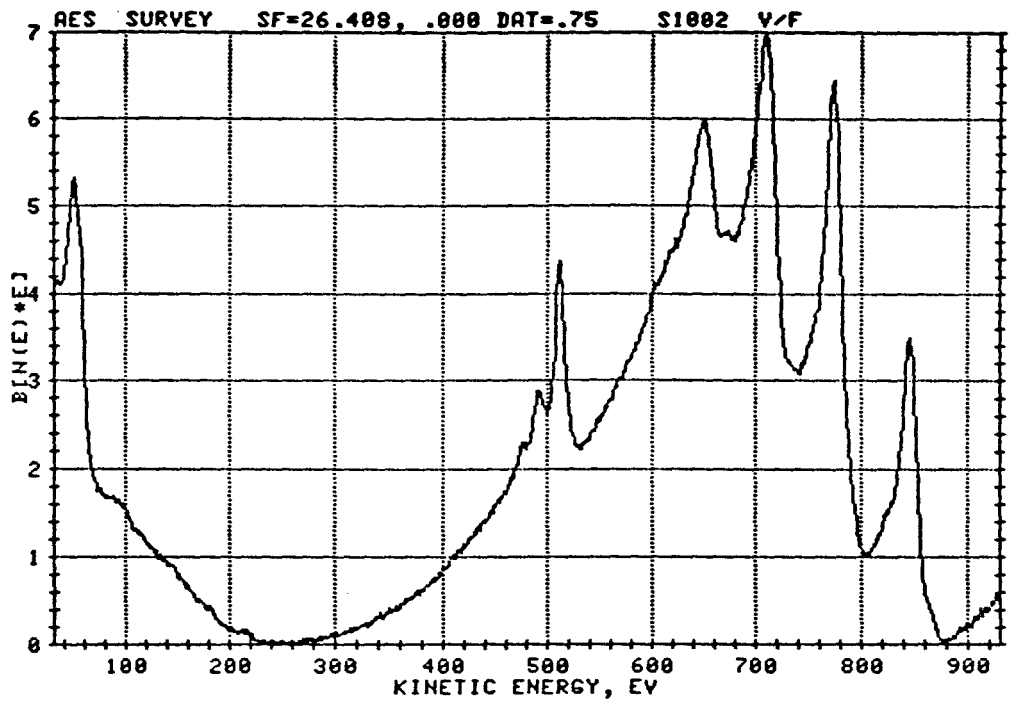
Typical N(E) Auger spectra of oxidized Ni-Co alloy.

Figure 7b
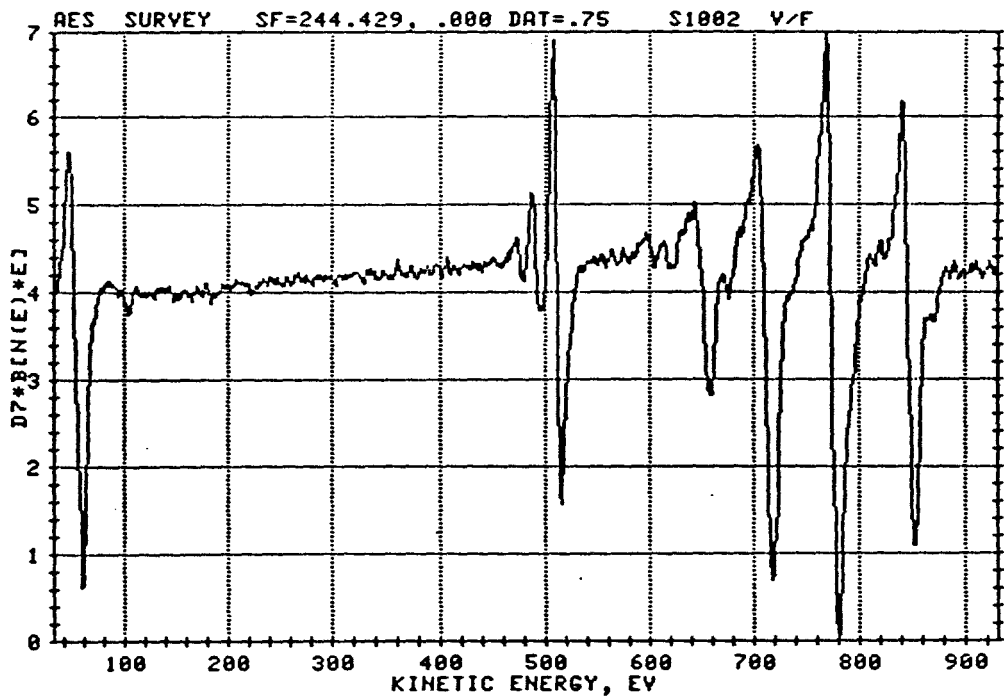
Same spectra as above except in dN(E)/dE mode.

s

5-II Considerations of Quantitative Auger Electron Spectroscopy

In order to obtain quantitative analyses via AES one must be able to relate the current of Auger electrons to the population density of the analyte in the surface region. A general expression for Auger current produced in an element A by the example transition WXY is given as;

$$I_A(WXY) = \int_\Omega \int_{E_W}^{E_p} \int_0^\infty I_P(E,Z)\sigma_A(E,E_W)N_A(Z)\gamma_A(WXY)\exp^{(-Z/\lambda)}d\Omega dZ dE \qquad 5.2)$$

where Ω represents all space, I_P is the excitation flux density, σ_A is the ionization cross-section of the core level W, $N_A(Z)$ is the atomic density of element A at a depth Z from the surface, $\exp^{(-Z/\lambda)}$ is the probability for escape and $\gamma_A(WXY)$ is the Auger transition probability factor. This equation assumes two dimensional homogeneity. A simplification of eqn. 5.2) can be made if three dimensional homogeneity is assumed. That is to say that the composition does not change over the depth of analysis. Furthermore the excitation flux density can be divided into two components. The first component is the Auger electron current due to the primary beam and the second is the contribution from the secondary electron cascade. The parameter T can also be introduced which represents the transmission factor for the analyzer being used. Thus the simplified expression for Auger current would be;

$$I_A(WXY) = I_P T N_A \gamma_A(WXY)\sigma_A(E_P,E_W)\lambda(1 + R_B)A_s \qquad 5.3)$$

where 1 + R_B now is defined as the backscattering factor, A_s is the sampling area and λ is the attenuation length for electrons from the WXY transition. Even with this simplification, quantitation from first principles would be very complex and, for practical purposes, impossible. It is to avoid the direct use of eqns. 5.2) and 5.3) that sensitivity factors and standards are used to obtain quantitative analyses via AES. However the factors for attenuation length, backscattering, as well as the so far unmentioned factors, of surface morphology and damage from sputtering, need to be dealt with as there may be differential effects for specific systems. A brief discussion of those factors is presented next, followed by details of the analysis procedures used in this work.

a) Attentuation Length

i) Inelastic Mean Free Path An electron travelling through a material will only be able to travel a distance determined by the energy of the electron. This distance is called the Inelastic Mean Free Path (IMFP) and in AES and XPS these distances are always longer than the thickness of one monolayer. The result of the IMFP being longer than one monolayer thickness is that any signal in an Auger spectrum will be composed of dwindling contributions from the first monolayer and deeper layers.   It is therefore essential that the inelastic mean free path be known before a composition of the first monolayer can be reported from Auger or X-ray Photoelecton Spectroscopies.

Predictions of IMFPs from first principles are based on highly complex mathematical models[53,54] that will not be dealt with in detail

here. The major detraction from such models is the fact that the predictions rely on a knowledge of the behaviour of the dielectric constant $\varepsilon(q,\omega)$ function that is not known. Penn[54] most recently used the observed optical dielectric constant in his equations to predict λ's and his predictions are quite close to experimentally determined values.

The experimentally determined λ's that Penn and most workers refer to, were compiled by Powell[55] and more recently and completely by Seah and Dench[56]. In the Seah and Dench article 215 experimental determinations of elemental IMFPs were found to obey a universal curve with some appreciable error. The fit of the experimental data to a universal curve was substantially improved by including a factor for atomic size which was not accounted for by the individuals who determined the IMFPs for specific elements i.e. lattice parameters and crystallographic orientation was not originally accounted for in most of the determinations. The size corrected curve showed a minimum at approx 40 eV and experimental scatter was greatest in this energy range. For electrons above 150 eV the fit to the universal curve was substantially better than the 10-150 eV range as was the fit for electrons with < 10
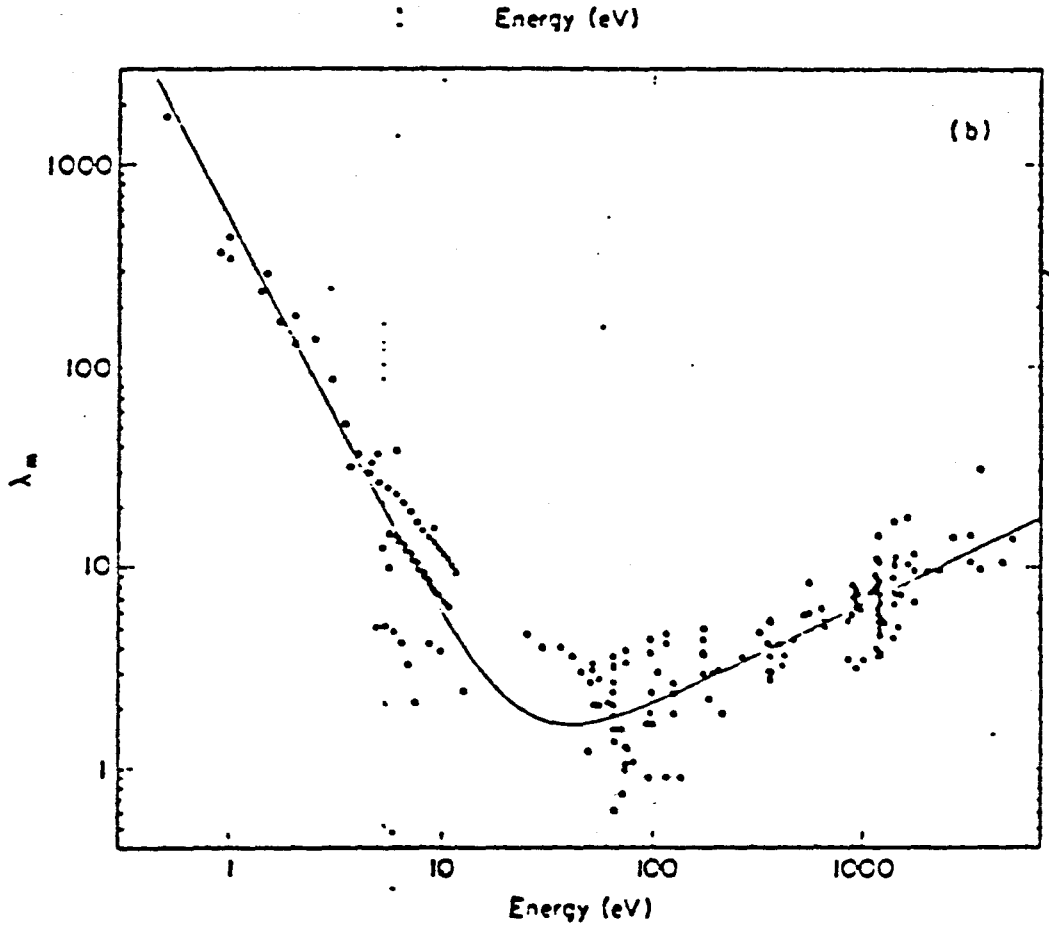
Energy (eV)

Figure 8 from Seah and Dench: IMFP vs. electron energy

ev. The universal curve above 150 eV and below 10 eV gives a strong indication that the scatter around the universal curve in the range 10 eV to 150 eV is due, as indicated by Powell[55], to the experimental difficulties in this range and not any inappropriateness of the universal curve (see fig 8 from ref. 56). The recent work of Penn[54] also supports this assertion as the values that author predicts for IMFP, fit experimental data from Ag,Al,Au and Cu and also matches the fitted curve of Seah and Dench very well in this energy range. The equation of best fit as determined by Seah and Dench is;

$$\lambda_m = \frac{538}{E^2} + 0.41(aE)^{0.5} \text{ monolayers} \qquad 5.4)$$

for electrons with energies from 1 eV to 10,000 eV in elements. In equation 5.4) the variable E is the energy of the electron and a is the thickness of one monolayer. This dependency on the monolayer thickness allows for a variation of sampling depth with crystallographic orientation and is vital to this thesis. Using a monolayer thickness of 2.03 Å we may calculate the λ_m for the low energy (50-60 eV) peaks most often used in this thesis: λ_{Ni}= 1.587 monolayers (3.22 Å) and λ_{Co}= 1.536 monolayers (3.12 Å). From this calculation it is possible to see that the effective sampling depth for both elements will be the same in the 50-60 eV region.

ii) Corrections due to λ in the Retarding Field Analyzer The first analylses done for this thesis were performed in a static Auger Spectrometer equipped with a Retarding Field Analyser (RFA). The RFA conisted of four (4) concentric grids which could selectively allow electrons of specific energies to pass to an electron amplifier . The electron gun was coaxial with the grid system and as such, electrons were collected from 5° to 60° off of the sample surface normal. A computerized routine was developed in house by Dawson and Burke[57] that could, given the IMFP and the monolayer thickness, calculate the composition of the first monolayer by allowing contributions to the observed signal from an infinite depth (∞ = 40 monolayers for the calculation) into the bulk. The method can be summarized as follows:

The .total signal received by the analyzer is composed of two parts, the first monolayer contribution and contributions from all subsequent layers.

$$I_{Ni} = X^{s}_{Ni} \overset{\circ}{I}_{Ni} = X_1 I_1 + X_b \sum_{i=2}^{\infty} I_i \qquad 5.5)$$

Where I_{Ni} is the total Auger signal, X^{s}_{Ni} is the experimentally determined composition in the sampling region of the Auger electrons (how this number is arrived at, is discussed later), X_1 is the first monolayer composition, X_b is the bulk composition and I_i is the signal from the ith layer. If

$$\overset{\circ}{I}_{Ni} = \sum_{i=1}^{\infty} I_i \qquad 5.6)$$

then

$$X^{S}_{Ni} = (X_1 I_1 + X_b \sum_{i=2}^{\infty} I_i)/ \sum_{i=1}^{\infty} I_i \qquad 5.7)$$

and

$$X_1 = (X^{S}_{Ni} \sum_{i=1}^{\infty} I_i - X_b \sum_{i=2}^{\infty} I_i)/ I_1 \qquad 5.8)$$

The Auger current to the analyzer is given by;

$$I_i = \int_{\theta=5°}^{\theta=60°} C \sin\theta \cos\theta \exp^{(-i/n_\lambda \cos\theta)} d\theta \qquad 5.9)$$

where C is an experimental constant and n_λ is the IMFP in monolayers.

iii) Corrections due to λ for the Cylindrical Mirror Analyzer

The CMA collects electrons over a solid angle of $\theta = 42°$ by focusing electrons of specific energy onto an electron multiplier and usually has better energy resolution than an RFA. The correction procedure used for spectra collected by a CMA is somewhat simpler as the geometry is straightforward. If I_b is the Auger signal corresponding to the bulk then

$$I_b = AC(1 - \exp^{-n_\lambda/d\cos\theta})^{-1} \qquad 5.10)$$

where C is the composition and A is a constant related to the elemental sensitivity factor. n_λ is the attenuation length of electrons in nm, d is the monolayer thickness in nm. Then if ΔC is the change in the surface concentration

$$I_s = I_b + A\Delta C \qquad 5.11)$$

and

$$(I_s - I_b)/I_b = \Delta C/C(1 - \exp^{-n\lambda/d\cos\theta})^{+1} \qquad 5.12)$$

putting $(I_s - I_b)/I_b = R$ then

$$R(1 - \exp^{-n\lambda/d\cos\theta})^{-1}C = \Delta C \qquad 5.13.$$

The value of R then is obtained from the experiment and ΔC is calculated.

b) Preferential Backscattering

As mentioned previously the total Auger signal will have a com-
ponent arising from the electrons that are scattered (elastically or
inelastically) off of subsurface atoms with enough energy to carry out
the initial ionization event in the Auger process. The yield of
electrons from this process is a function of[58] atomic number (Z), angle
of incidence (Ψ) and the ratio of the incident electron energy to the
energy required to carry out the initial ionization event ($U = E_b/E_p$).
Ichimura et. al.[59-61] did a large number of Monte-Carlo type calculations
in an attempt to arrive at an easy to use relation for the backscatter
yield R_B. The resultant equation for normal incidence of the electron
beam (the arrangment in our spectrometers) is;

$$R_B = 1 + (4.35 - 3.93\ Z^{0.1})U^{-0.25} + (4.85\ Z^{0.1} - 5.45) \qquad 5.14).$$

Recent experimental evidence[62] has indicated that relation 5.14) predicts
a backscatter factor, $(1 + R_B)$, in excellent agreement with determina-
tions using $E_P = 15$ keV, but overestimates the effect when the primary
beam energy is low. The experiments done in this thesis used primary
beam energies of 1 keV, 2 keV and 5 keV which would be considered low,
and as such, eqn. 5.14) would represent an upper bound to the effect of
backscattered electrons in this study. When estimates are calculated for
the elements of interest here under the worst of circumstances ($E_P = 1$
keV and $E_b = 60$ eV, where the overestimate of the effect is at a maximum)
the backscatter factors are;

$$(1 + R_B)_{Co} \ (\Psi = 0, \ E_P = 1 \ keV) = 1.742$$

$$(1 + R_B)_{Ni} \ (\Psi = 0, \ E_P = 1 \ keV) = 1.737 \quad .$$

Since the effect of backscattering is only detrimental if the elements of interest have differing backscatter factors, it is very safe to assume that preferential backscattering is not significant for this alloy system.

c) Effects of Surface Morphology and Preferential Sputtering

No surface is actually smooth on an atomic scale unless some very special procedures are followed, and practical surface analysis usually accepts a certain degree of roughness. As mentioned in the previous chapters on sample preparation, all the samples studied here were prepared and polished to the same extent outside of vacuum and sputter cleaned under identical conditions in vacuum. It is a well accepted fact that the yield of Auger electrons from a sample is to some extent, dependant on the roughness of the surface. De Bernardez et.al.[63] have proposed a model of a surface roughened by ion sputtering that gives a triangular topography (a fairly common observation in practice). Those reseachers have concluded that increased surface roughness decreases Auger yield significantly when the dimensions of the roughness are small (on the same scale as that produced by sputtering). This effect could be significant to this study if standards used for analysis (see later discussion) have different morphologies on the scale of beam damage.

Another possible effect of beam damage is preferential sputtering. Simply put, preferential sputtering results from differences

in the rate of removal of atoms from a surface during cleaning by an ion beam. If the energy of an ion beam is held constant, then the variables that control the rate of removal of atoms must be, the nature of the substrate (Z, bond energy) and the temperature. Empirical determinations[64] of pure element sputter rates have been tabulated and can be used in estimating the relative rates of atom removal in alloys. A common model used[65-67] can be described by the following for this system;

$$Ni(s) \xrightarrow{k_{Ni}} Ni(g) \quad \text{and} \quad Co(s) \xrightarrow{k_{Co}} Co(g)$$
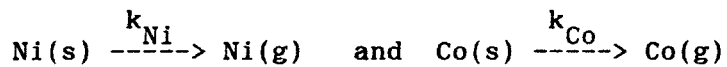
where k's are sputter rate constants. If we define the ion current as I^+ and the concentrations of Ni and Co are X_{Ni}^b and $(1 - X_{Ni}^b)$ respectively, such that the probability of a Ni atom being exposed at the surface is $X_{Ni}^s(1 - X_{Ni}^b)$, we can predict the rate of removal of Ni and Co atoms by;

$$dX_{Ni}^s/dt = k_{Ni}I^+X_{Ni}^s(1 - X_{Ni}^b) \quad \text{and} \quad dX_{Co}^s/dt = k_{Co}I^+X_{Co}^s(1 - X_{Co}^b)$$

respectively. After some time a steady state will be established such that $dX_{Ni}^s/dt = dX_{Co}^s/dt$ and we arrive at the relation;

$$\frac{X_{Ni}^s}{X_{Co}^s} = \frac{k_{Co}(1 - X_{Co}^b)}{k_{Ni}(1 - X_{Ni}^b)} = \frac{k_{Co}X_{Ni}^b}{k_{Ni}X_{Co}^b} \qquad 5.15)$$

which can be simplified to;

$$X_{Ni}^s = \{1 + \frac{k_{Ni}X_{Co}^b}{k_{Co}X_{Ni}^b}\}^{-1} \qquad 5.16)$$

The relation 5.16) relies on the assumptions that the pure metal sputter yields are indicative of sputter rates of individual atom species in alloys, that relative rates will remain the same for different energy ions and the effect of substrate temperature will be equal for both elements. The first assumption is most likely valid in this case since Co and Ni form a continuous series of solid solutions with no specially stable compounds, but in general this assumption may not be entirely valid[67]. The second assumption is likely also valid as a study of the effects of ion energy on sputter rates[68] has shown no relative change in preferential sputtering, although ion yield increases with increasing primary energy. Temperature does have an effect on the observed composition[69,70] but the effect is secondary because the ion damage creates enhanced diffusion pathways which allow segregation at very low temperatures. The effect is difficult to quantify however since higher temperatures may also initiate the removal of defects created by the ion beam.

Since this study was primarily intended to focus on segregation, the only comparative study done here was at room temperature for all compositions studied and the results of that work are reported later. Higher temperature preferential sputtering was not considered to be very significant since segregation alters the surface composition depending on the driving force for segregation. Any investigation into the effect of

sputtering at elevated temperatures, in this system, would therefore be too complex and uncontrolled for a useful scientific study.

5-III Analysis Method

a) Sputtered Pure Element Standards

The considerations covered in the preceeding sections have all emphasized the need to make corrections to observed compositions, but not covered so far is the method by which compositions were arrived at. There are, in reality, two methods commonly used to determine compositions from Auger spectra. The first method relies on tabulations of relative Auger yields (sensitivity factors) which may be applied to either differential or N(E) spectra. The problem with this method is the variation of sensitivity factors with the conditions of analysis and the best expected accuracy would be ± 10%. More usually pure element standards are used along with the expression of Hall and Morabito[71].

If we define the relative peak intensity I'_{rel} as the ratio of one peak (z) due to an element A of concentration X_A, to another peak (y) due to an element B of concentration X_B

$$I'_{rel}(z,y) = (I'_z/X_A)/(I'_y/X_B) \qquad 5.17)$$

and

$$I'_z = X_A N'(1 + R_z)\lambda_z k_z SR \qquad 5.18)$$

where $(1 + R_z)$ is the backscatter factor as previously described, k_z is an instrumental parameter and λ_z is the effective escape depth. We may determine the concentration of element B by;
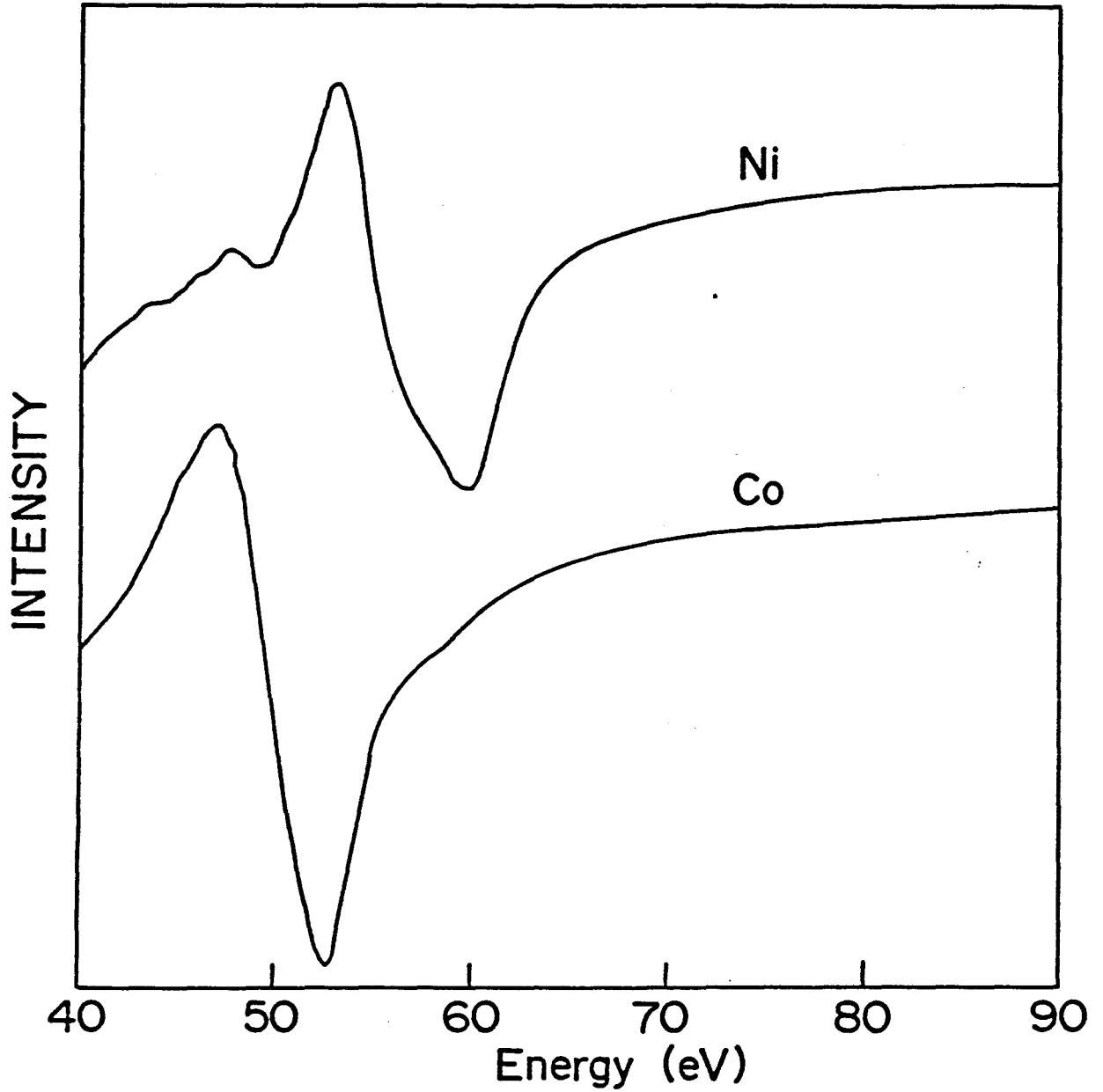
Figure 11
Low energy pure element Auger spectra for Ni and Co
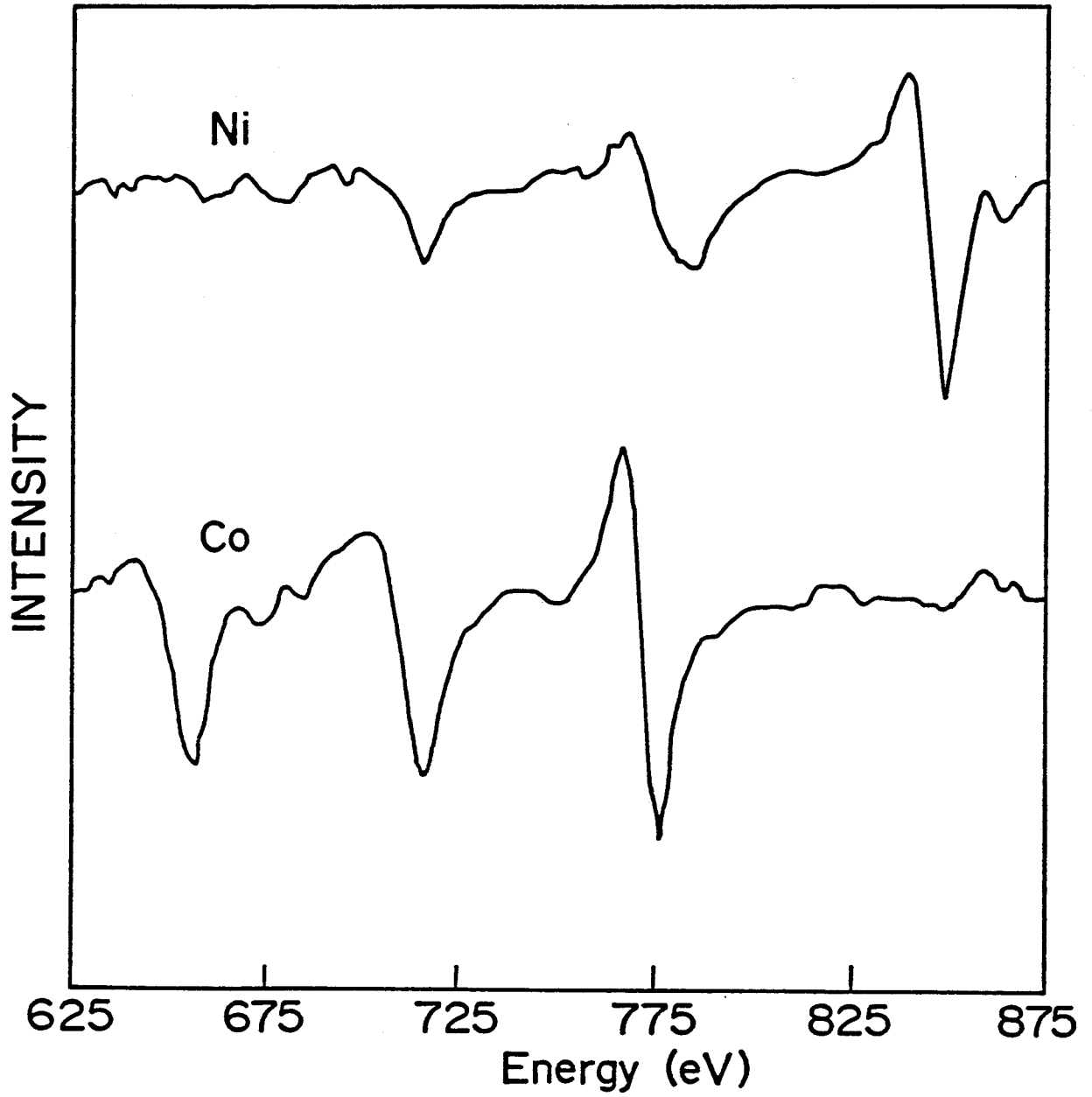
Figure 12
High energy range Auger spectra of pure Ni and Co

$$X_B = I_y' / \sum_z [I_z'/I_{rel}'(z,y)] \qquad 5.19)$$

This assumes that; $\Sigma X = 1.0$, the secondary electron distribution is additive and there is no change in elemental peak shape upon alloying. In eqn. 5.19) and it's component eqns. 5.17) and 5.18), the factors $(1 + R_z)$ λ_z and k_z must be considered. The relative backscatter factor $(1 + R_z)$ has already been dealt with and it is now known that for the Auger peaks in the range 50-60 eV the backscatter factors are virtually the same and hence will cancel in eqn. 5.19) and no longer need to be considered if this procedure is followed. The sampling depths for these peaks have been shown to be effectively the same and hence they also cancel in eqn. 5.19). k_z may be the same for both elements if all instrumental conditions are kept constant while standards are collected. The factor SR in eqn. 5.18) does not appear in the original Hall and Morabito[71] but is included here since, as has already been discussed, surface roughness (SR) will affect the yield of Auger electrons from a surface.

Given eqn. 5.19), all that is necessary for quantitative Auger of Co-Ni spectra is the measurement of peak heights in standard and alloy spectra. The difficulty encountered is that for this system the characteristic Auger spectra for Co and Ni overlap so much that easy peak height determination is impossible (see figs. 11 and 12). In fig. 11 it is clear that no distinct peak for either element will emerge as being useful in alloy spectra. In fig. 12 the highest energy (848 eV) Ni peak will be clear of peak overlap and appears to be a useful peak while the

lowest energy Co peak (654 eV) will also be unmixed. There are two reasons why this still poses a problem. The first is that the 654 eV Co peak is small, even in the elemental standard, and does not have a well defined peak shape for the determination of a peak height. The second reason is that the sampling depths for the two peaks will be quite different. If we again assume a monolayer thickness of 2.03 Å the 848 eV Ni peak will have λ_{Ni} = 5.38 monolayers (10.9 Å) while the 654 eV Co peak will have λ_{Co} = 4.73 monolayers (9.6 Å). This means that analyses based on these two peaks will have to be corrected for differing sampling depth if the composition in the analysis range is inhomogeneous, which is complicated by the fact that measuring the Co peak is extremely difficult for compositions less than 50 a/o Co. These difficulties in analysis have almost certainly been a deterrent to more investigation into this system and the work of this thesis has sought to circumvent the difficulty.

The solution to the difficulties in analyzing these spectra has been the introduction of computer simulation. Fractions of pure element spectra are mixed together to generate a "simulated" spectrum that is then compared point by point to an observed spectrum and optimal fitting fractions without a shift in the energy scale are reported. The "best-fit" fractions of the standard spectra are then used to determine the observed composition. The assumptions involved in this type of analysis are exactly the same as those for peak height determination since what
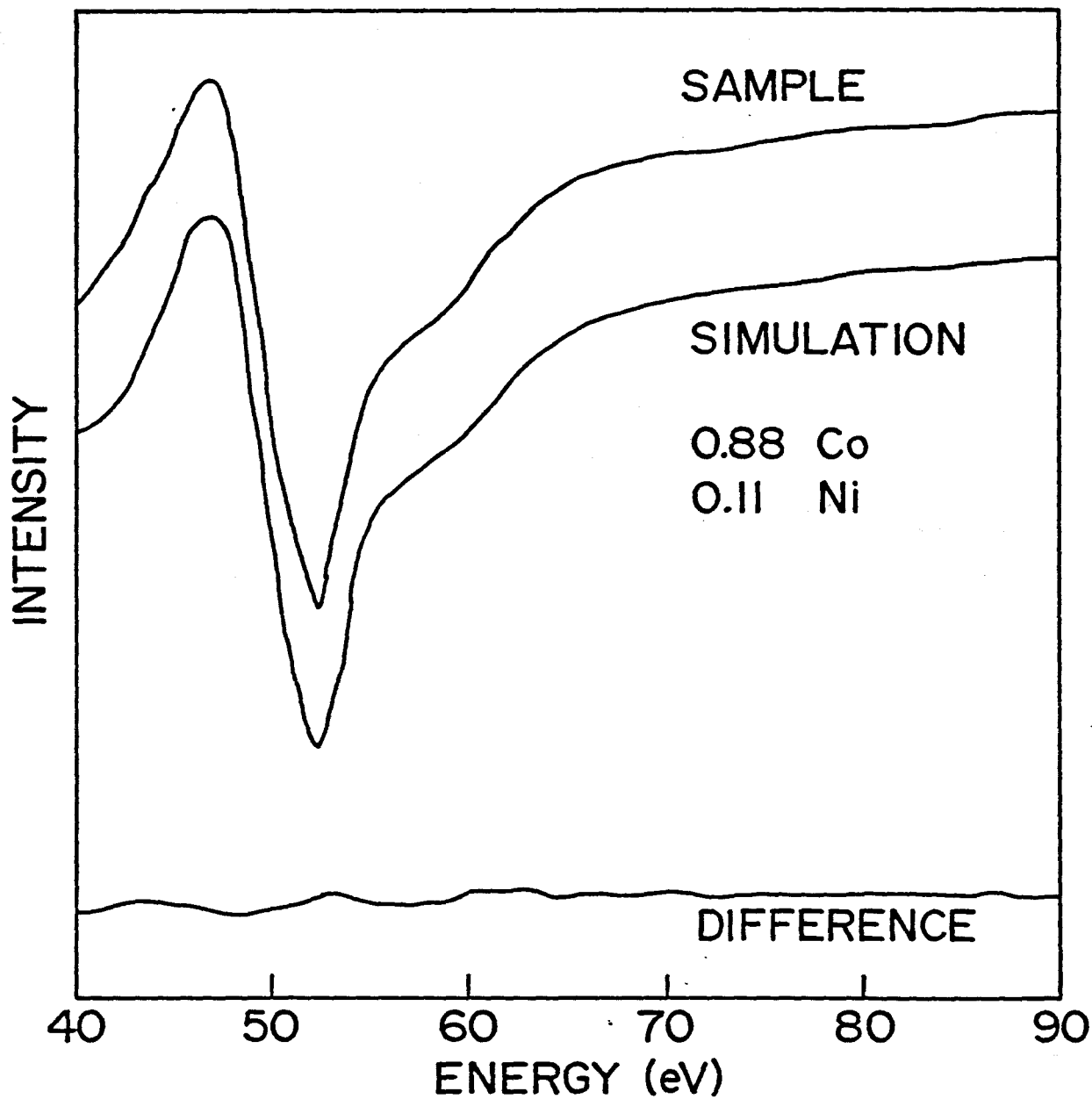
Figure 13
Sample spectra with simulation and the difference spectra.

the computer simulation does, is compare peak heights at every point in the spectrum. The assumptions that the secondary background is additive and that there is no peak shape change on alloying are justified by the fact that near perfect simulations are possible over the peaks and background simultaneously in the low energy range (see fig. 13 where a sample spectrum is presented along with the computer simulation and a difference spectrum i.e. the difference between sample and simulation at every point).

Simulations in the high energy range are equally good for sputtered spectra but simultaneous matching in annealed spectra for the 848 eV and 654 eV peaks has been poor. This poor matching of high energy spectra in annealed samples is discussed later.

The assumption that $\Sigma X_i = 1$ must now be addressed. In fig. 13 the fractions of sputtered standards used to generate the simulation were 0.88 Co and 0.11 Ni which add to 0.99 and is therefore close enough to 1.0 to believe that the assumption is valid. This sort of result is repeated whenever sputtered standards are used to simulate sputtered alloy spectra, however spectral fraction totals rarely add to 1.0 when sputtered standards are used to simulate annealed alloy spectra. An hypothesis of this thesis was that when there are no detectable contaminants of any kind (the case for all spectra accepted for quantitative analysis here), the spectral fractions should be normalized to 1.0 after fitting, because the surface roughness of the annealed alloy was different from that of the sputtered standards. In order to test
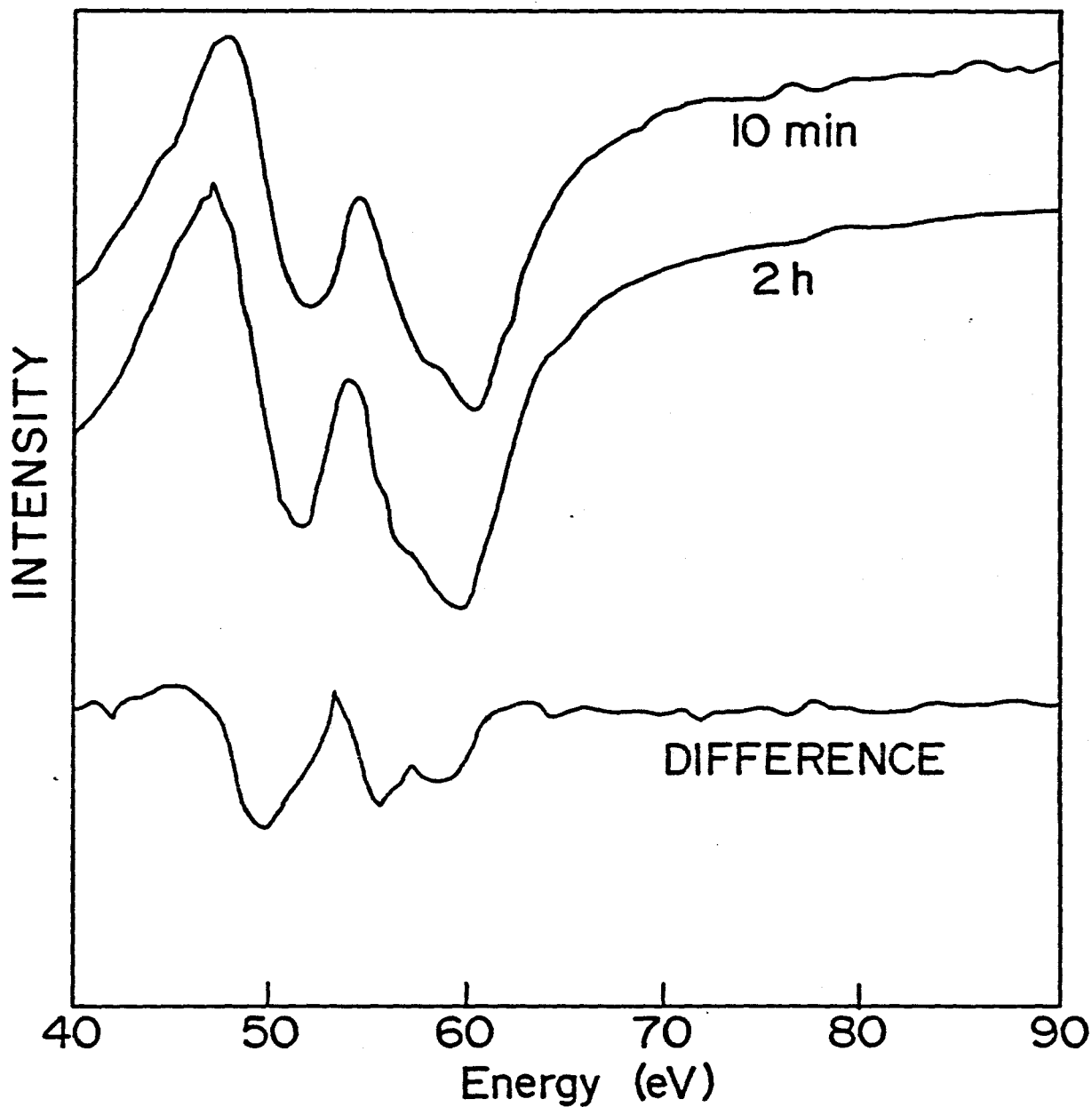
Figure 14
Annealed spectra taken after 10 mins. and 2 hours, showing the
difference in total Auger current. Same scale is preserved throughout.

this hypothesis, two experiments were performed. The first experiment involved annealing an alloy for 10 minutes (a time thought to be sufficient for the establishment of an equilibrium segregated surface) and two hours. The primary difference between these two samples was thought to be the surface roughness, since the two hour anneal would have allowed more time to change the morphology than a ten minute anneal. The result of this experiment is presented in fig. 14 where the multipliers were;0.53 Ni, 0.38 Co for the ten minute anneal and 0.64 Ni, 0.44 Co for the two hour anneal. The normalized compositions were thus 58% Ni,42% Co for ten minutes and 59% Ni,41% Co for two hours, virtually the same. This is consistent with a picture where some subsurface defects (due to ion beam damage) are removed after 10 mins. and more significant smoothing (as indicated by the increase in Auger signal, see section on morphology above) of the surface is achieved after two hours. If this interpretation was correct, then pure element sputtered spectra would have lower total signal than annealed pure element spectra and this was the second experiment. Pure standards were annealed for 30 min. after sputtering and total signal intensity compared. The result was that the annealed spectra showed approximately a 10 % increase in signal over the sputtered spectra for both Ni and Co, consistent with the hypothesis. These results then confirmed the standard practice of this thesis, of not requiring that the fractions add to 1.0 during fitting but normalizing the fractions to 1.0 after fitting.

The computer simulation and normalization procedure described above was developed using dN(E)/dE spectra but is also valid for N(E) spectra. Recently Underhill[72] used a one pass linear least squares

fitting routine to perform simulations on N(E) spectra and also found that excellent simulation matches were possible over both the analysis peaks and the background for determinations on samples at ambient temperatures. This procedure used the background above the peaks to normalize for different total currents from the standards and hence corrects for differences in surface morphology. All N(E) spectra used for quantitative analysis in this thesis were performed using that method since it represented a significant improvement in the time needed to complete an analysis. The only change made to that procedure in this work was the optimization of an energy shift applied to the standards which was routinely less than 1 eV. This energy shifting was necessitated by the fact that most of the N(E) spectra were collected at elevated temperatures where the sample mounted as described in chapter 4 could twist and change the distance from the sample to the analyzer. A small change in the distance from sample to analyzer is not important when an RFA is being used, but is critical when a CMA is used, because the distance from sample to analyzer affects the calibration of the energy scale directly. An example of an N(E) simulation along with the corresponding observed spectra is given in fig. 15. This procedure then allows the analysis not only of the higher energy (654eV-848eV) peaks but also the lower energy peaks which have not been accessible to this point.

One final point to mention is the fact that it was possible to obtain good simulation matches for high energy peaks when the sample was sputtered while good matches were not possible with annealed high energy spectra. The reason for this is the fact that the first monolayer is modified by segregation and the differing sampling depths of the 848 eV

and 654 eV peaks means that contributions from the first monolayer are different for those two peaks and hence the observed composition is different. It was this restriction along with the fact that the low energy peaks (which have the same sampling depth for both elements) are more surface sensitive that, led to the almost exclusive use of these low energy peaks for quantitative analysis.

Figure 15
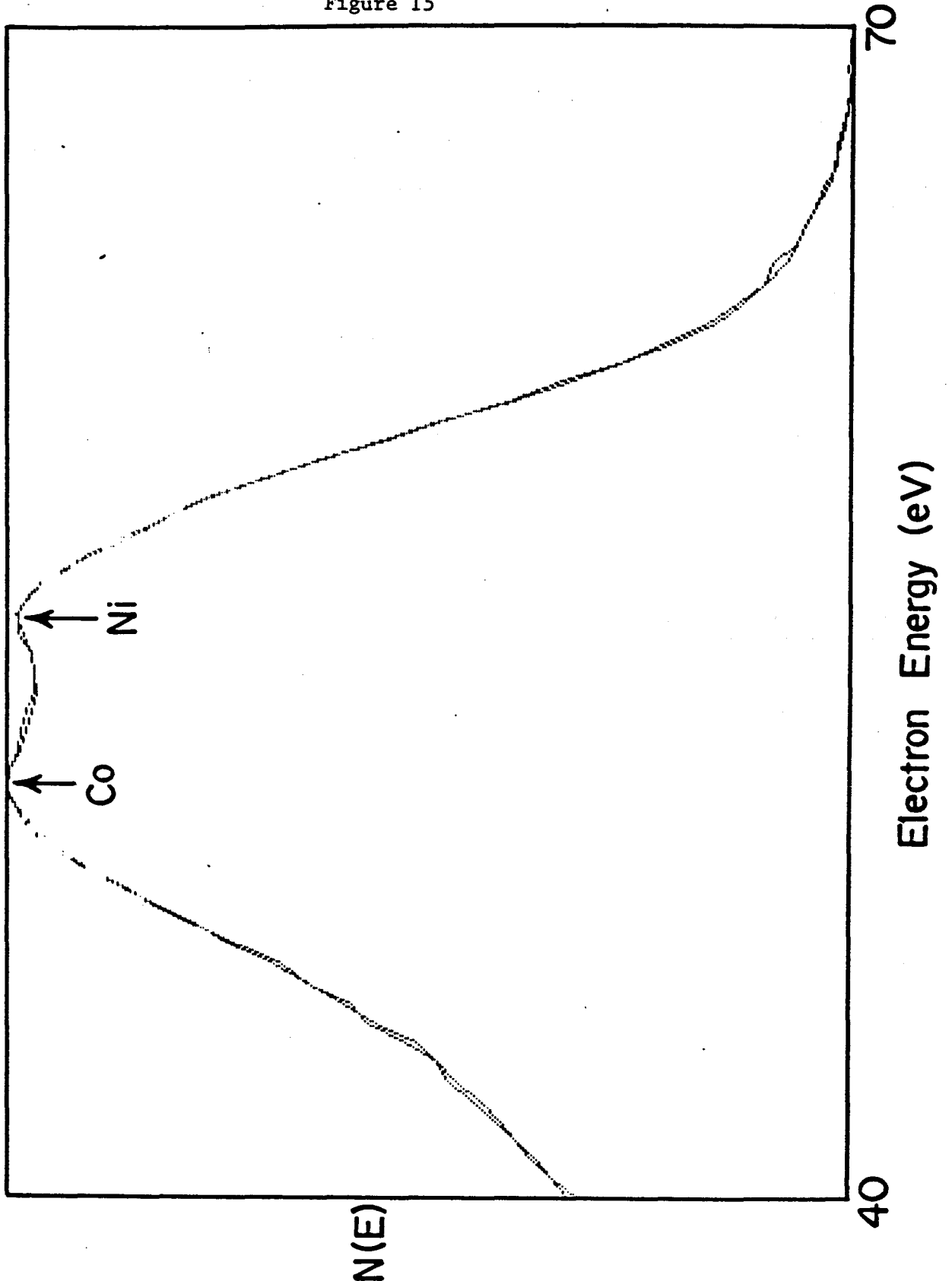
Sample spectra and simulation in the low energy range.

b) Scratched Alloy Standards

An alternative analysis procedure would be to use freshly made (in vacuum) scratches on an alloy at room temperature, where the bulk composition is known, as a standard in a computer simulation procedure. A series of experiments were performed where spectra were collected in fresh scratches made on alloys by a diamond scribe. The spectra collected in these scratches were then analyzed using sputtered pure element standards in the manner described above. The analyses of these scratched alloys should have shown a composition the same as the known composition of the bulk if the standard was appropriate. Unfortunately the resulting analyses consistently yielded compositions 2-3 % higher than the known bulk composition of Ni. As will be discussed in some detail later, Ni is the segregating component in this system. It is felt that since Ni is always enriched at the surface upon scratching, the physical work of creating the scratch either caused some local heating or sufficient damage to allow segregation to proceed to a limited extent even at room temperature and as such, scratched alloy standards were judged to be inappropriate for quantitative Auger analysis.

Chapter 6

A Study of Preferential Sputtering

The nature of preferential sputtering and the method used to determine compositions was dealt with in chapter 5 and will not be repeated here. The only modification to the procedure for quantitative analysis of sputtered alloy surfaces was the omission of the correction for the IMFP (λ) because it is assumed that the sputtered sample will have a homogeneous composition over the sampling depth of both the low and the high energy Auger electron ranges. This is a reasonable assumption since 3 keV Ar^+ ions were used to sputter-clean these surfaces and the mean depth of modification is thought to be deeper into the sample than escaping Auger electrons of even 848 eV.

The polycrystalline samples in this study were analyzed in an AES spectrometer with an RFA and sputtered at ambient temperatures with 3 keV Ar^+ ions directed at an angle of 71° from sample surface normal, with a raster size sufficient to cover the entire sample, for at least 10 mins. Data collection was performed with the ion beam off and a sample spectrum was generated using signal averaging of 10 sweep repetitions with 20 samplings per point. Sample spectrum simulations were indistinguishable by eye for both the high and low energy windows of interest from the observed spectra. The sputtered compositions for these polycrystalline alloy surfaces are reported in table 6-1 and graphically represented in fig 16.

Table 6-1: Observed and Predicted Sputter Compositions

Bulk Composition a/o Ni	Composition Observed: Average of low and high ranges	Predicted Comp. From Eqn. 5.16
14.1 ± .04	10.7	12.1
22.6 ± .01	18.5	19.7
43.1 ± .10	37.8	38.7
56.0 ± .06	53.0	51.7
78.7 ± .01	77.0	75.7
89.6 ± .01	86.7	87.9

Figure 16: Surface Excess (Depletion) vs. Bulk Composition

3 KeV Ar sputtering

calculated curve eqn (5)
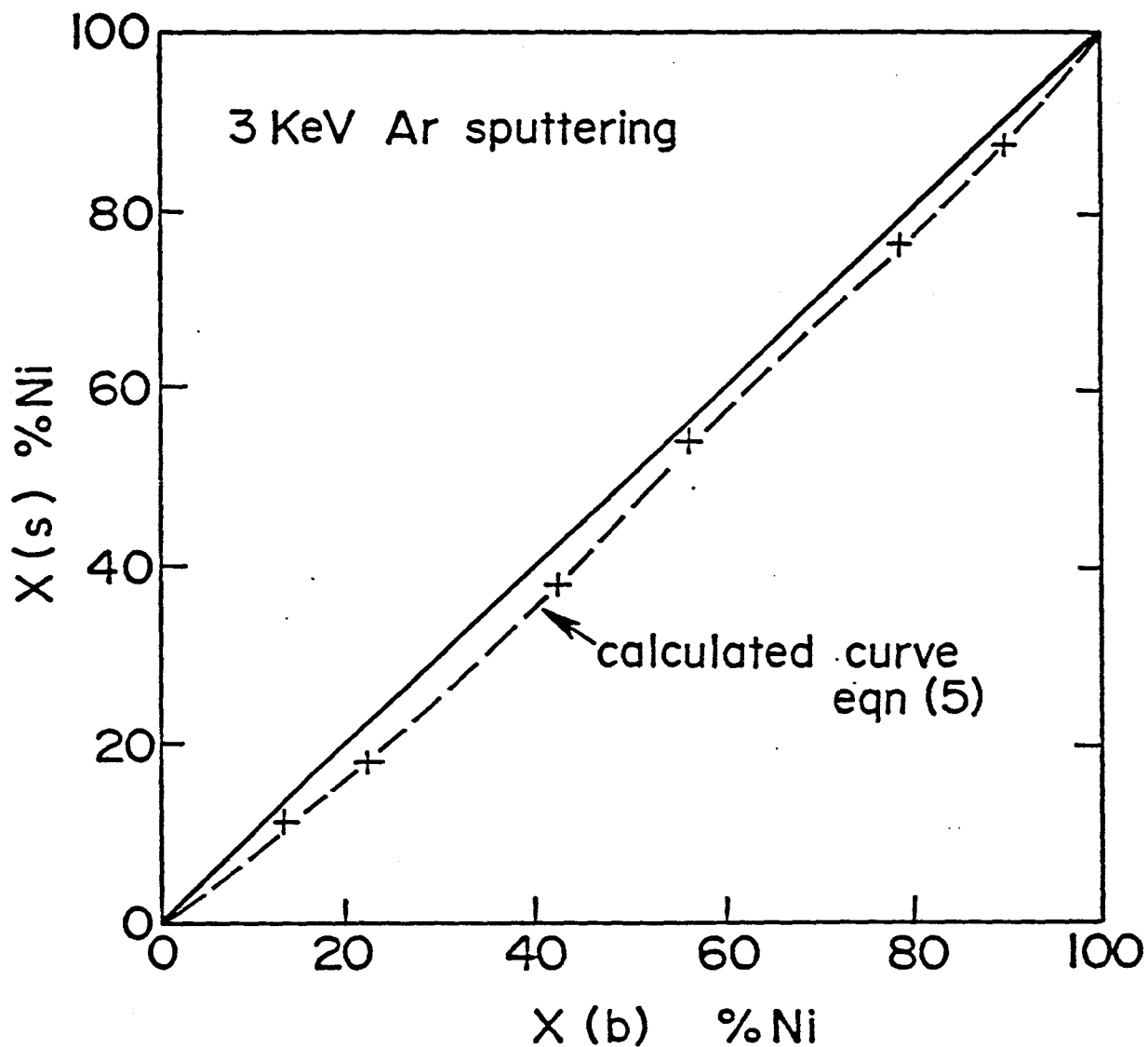
There was very good agreement between the two energy windows and the average of all determinations is presented in table 6-1. A detailed error breakdown is not presented, as precisions of repeat experiments were less than 1 %, which is less than the estimated accuracy of this equipment and this technique.

From table 6-1 and fig. 16 it is clear that Ni is preferentially sputtered over the entire composition range and this result is in agreement with the previous studies of this system refs. 45-48.. Pure element sputter yields[73] for 0.5 keV Ar$^+$ were used in the calculation of predictions listed in table 3 column 3 using eqn. 5.16) as there is no available data for 3 keV Ar$^+$ sputtering on Ni and Co. There is in general, very good agreement between the predicted compositions and the observed compositions and it is therefore concluded that preferential sputtering in these alloys can be adequately predicted on the basis of pure element sputter yields.

Chapter 7

Quenched Study of Segregation: Polycrystalline Samples

In this part of the study, six polycrystalline samples were mounted and heated in the static Auger spectrometer equipped with an RFA. The experimental arrangement in this instrument (see fig 3b chapter 4) was such that simultaneous heating and collection of spectra was not possible, and therefore all annealing experiments were quenchings from one temperature. The one temperature examined here was 580 $\pm$ 10 C° (853 K) as determined by a W/Re thermocouple welded directly to the sample (see chapter 4 for details). Samples were allowed to equilibrate at the desired temperature and 100 to 1000 eV surveys were taken with a 2 keV primary beam voltage and 25 mA filament current, to check for the typical contaminants; C, S, O, Cl and N.. Separate surveys were collected in the range from 30 eV to 100 eV with 1 keV primary beam voltage and 15 mA filament current to check for contaminants such as Si, Al and Mg. If any contaminants were detected, 3 keV Ar$^+$ sputtering was used until contaminants were removed. When the sample surface was judged to be clean, the ion gun was turned off and the sample was annealed for 10 minutes, at which time the heating gun was abruptly turned off and the sample rotated away to facilitate the maximum cooling rate possible and hence quench the surface at the equilibrium segregated composition for 580 C°. The sample was then re-positioned and contaminant checking

sweeps were then conducted. If the sample was still clean, spectra were collected from the two energy windows. If after the sample spectra were collected, the sample surface was still contaminant free, the sample spectra were accepted for analysis.

The time allowed to reach equilibrium was thought to be adequate since the work of Goretzki et. al.[45] concluded that there was no visible change in composition after 8 minutes. Furthermore, the study conducted and reported in the previous section on surface morphology concluded that there was no appreciable difference in composition between a sample annealed for 10 mins. and one annealed for 2 hrs. at the same temperature, reinforcing the belief that 10 mins. was an adequate amount of time to achieve equilibrium.

A pair of typical low energy spectra are shown in fig. 17 where the top curve is a room temperature sputtered surface and the bottom curve is the same sample after having been annealed and quenched from 580 C° . The bulk composition of the sample was 56.0 ± 0.06 a/o and the surface compositions as determined by the computer simulations were 53 a/o for the sputtered surface (a slight preferential sputtering of Ni as has already been discussed) and 65 a/o for the segregated surface (these compositions are "as observed" and have not been corrected to reflect the composition of the first monolayer only). It is clear in this representation that Ni is segregated upon annealing. The simultaneously collected high energy spectra showed approx. a 3-4 % enrichment of Ni and are not shown here since this difference is very difficult to see.

Figure 17
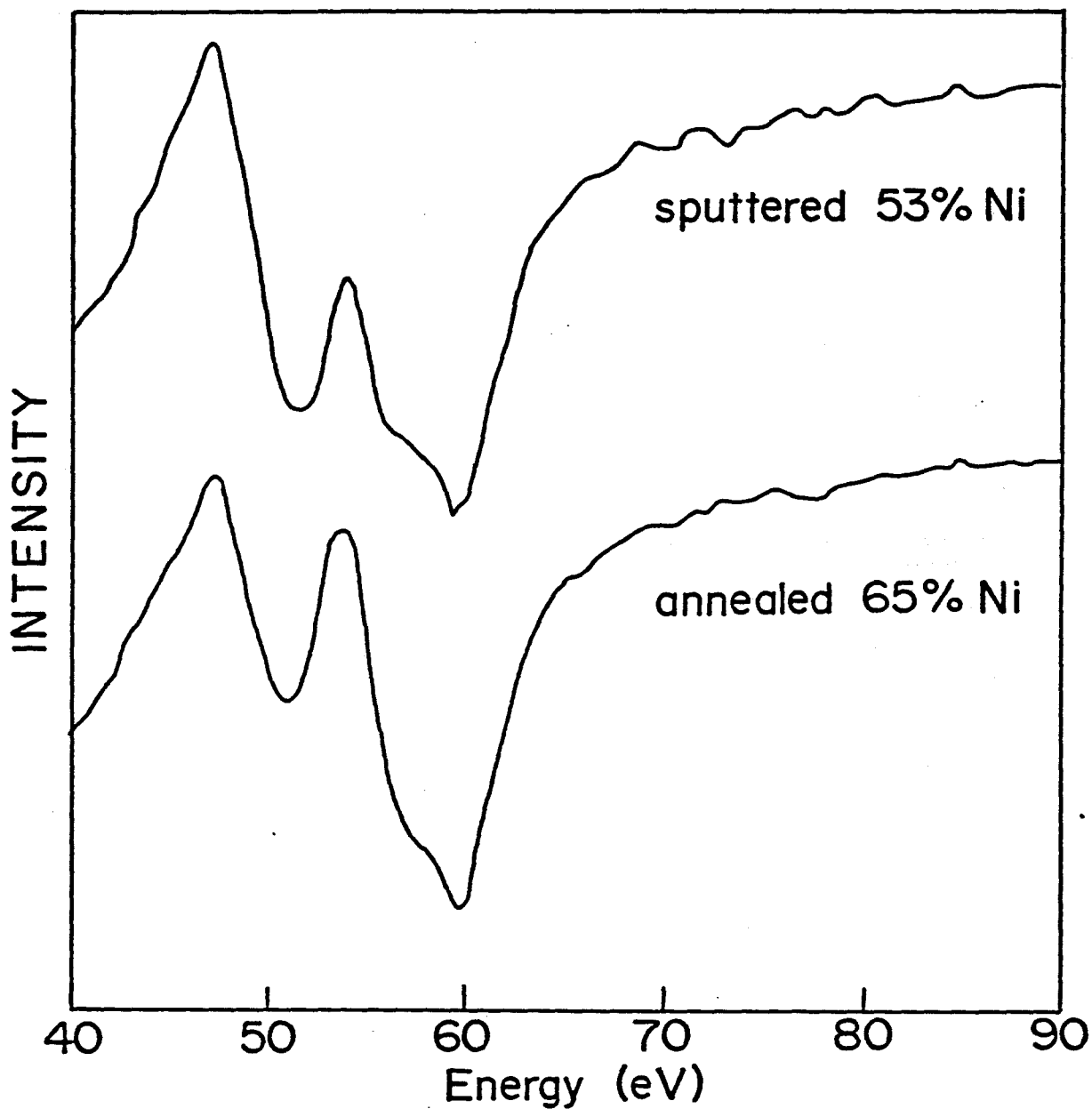
Sputtered and annealed spectra showing that Ni is noticeably enhanced upon heating. Ni segregation.

Furthermore it was impossible to achieve perfect simulation matches over the entire high energy window. Compositions determined from this region were necessarily determined from only the 654 and 704 eV peaks since these two peaks could be simultaneously matched.

The reason that it was not possible to simultaneously match the two extremes of the high energy window is quite simple. If the segregation of Ni is confined to the first monolayer, or even if there is some effect on the second monolayer, the signal from both the 654 eV and the 848 eV peaks will be largely made up of signal from unsegregated sub-surface layers. The difference between the two peaks is the relative proportion of surface layer to sub-surface layer. The 848 eV peak therefore contains more signal from bulk (i.e. unsegregated) layers, than the 654 eV peak and hence will have lower apparent composition w.r.t. Ni. Reasoning along these same lines, it is obvious (given the smaller sampling depth) that the low energy window will have a much higher proportion of signal arising from the first monolayer and hence the segregation phenomenon is much more noticeable. In a previous attempt at determining the segregation behaviour of this system by Tanaka et.al[48], computer simulations of only the high energy range peaks were used to determine compositions. The conclusion of that study was that "the segregation trend is not sufficiently large for detection of any change between the surface and bulk compositions.". That study however did not attempt to compensate for sampling depth and the spectra shown did not include the 848 eV peak in any simulation. It is therefore clear that that study did not observe segregation because the peaks used for

analysis were not sufficiently surface sensitive. The reported composi-tions in this study shall therefore hereafter be based on the low energy window exclusively, in order to have the best surface sensitivity and equal sampling depths for both components.

The observed X_{Ni}^{s} and X_{Ni}^{1} values in fig. 18 and table 7-1 are the result of 7 repetitions each, with the X_{b} = 89.6 a/o Ni sample being the exception having only three repetitions completed. Reported errors are based on standard deviation precisions of these experiments where each individual composition was determined to ± 1 %.

The results of this study are graphically depicted in figure 18 where the "as observed" compositions are presented along with the first monolayer compositions calculated from the observed values using eqn. 5.9). The monolayer thickness used to calculate n_{λ} via eqn. 5.4), was based on an average of monolayer thicknesses from the three low index orientations ((111), (110), (100)) which were in turn defined as being the distance from the topmost atom to the deepest atom with coordination less than that of the bulk. The resulting monolayer thickness was 1.83 Å and hence the n_{λ} = 1.44 monolayers. As was expected, the calculation of the first monolayer composition enhanced the observed segregation of Ni to the point where at 50 a/o the enrichment is approx. 19 %.

Figure 18
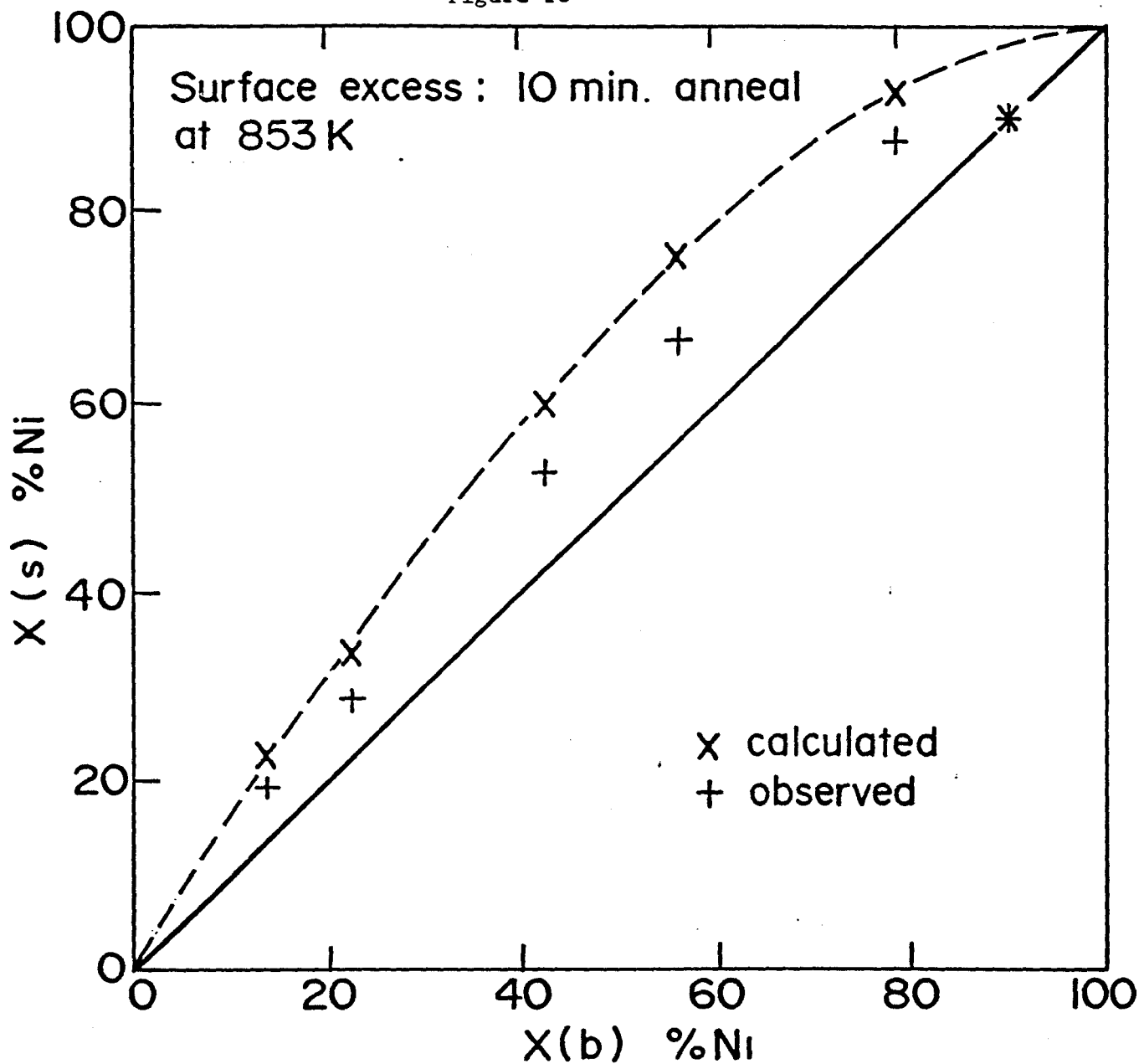
Surface excess diagram Ni-Co system determined after a 10 min. anneal at 853 K. Symbols do not imply error bars from precision because the precision error is smaller than the symbols used here to represent the data points. * is a superposition of two symbols.

It is now possible to compare this result to the results reported for this system by other workers. As has already been mentioned, Tanaka et.al.[48] reported essentially no segregation and the point has already been made that the peaks used for analysis there, were not sufficiently surface sensitive to detect segregation. This explanation would also tend to explain the result of Cherepin et.al[46] who reported very slight segregation of Ni but offered no quantitative assessment and also used the high energy peaks. The result of Shpiro et.al[47] is directly contradicted here as those researchers reported Co segregation. There is however a simple explanation for that result also. The main thrust of that work was to investigate how the Ni-Co system reacted with various gases, oxygen included. The background pressure reported for that work was 10^{-7} torr, which is not a very good vacuum for these studies. As part of this thesis Ni-Co alloys have been exposed to oxygen at 10^{-8} torr and it was found that Co is preferentially oxidized at room temp. even at these low pressures. It is therefore logical to assume that in a system where oxygen was being reacted with the substrate alloy routinely, the surfaces of those alloys could be slightly oxidized by residual oxygen either from the background gas or segregated from the bulk, and hence present a slightly higher ratio of Co to Ni. This observation of Co segregation was therefore probably due to preferential oxidation of Co on these alloy samples. Finally the earliest result of Goretzki et.al.[45] found that there was approximately 10 % enrichment of Ni in an alloy that was 30 a/o Ni after an eight minute anneal at 350 C°. Comparison of this result to fig. 18 tends to point to general agreement, but the Goretzki annealing was done at a lower temperature and there are few experimental

details given regarding which peaks were used and how the quantitative estimate was arrived at.

In the chapter dealing with the theories proposed to predict the segregating component and quantify the extent of segregation, it was pointed out that the two main types of models yielded opposite predictions for this system. The results of this chapter may now be used to compare those models. Firstly, the observation must be made that the theories which use $\Delta H_{vap.}$ to predict segregation, the bond-breaking models (see table 3-1) indicate that there is negligible segregation of Co with the extent varying slightly, depending on the complexity of the relation. Since, from this work, it is clear that Ni segregates, these bond-breaking models are not appropriate for predicting segregation in this system. In table 7-1 below, only one prediction based on $\Delta H_{vap.}$ is listed since modifications to bond-breaking theory will similarly predict the incorrect segregating component. The energy term equation used for the prediction there is eqn. 2.38) since it is the simplest bond-breaking equation with easily available data. Not listed in table 7-1 are the predictions for segregation from bulk diffusion data (eqn. 2.59)), because although values of the diffusion coefficients and pre-exponential factors can be found which yield excellent agreement with experiment, the variation in tabulated values is so large that any result could be extrapolated depending on the experimental values chosen. The correlation to bulk diffusion is therefore interesting but not practically applicable with the experimental data available.

The other main type of model is the surface free energy model that relies on the difference in surface tensions of the pure solid

metals ($\Delta\gamma$) as the driving force for segregation. It is unfortunate however, that the surface tension of a pure solid metal is not an easily determinable quantity in practice. Instead of measurements, predictions based on more readily available physical properties are commonly used. One of the simplest methods for predicting the surface tension of a solid metal at a given temperature, is to extrapolate the surface tension of the liquid element back to the temperature of interest using the following equation;

$$\gamma = \gamma_o + (T - T_o)d\gamma/dT \qquad 7.1)$$

where γ_o is the surface tension at T_o and the temperature of interest is T. Using the values from ref. 74 in eqn. 7.1) the projected surface tensions are 2320 and 2110 mNm^{-1} at 853 K for Co and Ni respectively. The corresponding compositions for the alloys studied here are predicted using the relation of Miedema eqn. A.24) and listed in table 7-1. An alternate expression for surface tension is that of eqn.A.25) where the $\gamma^{s,o}$ is related to the electronegativity Φ^* and an electron density at the boundary of a Wigner-Seitz cell[8]. Predictions using values from eqn. A.25) in eqn. A.24) are also listed in table 7-1.

Table 7-1: Results and Predictions of Segregation Quenched from 580 C°

Bulk % Ni	Bond Breaking	$\Delta\gamma$ eqn. A.24) data from 7.1)	$\Delta\gamma$ eqn. A.24) data from A.25)	Observed X^1_{Ni} a/o Ni
14.1±0.04	13.6	20.2	29.8	22.5±0.7
22.6±0.01	22.1	31.1	43.0	33.2±0.6
43.1±0.10	42.4	53.9	66.2	60.0±4.0
56.0±0.06	55.3	66.3	76.7	74.7±1.7
78.7±0.01	78.2	85.1	90.5	92.6±0.1
89.6±0.01	89.3	93.0	95.7	90.0± *

* Only three repetitions completed, all with the same result to ± 1%

$$\gamma^{s,\circ} = n_{ws}^{5/3}(\Phi^* - 0.6)^2 \quad A.25)$$

From table 7-1 it is obvious that the bond-breaking theory does not predict even the correct component. The surface tension approach does predict the correct component but the extent of segregation seems to vary depending on the values assigned to the γ's. Assuming that the calculation of n_λ and the monolayer spacing are correct, the prediction of γ from the liquid metal values yields less segregation than what is observed. This points to the underlying assumption involved in using eqn. 7.1), which is that $d\gamma/dT$ is constant through the liquid/solid phase transformation, an assumption that is unlikely to be valid. The predictions of γ's from eqn. A.25) overestimate the extent of segregation and this is also not very surprising since the γ's are clearly estimates at 0 K and the difference between solid surface tensions may not be constant over the entire solid temperature range.

There is one other problem in using eqn. A.24) that must be addressed whether one uses γ's predicted from the liquid data (eqn 7.1)) or the Miedema prediction of eqn. A.25), That problem is the inclusion of the dependence of γ on crystallographic orientation. There is no easily

recognizable crystallographic dependence in eqn. 7.1) and it is known that surface tension does vary with crystal faces. In eqn. A.25) however, it is worthwhile to point out that the electron density at a Wigner-Seitz cell boundary $n_{ws}^{5/3}$, or in reciprocal space the first Brillouin zone, will most certainly vary with crystallographic orientation, but the listed values of $\gamma^{s,\circ}$ in ref. 31 have no explicit dependance on orientation. It would then seem to be a logical step to investigate the proposed crystallographic dependence of segregation. In order to do this it is necessary to determine the temperature dependence (ΔH_{seg}) of different crystal faces. The next chapter deals with the results of a study of the temperature dependence of segregation for different crystal faces.

Chapter 8

Temperature and Crystallographic Dependence of Segregation

8-I Large Grains in A Polycrystalline Sample: (111) and (210) Faces

In order to investigate the commonly held belief that there is a crystallographic dependence of segregation, a determination of the driving force over a temperature range for a several faces, is most desirable. In order to measure the driving force for segregation, it is possible to begin with the simplest equation relating the driving force for segregation to composition.

$$X_A^s/X_B^s = X_A^b/X_B^b \exp^{(-\Delta G^o_{seg.}/RT)} \quad c.f. \text{ eqn } 2.6)$$

where s and b refer to the surface and bulk as usual for atoms of type A and B. In order to use this equation, a definition of the surface region was necessary (see chapter 2) and in this system, the segregation was assumed to be confined to a monolayer. The monolayer assumption, while perhaps not generally applicable, is probably very good in this case since most models agree that ideal systems will have segregation confined to the first layer[1,9] and in Co-Ni alloys this is very close to being true. Also if there were some slight enrichment in the

second layer, the contribution of this change to the Auger signal would be very small relative to the first layer signal. Implicitly the above equation also lumps together all other components to the total driving force for segregation such as mixing enthalpies and differences in size. It has been determined and stated in chapters 2 and 3 that these other possible components of the total driving force are so small as to be considered absent in this case. If it is recognized that $\Delta G = \Delta H - T\Delta S$, we may re-write the simple expression above as;

$$X_A^s / X_B^s = X_A^b / X_B^b \exp(-\Delta H_{seg.}^o / RT + \Delta S_{seg.}^o / R) \qquad 8.1)$$

and if we define

$$C^* = X_A^s X_B^b / X_B^s X_A^b$$

a Van't Hoff type plot of $\ln C^*$ vs. $1/T$ will have slope = $-\Delta H_{seg.}/R$ and y-intercept = $+\Delta S_{seg.}/R$. Note here that most models assume that the remaining entropy component is very small and would pass through the origin in such a plot as described above. In eqn. 8.1) the assumption is made that there is no variation of $\Delta H_{seg.}^o$ or $\Delta S_{seg.}^o$ with temperature or composition. There may in fact be an additional temperature or compositional dependence but that would be indicated by curvature in the plots of $\ln C^*$ vs. $1/T$. In the system under study here, the component A is Nickel while component B is Cobalt.

As has already been mentioned, the 56.0 a/o Ni sample contained two very large grains which were determined to have (111) and (210)

surfaces. Measurements of relative Auger yields were taken at the temperatures of interest in the PHI 600 Scanning Auger Multiprobe (SAM), with the temperature determined via a Chromel-Alumel thermocouple welded directly to the sample. In this part of the study the maximum stable temperature achieved was 1036 K but this could not be maintained long (see chapter 4). Below 1000 K temperatures were stable enough to permit experiments up to 3 hrs. in length.

Experiments were conducted over several different days for each grain and care was taken to ensure that several different areas on each grain were sampled. It was found that as long as the same grain i.e. orientation, was being analyzed, the only variables associated with surface composition were contaminants, temperature and time.

As always, contaminants played a very large role in determining the exact experimental conditions used. At room temperature, the surface of the sample was usually found to contain some C, O and S which could be easily cleaned by Ar^+ sputtering and remained clean for up to 3 hrs.. When heated to approx. 813 K all C and O that was not cleaned away by sputtering, disappeared and the sample surface would be contaminant free for several hrs. until a S peak was just detectable. Reducing the sample temperature below 813 K allowed the eventual re-appearance of C and O, which presumably had dissolved into the bulk at higher temperatures and was now segregating back to the surface. This resulted in a practical limitation of the temperature dependence study to temps. higher than 813 K. At higher temps. S segregated more rapidly until at around 987 K it (S) segregated faster than the surface could achieve the equilibrium segregated composition. This condition defined the upper temperature

limit to be approx. 987 K and a maximum time at that temperature determined by the appearance of S. The time until S segregated noticeably to the surface was considerably extended by anneal-sputter cycles that apparently depleted the near surface region of S.

Time was a variable because after the sample was equilibrated at the desired temperature, the surface was sputtered just long enough to remove any S that had accumulated while the temperature was stabilizing. This sputtering created a surface slightly depleted in Ni (see chapter 6). The surface was then allowed to recover from this depletion and segregation was allowed to proceed to equilibrium. In order to ensure that the surface had reached equilibrium, spectra were collected continuously and a typical tracking of the surface composition with time is shown in fig. 19. This recovery chart was taken at 805 K (with no C or O visible during this collection), since it has been observed that the early rapid rise in fig. 19 is completed too rapidly at elevated temperature to collect spectra while the surface is close to the sputtered composition. This early rapid rise is usually interupted by a slight dip which may be associated with the removal of near surface damage caused by the ion bombardment[70]. The segregated composition is approached asymptotically and an average of spectra over this plateau was used to determine the equilibrium surface composition. The rise at the longer time end of fig. 19 is correlated with the appearance of S at the surface which may preferentially sit on top of, or displace, Co atoms. Since S below the detection limit may affect segregation, a study of the effect of S on the segregated composition was completed and the results of that study are presented in fig 20. In fig. 20, which was collected at 984 K

on a single crystal with surface orientation (111) and bulk composition 50.0 a/o Ni (see following section), Sulfur was allowed to build up and the observed relative Auger yield reported with the S peak height. It is clear that the Ni content of the signal rises slowly with the S content in a linear fashion and that below the detection limit, the Ni content is constant once equilibrium has been established. This observation indicates that sulfur below the detection limit does not have any appreciable affect on segregation in this system.

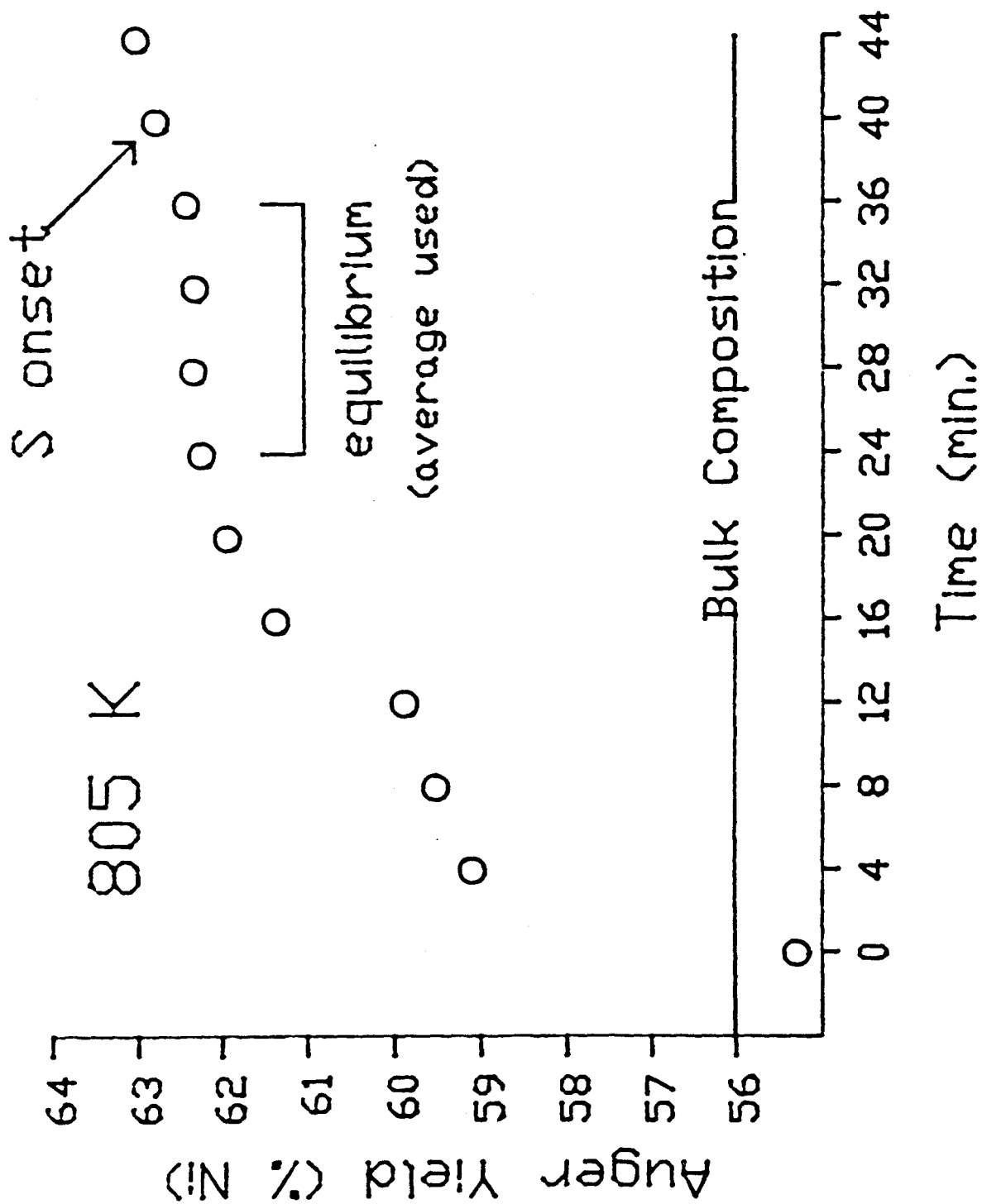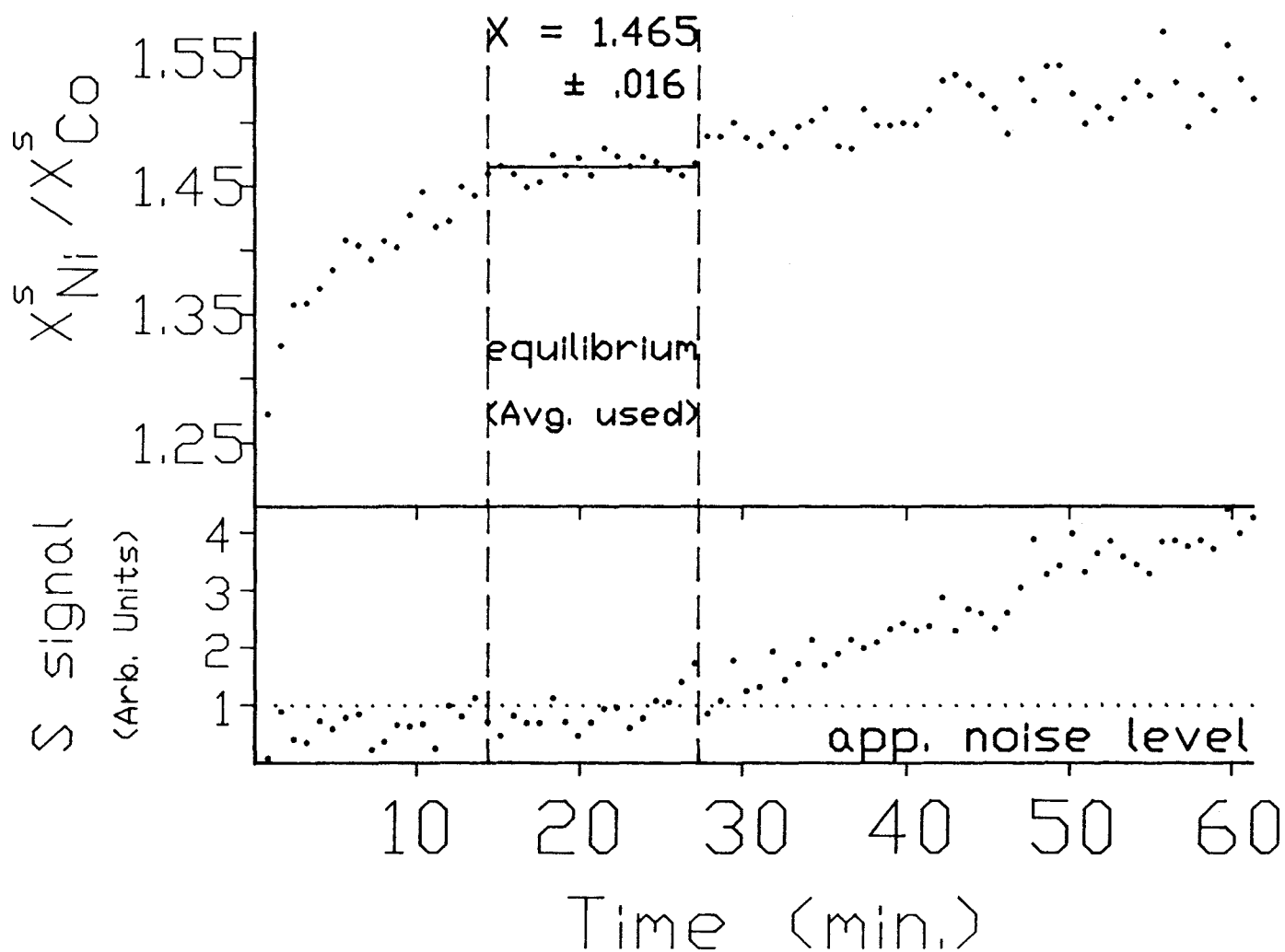Figure 19: Typical recovery from sputtering to segregated surface. Data taken from the (111) face of a 50 a/o Ni single crystal.

Figure 20: High temperature recovery track with the effect of sulfur segregation on Nickel content shown.
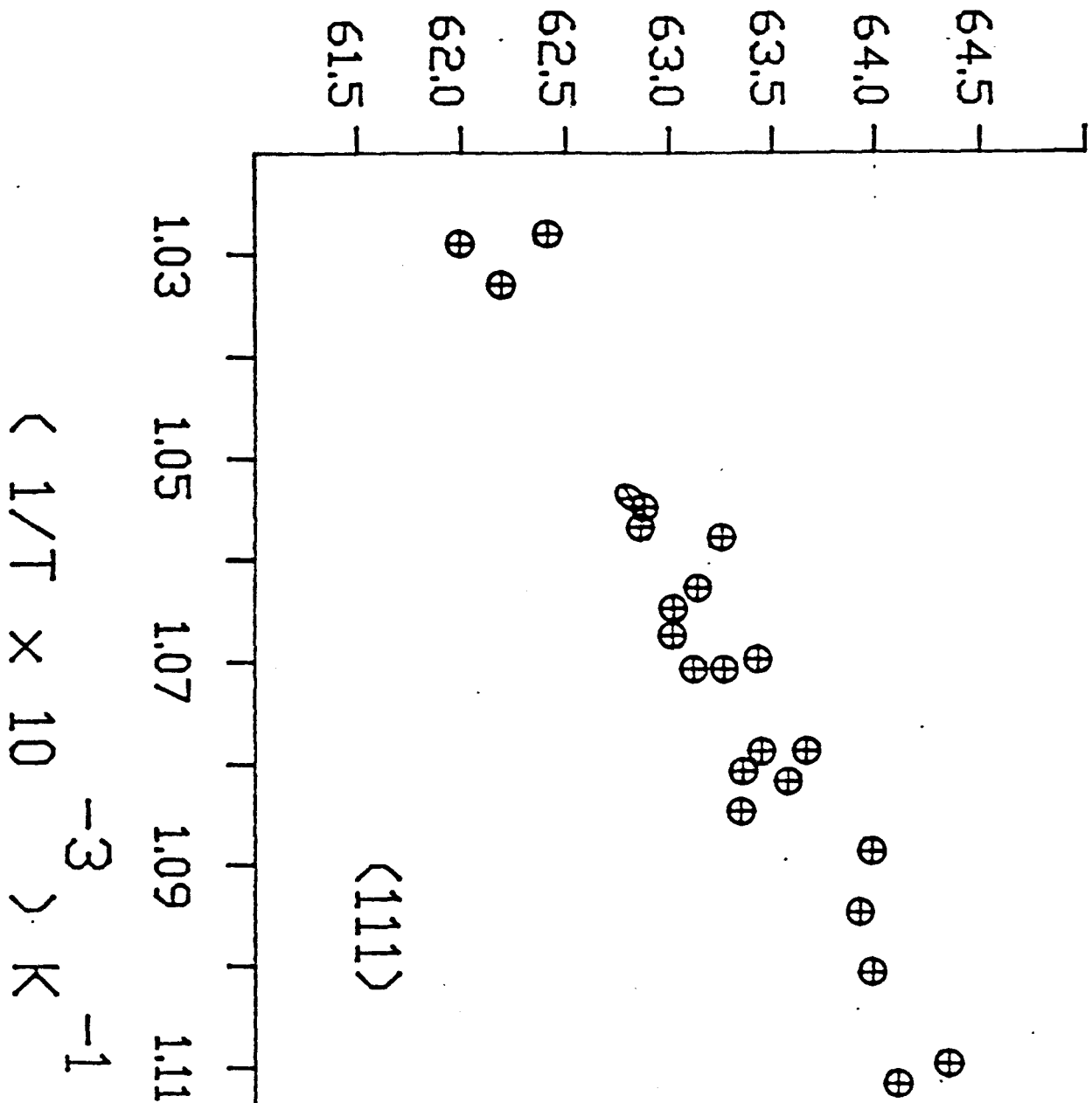
Figure 21: Relative Auger yield (as %Ni) vs. 1/T K^{-1}.
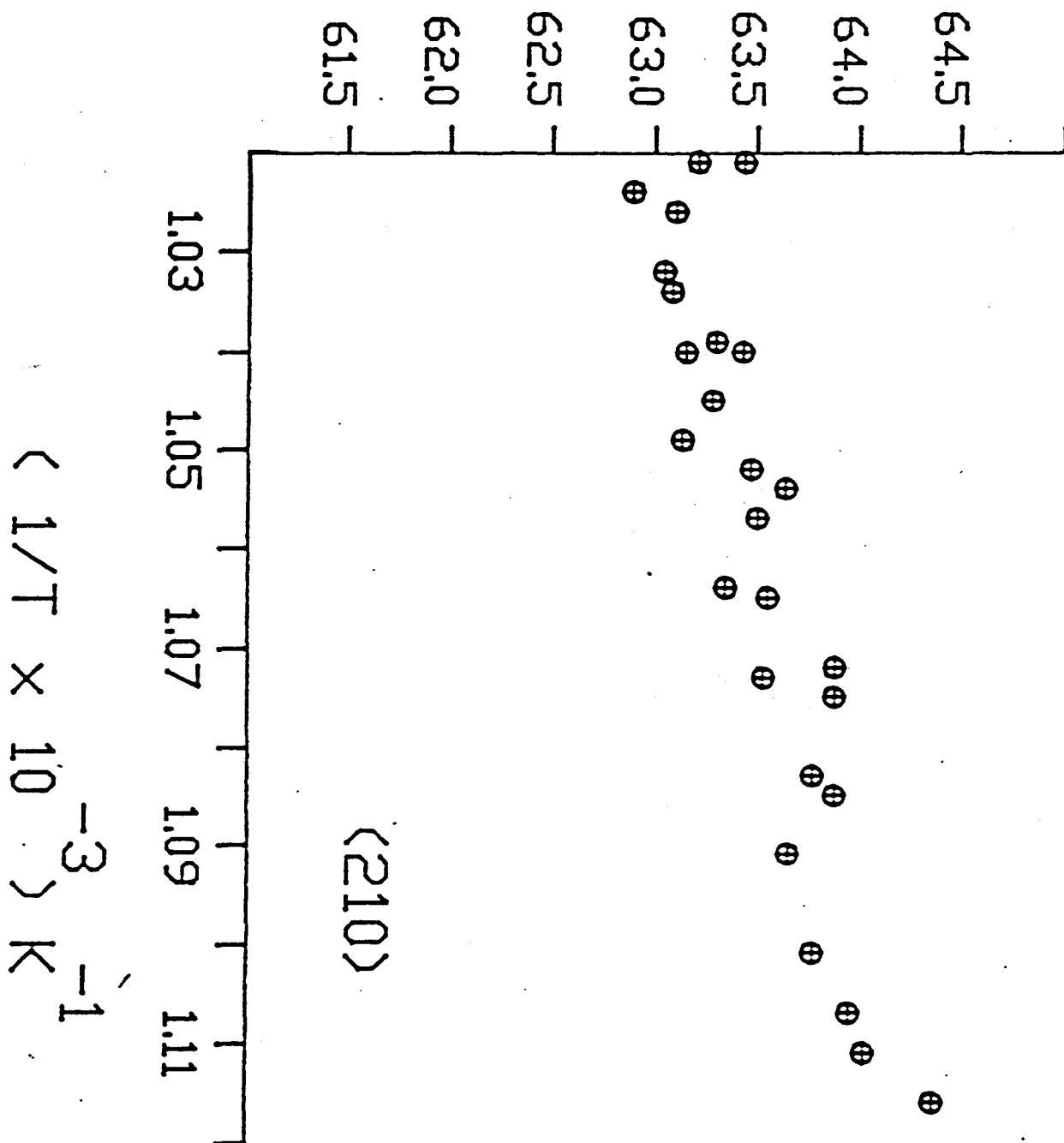Bulk composition 56 a/o Ni. (111)

Figure 22: Relative Auger yield as %Ni vs. 1/T for (210) face. Bulk composition 56 a/o Ni.

The raw (uncorrected for attenuation length) relative Auger yields expressed as atomic percent of Ni are plotted versus 1/T in figs 21 and 22 for the (111) and (210) faces of this alloy respectively. In order to convert the relative Auger yields to surface compositions, a monolayer of segregated surface was assumed and the attenuation length correction procedure given in chapter 5 for a CMA followed with d = 2.03 and λ = 3.17 Å.

With these two dimensions, the corrected first monolayer composi-tions were then calculated and converted into values of $\ln C^{*}$ and plotted vs. 1/T in figures 23 and 24 for the (111) and (210) faces respectively.

The resulting slope from fig. 23 was 2400 ± 200 K^{-1} and the y-intercept was -1.70 ± 0.21. The slope and intercept here were deter-mined by wieghted least squares analysis and standard errors are reported. These values were then converted to molar thermodynamic quan-tities and $\Delta H^{o}_{seg.}$ for this (111) face was -17.4 ± 1.6 kJ/mol while $\Delta S^{o}_{seg.}$ was -14.1 ± 1.8 J/molK. From fig. 24 the slope for the (210) face was 878 ± 94 and the y-intercept was $-.372 \pm .095$. These measurements convert to a $\Delta H^{o}_{seg.} = -7.3 \pm 0.9$ kJ/mol and $\Delta S^{o}_{seg.} = -3.1 \pm 0.8$ J/molK.

From the above results comes an interesting observation: the low index (111) surface indicates a more negative $\Delta H_{seg.}$ than the higher index (210) surface. It has been the conventionally accepted view that the smallest $\Delta H^{o}_{seg.}$ would be observed on the closest packed face and higher index faces would have higher $\Delta H^{o}_{seg.}$'s. This expectation arises from the bond-breaking models which stated that the driving force would be proportional to the number of missing bonds per atom at the surface. Surface free energy models also predict that, since higher index faces

have higher surface tensions, the driving force for segregation would also be higher. Since there was no immediately obvious explanation for this observation, further study of the crystallographic dependence was indicated.

The composition selected for this additional study was 50 a/o because Underhill[78] has completed an embedded atom calculation study of this system with a hypothetical bulk slab composition of 50 a/o. The initial results of that study were very encouraging because Nickel was predicted to segregate and the $\Delta H^o_{seg.}$ for a 50 a/o (111) face was -16.1 ± 0.6 kJ/mol which compared very well with the value of -17.4 ± 1.6 kJ/mol experimentally determined here on a 56 a/o Ni alloy. It was hoped that an exact comparison to the predicted $\Delta H^o_{seg.}$'s would be valuable, and the result of a determination on a (110) face would help to clarify the (210) result given above. It was also hoped that a wider temperature range could be investigated since there was no visible curvature in $\ln C^*$ vs. 1/T plots and it was possible that a temperature dependence of $\Delta H_{seg.}$ was masked by a temperature range narrow enough to have any curvature approximated by a straight line in this study.

Figure 23: lnC* (see text) vs. 1/T for the (111) face of a 56 a/o Ni alloy.
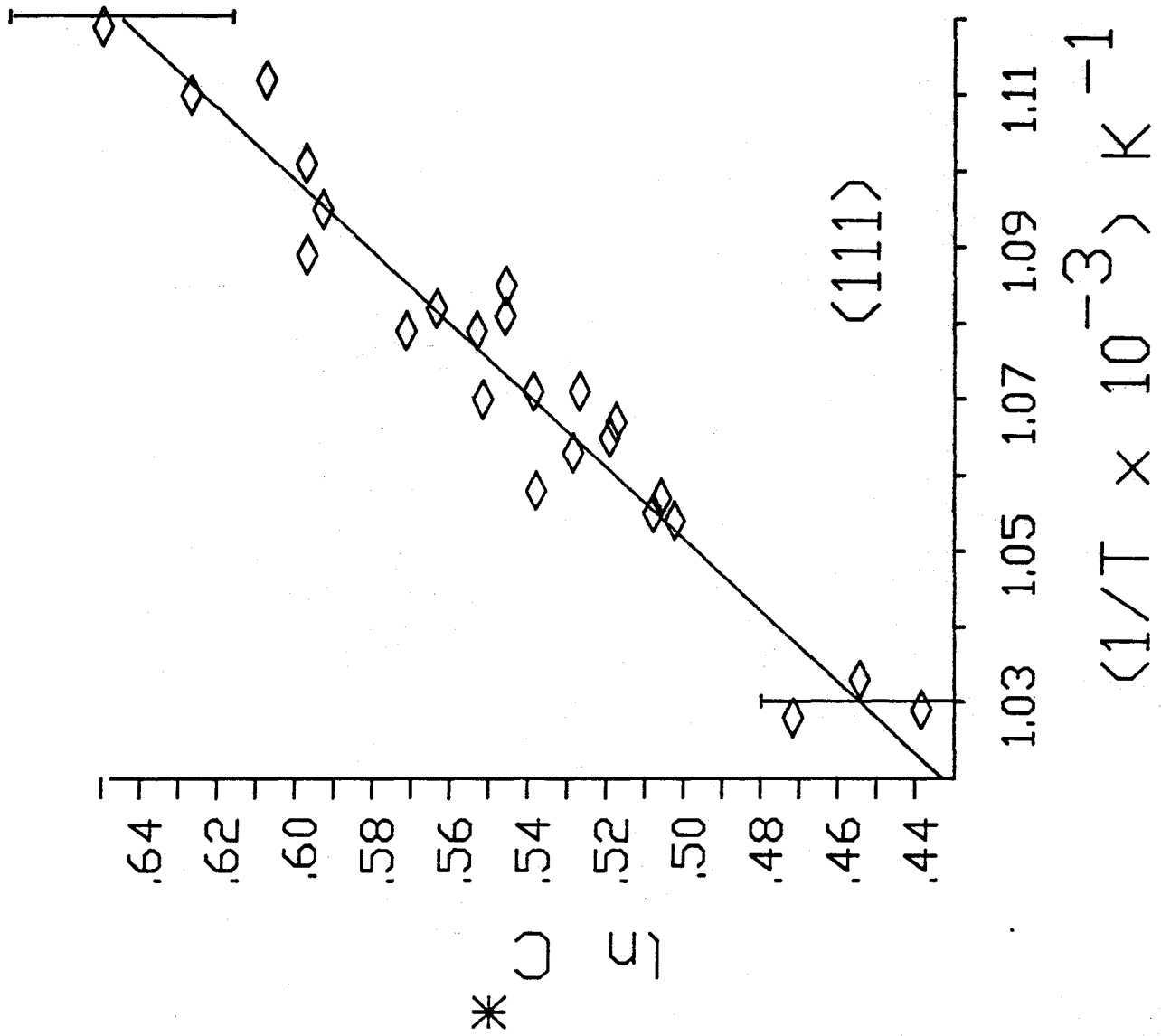
Figure 24: ln C* vs. 1/T for the (210) face of a 56 a/o Ni alloy.
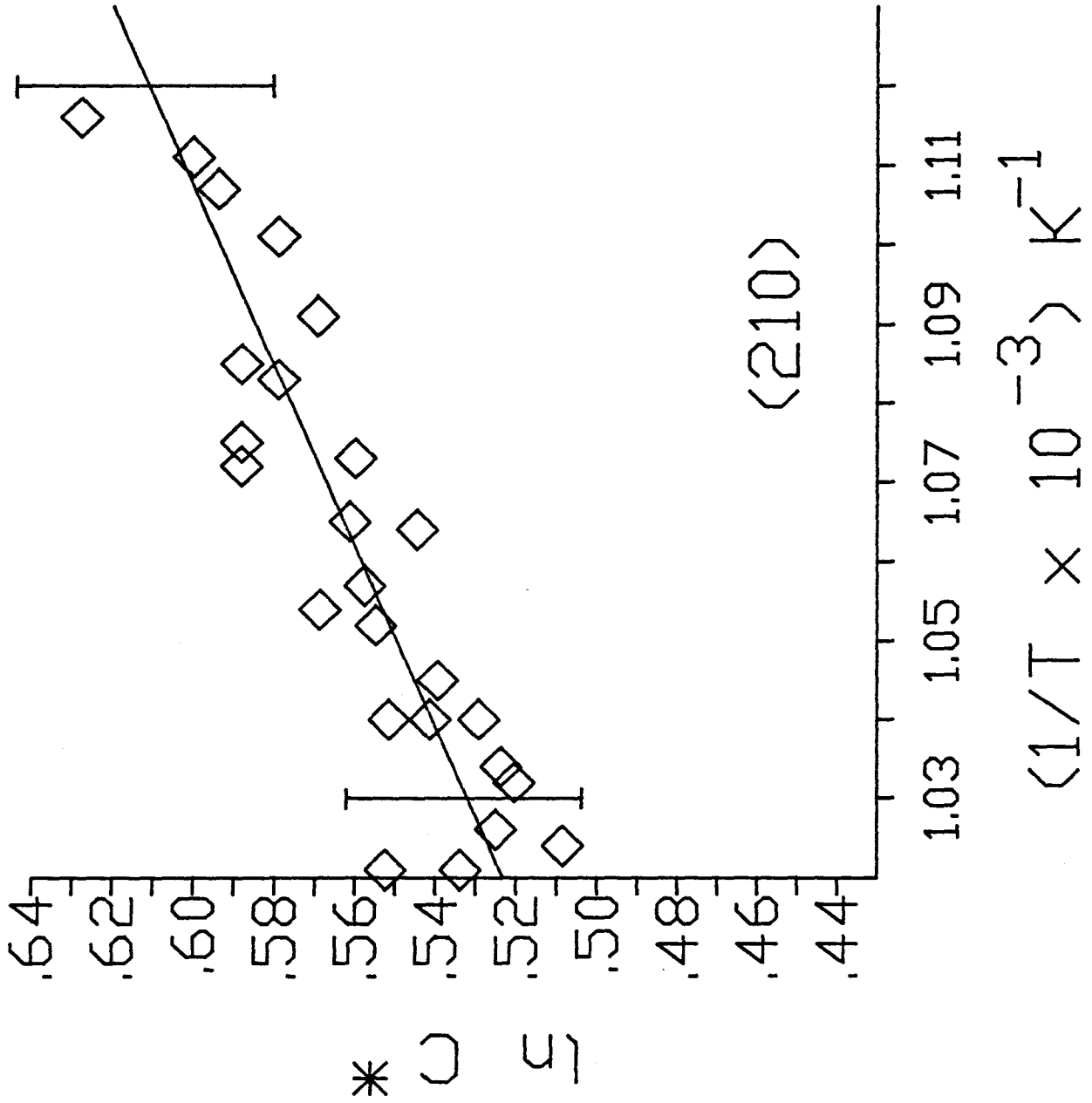
8-II (111), (100) and (110) faces of a 50 a/o Single Crystal

A single crystal was prepared (see chapter 4 for details) to have bulk composition 50.02 ± .005 a/o Ni. Samples of the three principle orientations ((111), (100) and (110)) were sliced from the crystal and found to be within 1° of the desired orientation by Laue back reflection. Uniform 7 mm diameter discs were spark-cut from the oriented slices and polished in the afore mentioned manner. Samples were then mounted as described previously and experiments performed in the same manner as had been used in the preceeding section.

The smaller diameter sample discs i.e. lower rate of heat loss because of the smaller size, as well as, an apparently lower bulk S content, allowed the upper limit of experimentally achievable temperatures to be raised to approx. 1100 K and thus greatly expanded the temperature window used to determine ΔH^o and ΔS^o. Sulfur was still a problem to be dealt with as in the previous experiments, but anneal sputter cycles proved very effective at removing it from the near surface region and contaminants in general did not cause any severe difficulties here.

The monolayer thickness and attenuation length were the same as in the previous study. Plots of $\ln C^*$ vs. $1/T$ for these faces are given in figs. 25-27 and the results summarized along with the results from the previous study in table 8-1.
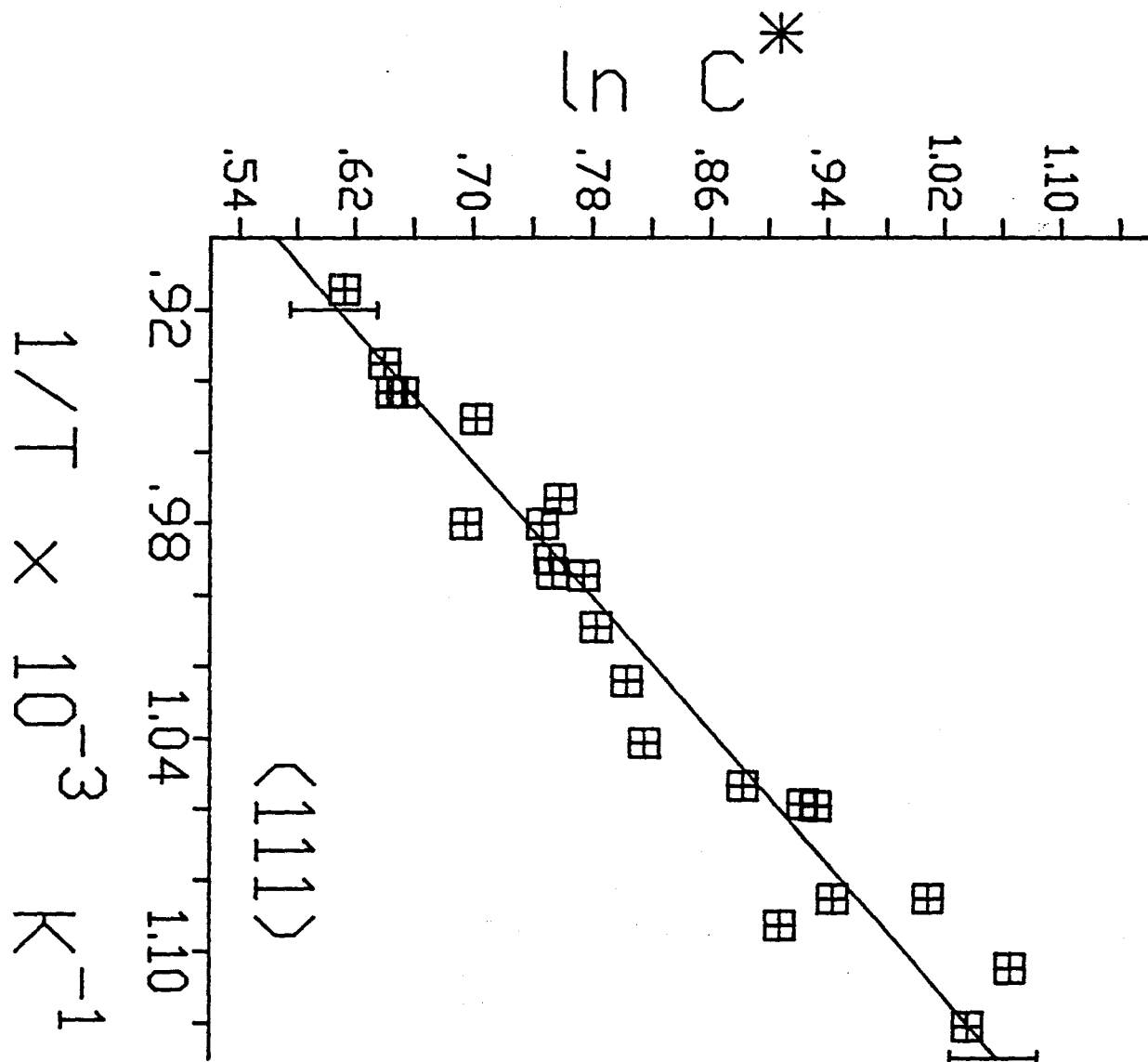
Figure 25: Plot of lnC* vs. 1/T for the (111) face of a 50 a/o Ni single crystal.
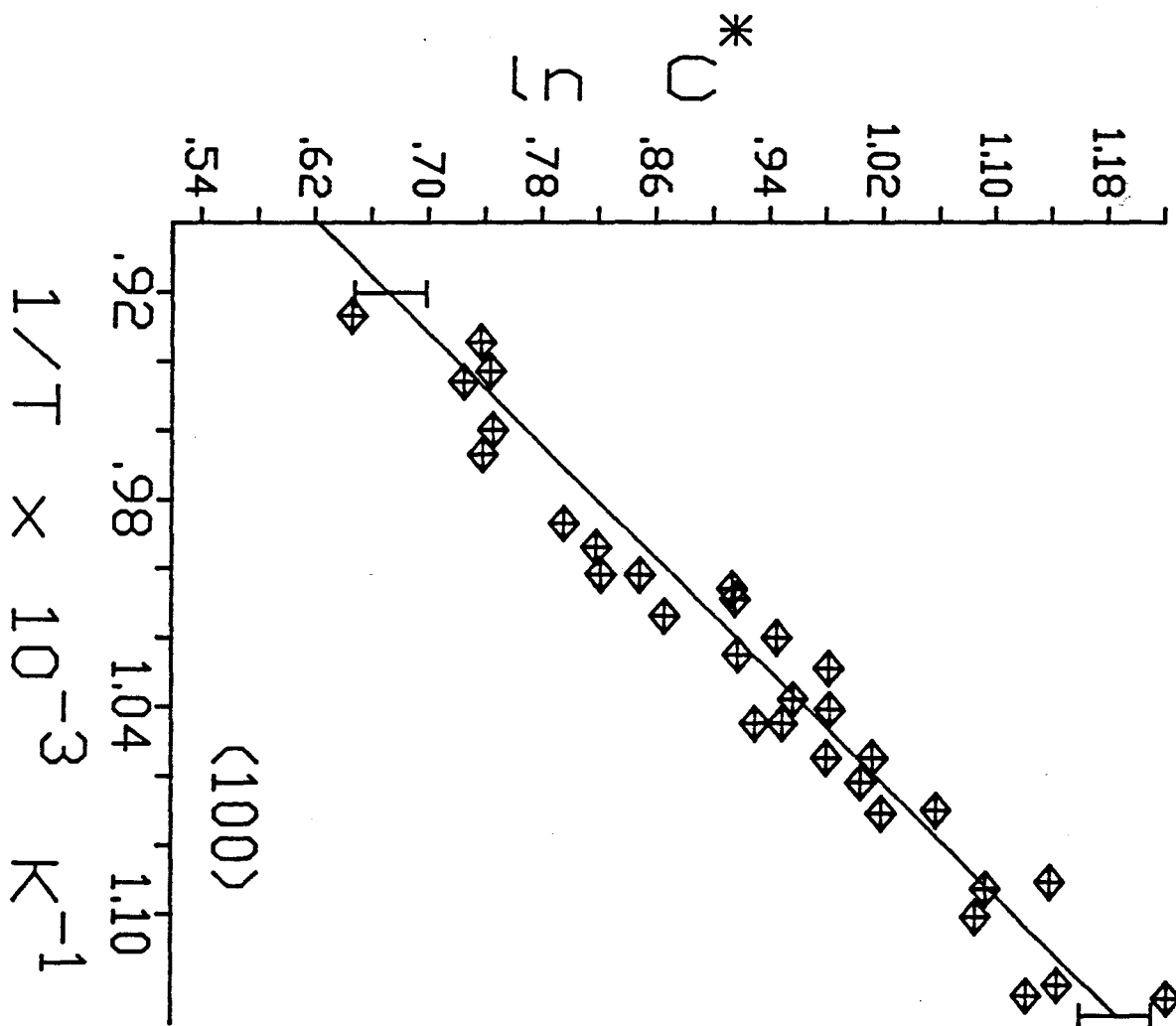
Figure 26: Plot of lnC* vs. 1/T for the (100) face of a 50 a/o Ni single crystal.
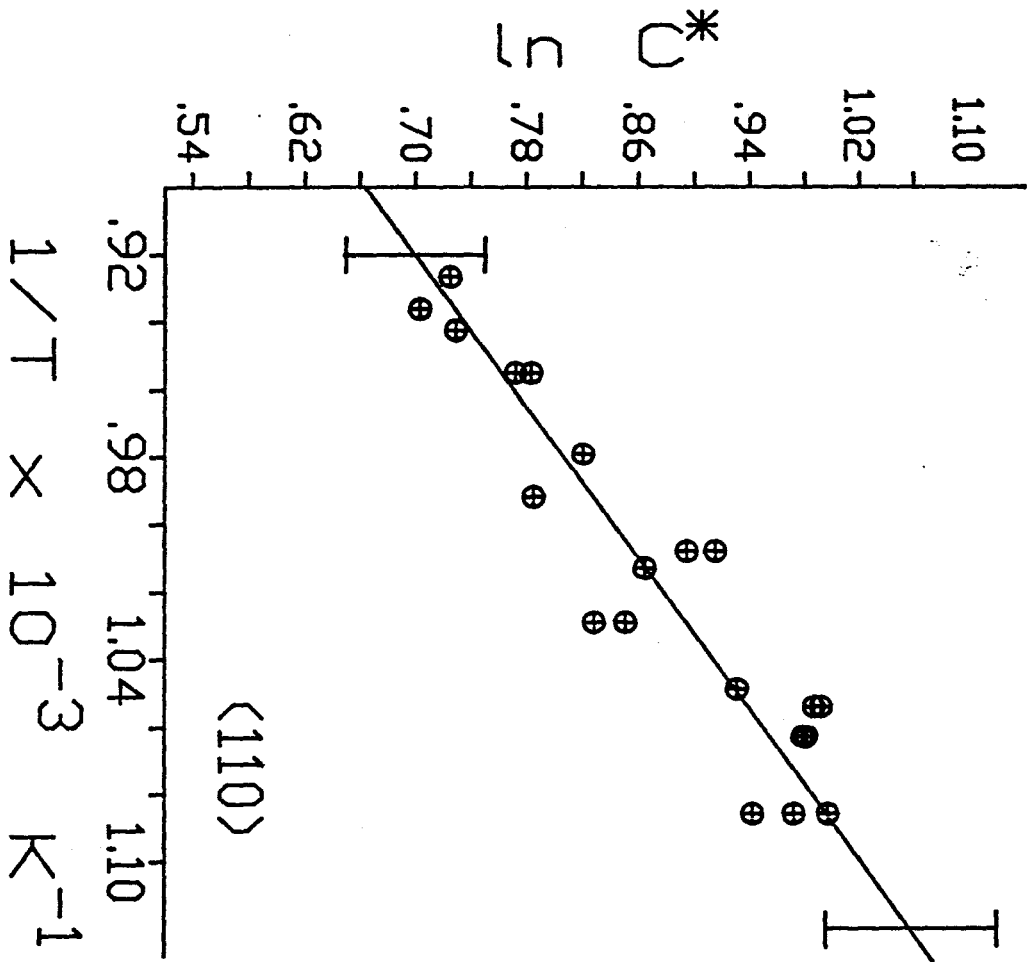
Figure 27: Plot of lnC* vs. 1/T for the (110) face of a 50 a/o Ni single crystal.

Table 8-1: Enthalpies and Entropies of Nickel Segregation for Different Faces All With The Same Monolayer Thickness

Bulk Comp.	Orientation	$-\Delta H_{seg}$ kJ/mol	$-\Delta S_{seg}$ J/molK
56.0 a/o Ni	(111)	17.4 ± 1.60	14.1 ± 1.74
	(210)	7.3 ± 0.94	3.1 ± 0.79
50.0 a/o Ni	(111)	17.8 ± 1.08	11.3 ± 1.09
	(100)	20.4 ± 0.87	13.2 ± 0.86
	(110)	14.9 ± 1.54	7.9 ± 1.59

Upon observation of figs. 25-27 it is clear that there is no residual curvature in the plots of ln C* vs. 1/T for this temperature window. This indicates that a further temperature dependence of ΔG^o is not evident and the approximation used to assign $\Delta H^o_{seg.}$ and $\Delta S^o_{seg.}$ to the values from the slopes and intercepts is probably valid over this temperature range.

From table 8-1 it is obvious that:

i) The more open faces, the (110) and (210), have apparent $\Delta H^o_{seg.}$'s that are lower than the corresponding more compact (100) and the closest packed (111) faces.

ii) The (100) has $\Delta H^o_{seg.}$ higher than the (111) which is what would be expected according to conventional models.

iii) There is significant variation in the entropy term which is definitely not equal to zero and is lowest for higher index, more open faces.

These apparently contradictory results presented something of a dilema since point ii) agrees with conventional models and point i) disagrees strongly. This discrepency may be partially interpretted via the observation that the driving force for segregation must be a free

energy ($\Delta G^o_{seg.}$) and the literature routinely ignores the entropy component of the free energy expression with the assumption that it is insignificant and configurational only. This approach to the interpretation of the data is the result of the common usage of bond breaking models when discussing segregation, and it is clear from the results already presented, that bond breaking models predict an insignificant amount of Co segregation, which is contrary to the observed fact. It is clear from the observed values that there is certainly variation in the entropy term with crystallographic orientation and the size of the term is large enough to make a significant difference in the total driving force for segregation. The correct basis for comparison must therefore be the free energy of segregation over a specified temperature range.

From the data above it is possible to calculate and compare $\Delta G^o_{seg.}$'s for the three principle orientations. The results of this comparison are summarized in figure 28. Even though the error associated with the (110) result is quite high, as a result of the small number of data points available for this face, the trend at the high temperature end is obviously as had been expected if the driving force for segregation were related to a difference in surface tensions i.e. (111) lowest to (110) highest. It is of value to note that the variation of solid surface tension with crystallographic orientation is an observed fact, but the variation of the component enthalpy and entropy is not well understood.
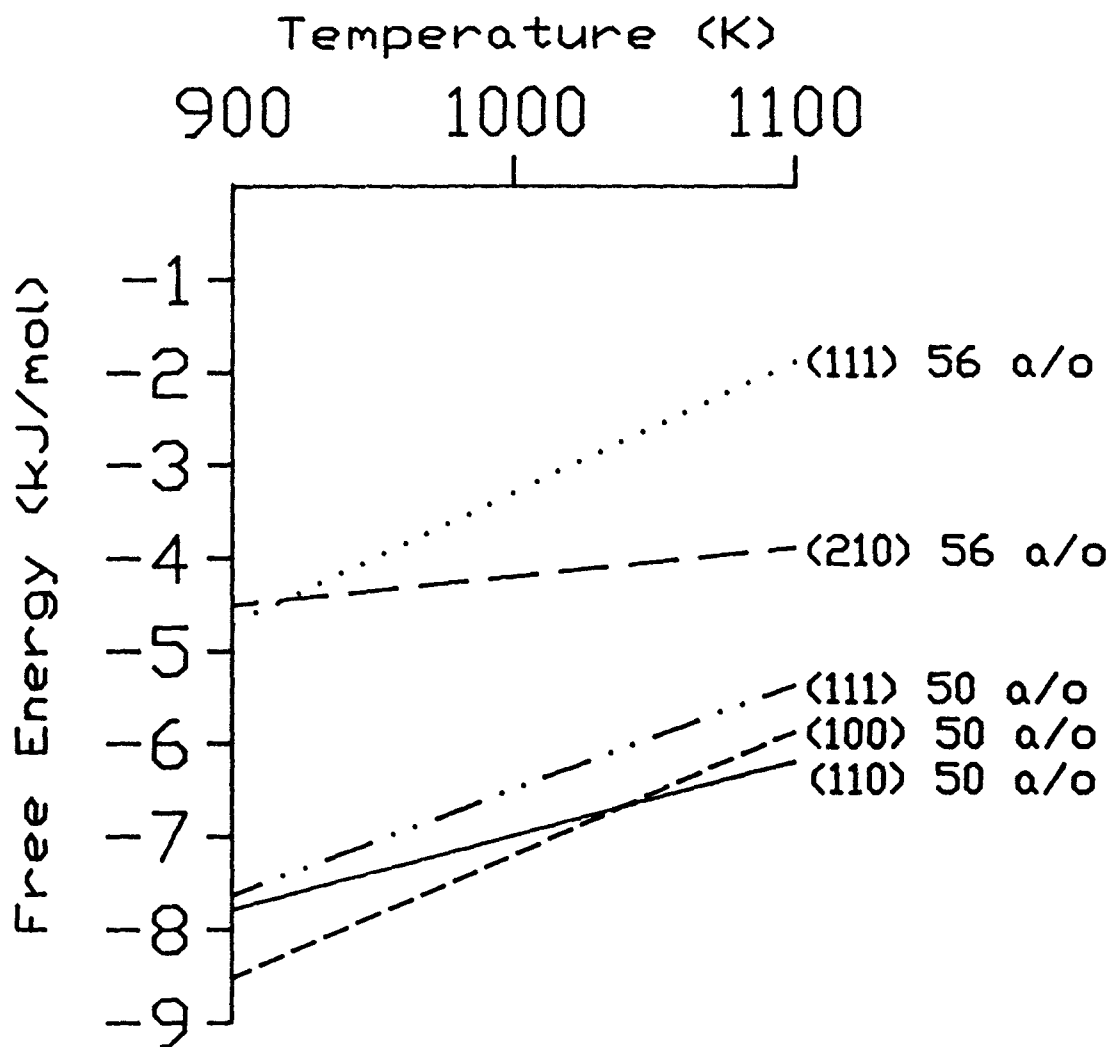
Figure 28: A plot of Free Energy of Segregtion vs. Temperature.

(for Ni-Co alloys with 56 and 50 atomic percent Ni).

If this basis for comparison were correct then a similar calculation of $\Delta G^{o}_{seg.}$ for the 56a/o(111) and 56a/o(210) faces should have the 56a/o(210) free energy result higher than that for the 56a/o(111). The observed $\Delta G^{o}_{seg.}$'s for the 56 a/o sample are shown in figure 28,

From inspection of figure 28 it is evident that the expected trend in ΔG^{o}'s is obeyed at the high temperature end of the plot. That is that $\Delta G^{o}_{seg.}$ (110) > (100) > (111) for the 50 a/o Ni sample and $\Delta G^{o}_{seg.}$ (210) > (111) for the 56 a/o Ni sample. At lower temperatures there is a crossover point such that the (110) and (210) lines fall out of the expected sequence. This may be partially the result of the fact that only one monolayer thickness was used in the calculation of the attenuation length correction and points out one of the problems associated with quantitative Auger from higher index or more open faces, the attenuation length is probably not the same for all faces, but the exact values are not certain.

Another interesting feature of figures 28 is the large difference in free energy between (111) faces of 50 and 56 a/o Ni. The ΔH^{o} values for both determinations are quite close, -17.4 and -17.8 for the 56 and 50 a/o Ni samples respectively as might reasonably be expected for alloys with such a small difference in composition, but the ΔS^{o} values differ quite markedly. These are interesting results but ones which require more study before any attempt at interpretation can be made.

The final questions concerning segregation in this system are; why does Ni segregate at all and why is the entropy component so important? The fact that the surface free energy models come closest to

predicting the correct surface enrichment, tends to point to the difference in surface tensions as the driving force, but accurate solid surface tensions are not readily available. It is useful to note that the predictions of surface tensions by Miedema[33] using equation A.25 in eqn. A.24 (a combined surface free energy, heat of solution and size model--see appendix 1) rely on the electron density at the edge of a Wigner-Seitz cell and the electronegativity for the element in question. Since electronegativity has been related to the effective nuclear charge by Allred and Rochow[79];

$$\Phi^* = (3590Z^*/r^2) + 0.744 \qquad 8.2)$$

and the effective nuclear charges (Z^*) for Ni and Co are[80] 12.530 and 11.855 respectively, the electronegativities (Miedema terms this as the "chemical potential for electrons" and is clearly the electronegativity by North American convention) are 5.20 and 5.10 ev for Ni and Co respectively. If relations 8.2 and A.25 hold true, then the driving force for segregation is at least partially related to the electronic structure of the metal atoms and the filling of the d bands.

The embedded atom calculation of Underhill[78] mentioned previously, has come very close to predicting the ΔH^o_{seg}'s that have been observed in this work. In that study it was pointed out that electronic theories qualitatively predict the correct segregating component but quantitation is very difficult. In an embedded atom calculation, the electronic contributions to the interaction potentials $\Phi_{ij}(r)$ and $F_i(\rho_i)$ (see chapter 2) are included if bulk thermodynamic and elastic constants are accurately

predicted. This ensures that the potential functions used for segrega-
tion data are correct. Inspection of plots of the interatomic potentials
(attractive and repulsive) as a function of the number of bonds to an
atom[78], reveals that the decrease in core-core repulsions in Ni is
offset to a greater degree than Co, by the decrease in attractive forces
upon going from bulk coordination to surface coordination. The reason
for this difference between Ni and Co seems to be the fact that Ni has 8
d electrons while Co has only 7. Samsonov and Krasnov[81] pointed out the
relationship between the surface tension of liquid transition metals and
the number of d-electrons. Those researchers demonstrated that, for rows
in the periodic table, surface tension is at a maximum when there are 5 d
electrons and decreases when there are fewer or more than 5 d electrons.
This observation parallels the predictions of the electronic theories for
segregation in transition metals[37,82].

Kerker et. al[37] (1977) pointed out that electronic density of
states calculations[83-88] indicate that surface segregation is highly
sensitive to d-band filling. In purely chemical terms, that is to say
that for atoms up to d^5 (assuming for the moment that all d-orbitals are
degenerate) all electrons are un-paired and any alloy element with fewer
d-electrons will have less internal energy and thus be favoured to take a
position at the surface. For alloys consisting of elements with > 5 d
electrons then, pairing of electrons in d orbitals decreases the internal
energy of the atom and hence the element with most d-electrons (fewest
unpaired electrons) will be favoured at the surface.

This model assumes that the only contribution to entropy is from
mixing, and other terms such as electronic entropy arising from the

density of states at the Fermi level contributes nothing to the total free energy. While this assumption may well be valid for simple metals, in the case of transition metals other considerations may have to be taken into account since the evidence of this thesis suggests an important contribution to the total energy term from entropy. If the above electronic interpretation is correct, then the pairing of electron spins might introduce a significant term if only on the magnetic moments of atoms in the system. Given this possibility then, it may also follow that symmetry at the surface may introduce a crystal field splitting effect which might account for the noted crystallographic dependence of the segregation.

It is now clear that segregation does occur in this system and that at equilibrium a clean Ni-Co alloy surface will be enriched in Ni. The reason that segregation has attracted such a large amount of interest in the past is the possibility that it may influence the reactivity of the alloy in question. Towards that end, the earliest stages of oxidation on Ni-Co alloys have been investigated here in order to try to elucidate the mechanisms governing reactions at metal surfaces. The balance of this thesis reports the results of that investigation.

The Initial Stages of Oxidation : Background

9-I General Stages

For many years the process of oxidizing metal surfaces has been thought of as proceeding via two stages: i) chemisorption of O or O_2 followed by ii) thickening of the oxide overlayer by one of the several possible kinetic schemes (parabolic, linear, logarithmic etc.). This view was altered in 1970 by Fehlner and Mott[89] and in 1974 by Holloway and Hudson[90] (HH) who pointed out that the oxide layer must be formed prior to thickening and that the kinetics of that process would likely be different than either the preceeding or following stages. By far the most often studied reaction of a metal with oxygen in the early stages has been that with Ni, and HH developed their mechanism for nucleation and growth of the first oxide layers by studying the interaction of Ni (111)[90] and (100)[91] faces with oxygen. In the present study, the initial stages of oxidation (oxide island formation and growth) on Ni-Co alloys has been investigated and compared to the model and observations of HH and others. Following is a brief synopsis of the HH model and some of the observations made on the Ni/O system.

9-II Chemisorption

The first stage of Oxygen uptake on Ni was thought to be dissociative chemisorption which obeyed a Langmuir type adsorption isotherm. This observation has been generally supported in the literature[92,93] with some early questions about whether or not the adsorption was non-dissociative, being cleared up by Benninghoven et. al.[94] and Verheij et. al.[95] via SIMS and flash desorption, who concluded that adsorption onto the metal was dissociative. Subsequent work[96-99] has also shown that there are two distinct surface phases of chemisorbed oxygen characterized by their LEED structural descriptions p(2x2) followed at slightly higher exposures by c(2x2).

Langmuir kinetics can be modelled simply by assuming that the surface contains a certain number of adsorption sites S, some of which may be occupied S_1 such that the number of sites available at any one time for adsorption would be $S_o = (S-S_1)$. If adsorption is assumed to be a non-activated process then the rate of adsorption is just proportional to the number of available sites, the surface collisional frequency (which must be proportional to the pressure) and the sticking probability, therefore;

$$\text{Rate of adsorption} = k_o P S_o = k_o P(S-S_1) \qquad 9.1)$$

Assuming first order desorption, the rate of desorption is proportional to a rate constant k_1 and the number of surface sites which are already covered in adsorbate S_1. At equilibrium the two rates are equal and if

we now define $\theta = S_1/S$ as the fraction of the surface covered by adsorbate, the Langmuir adsorption isotherm is obtained;

$$\theta = \frac{bP}{1 + bP} \quad \text{where } b = k_1/k_0 \qquad 9.2.)$$

This isotherm must be modified in the case of dissociative chemisorption (the proposed mechanism in this case) however, since two adjacent sites must be present to adsorb Oxygen and two O atoms must be present to reform O_2. The rate of adsorption $= k_0 P (S-S_1)^2$ and similarly the rate of desorption would then be $= k_1 S_1^2$, yielding;

$$\theta = \frac{bP^{1/2}}{1 + bP^{1/2}} \qquad 9.3)$$

Of course at higher pressures the rate of adsorption will far exceed the desorption rate and saturation will ensue. At very low pressures 9.3) will reduce to $\theta = bP^{1/2}$ since $1 >> bP^{1/2}$. The sticking coefficient is described as the probability that a particle striking the surface becomes chemisorbed, and the sticking coefficient s for a Langmuir dissociative isotherm onto a dissordered surface, as in the above idealized case is;

$$s = s_0 (1 - \theta)^2. \qquad 9.4)$$

In the case of the Ni/O system, the early works of Holloway and Hudson[90] and Mitchell, Sewell and Cohen[111] indicated that adsorption proceeded onto a disordered surface phase via a non-activated dissociative Langmuir

isotherm but, later work by Holloway[105] has stated that the chemisorbed

oxygen resides in two-fold bridge sites on Ni(111) and four-fold sites on

Ni(100). He further states that the sticking coefficient varies as $(1 - 4\theta)$ for the Ni(100) faces and $(1 - 3\theta)$ for the Ni(110) face. This meant

that only specific sites and not just any unoccupied site are needed for

chemisorption. A later work by Brundle[104] states that rather than a

four-fold site on Ni(100), the limiting available site is one called θ_8

which has two adjacent 4-fold sites with no nearest neighbours to repel

the two new incoming oxygen atoms. Clearly the exact nature of the

adsorption isotherm is face dependent and the exact mechanism is not

known for most of the faces. In this thesis however, the exact nature of

the chemisorption reaction is not of primary interest but the following

stage in the oxidation process is.

9-III Oxide Nucleation and Lateral Growth

The next stage in the HH model was the nucleation and lateral

growth of islands of oxide which were approximately 2-3 "layers" of oxide

thick. The existence of islands of NiO was suggested by the appearance

of a pattern consistent with domains of the oxide [p(1x1)] in LEED

photographs concurrent with the patterns identified as corresponding to

adsorbed O [c(2x2)]. This observation, coupled with AES peak height and

shape data, lead HH to conclude that NiO nucleated and grew as islands

after the adsorbed O layer reached $\simeq$ 0.35 mL of coverage. The model

proposed to explain the growth kinetics of the islands is as follows (see

fig. 29);

Oxide Island Growth Model

Figure 29

lateral diffusion

Desorption

Impingement

r

O_2

O_2

O_2

NiO

NiO

h

chemisorbed O

Nickel Substrate
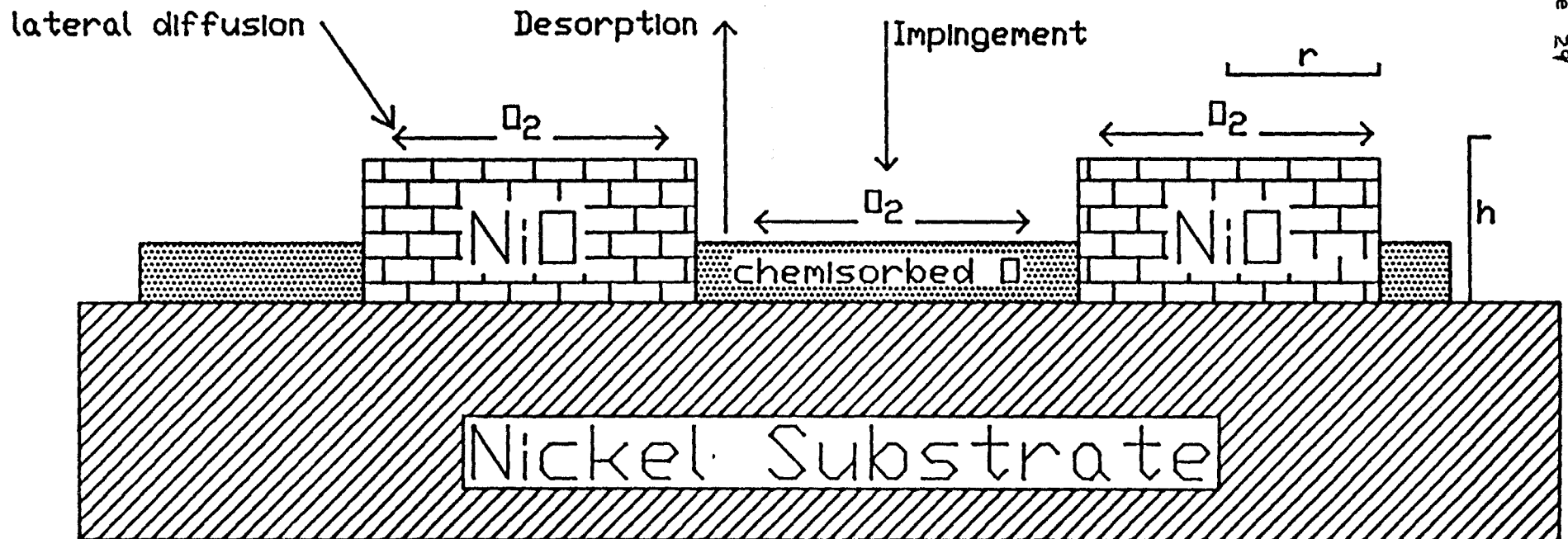
Five assumptions are made;

i)physisorbed O_2 exists on top of either chemisorbed O or oxide with a mean stay time of τ_p , a lateral diffusion coefficient D_s and an accomodation coefficient of 1 into the physisorbed state. These physisorbed O_2 molecules then diffuse laterally until they reach an island perimeter.

ii)O_2 dissociates at perimeter sites only.

iii)Islands have a circular shape, to simplify the mathematics.

iv)τ_p and D_s are the same for O_2 physisorbed on chemisorbed O and on the oxide.

v)all islands are nucleated in a short time relative to the time necessary to form a complete oxide coating.

It is possible to envisage growth in this model being limited by;

1)oxygen impingement from the gas phase,

2)surface diffusion of oxygen,

3)capture of oxygen at perimeter sites.

HH discounted case 1) because tracks of the Auger O peak height displayed non-linear variation with oxygen dose as would logically be expected if the island growth rate were simply proportional to the impingement rate of O_2. For cases 2) and 3) the results of the model development are;

$$(1 - \theta) = \exp^{(-K_i N_o P^2 t^2)} \quad \text{or} \quad (1 - \theta) = \exp^{(-K_i N_o L^2)} \qquad 9.5)$$

where L represents the unit of exposure Langmuir, which is 1×10^{-6} torr.sec. and where $K_i = (2A/n)(2mkT_g)^{1/2}[2B_i exp^{(E_i/RT)} + h]$ for both limiting cases with $B_1 = 2(Z\alpha^2\nu_1/\nu_2)^{1/2}$ and $E_1 = 1/2(E_a - E_d)$, $B_2 = A^{1/2}\nu_1/\nu_2$ and

$E_2 = E_a - E_c$. Here the 1 refers to the case of limitation by lateral diffusion and 2 refers to the case of limitation by conversion. The E_a refers to adsorption of O_2, E_d refers to desorption and E_c refers to capture. The A refers to the area of an island, ν_1 is the frequency of vibrations parallel to the surface, ν_2 is the perpendicular vibrational frequency, α is the mean jump distance and Z is the number of nearest neighbour adsorption sites.

The existence of island growth has been generally supported in other works[102-112] not only on Ni but also with other metals and there is a definite prospect that the mechanism is general[117]. There has been some significant disagreement however, as regards the exact model proposed by HH, as Brundle[104] and Mitchell et. al.[110,111] assert that the true mechanism must not involve a physisorbed O_2 since even at 300 K the residence time of such a species would be very short, but rather that the rate of island growth must be limited by direct capture at island edges from the gas phase. The exact thickness of the oxide islands has also generated some disagreement but Saiki et. al.[118] has most recently determined by X-ray Photoelectron Diffraction that the thickness of oxide islands generated by annealing a saturated Ni(100) surface at 523 K for 10 min. was 2-3 monolayers of O in the NiO lattice.

The existence of good LEED data along with the oxygen uptake curves from AES studies has been enough to convince other workers that an

island growth mechanism is operative in the Ni/O as well as other systems, but there has never been any unequivocal imaging of oxide islands at the 2 to 3 monolayer thickness level as has been done in this thesis. Goulden[119] (1976) and Milne and Howie[120](1984) have conducted SEM, RHEED and TEM investigations into oxide island formation on copper. These experiments generated islands by exposing clean copper to oxygen in the 10^{-4} torr range at tempertures from 250 to 400 C^{o} for from 1 to 150 min.. The islands so generated were at least 300 and more usually 600 - 800 Å thick and as such were very much larger than those observed in this thesis. The lack of chemical information during imaging, as well as, the very heavy oxidative treatment used to generate these features, leads to the question of whether or not these "islands" were either nuclei of columnar grains on an already completed compact oxide film or an example of the same island growth process under very dissimilar conditions. The next chapter of this thesis deals with the method used here to obtain unequivocal imaging of very thin oxide islands and a method by which the proposed mechanism of HH has been tested.

Finally the fact that this study has been conducted exclusively on alloy surfaces, must be addressed. The effect of an alloying element is thought to affect the early stages of oxidation in two ways. The first effect will be the preferential oxidation of the component with lower free energy of oxidation and the proportions of alloying elements may affect the kinetics greatly. Previous work (Cherepin et.al 1979[46] as well as numerous others) has established that Co is selectively oxidized with the content of Co increasing in the oxide as the thick oxide grows. Here in this study, only one composition has been investigated (79 a/o

Ni) and providing modification of the surface composition is confined only to segregation, the surface is initially of constant composition. The first part of this thesis has dealt in some detail with modifications of the surface composition with temperature due to segregation and the results of that study have been presented. From the previous experience of dealing with this alloy at elevated temperatures, it can be concluded that if sufficient time were allowed, the clean surface would become enriched in Ni. It is perhaps fortunate therefore that although few formal kinetic experiments were conducted, at the temperatures of interest in this oxidation study (<< segregation temps.) segregation is so slow as to have very little effect on the surface composition.

The second effect of the alloying component is likely to have more impact on the kinetics of oxide island growth, that being island growth limited by diffusion of the most reactive component. This possibility has been given careful consideration but the fact that the oxidation reaction proceeds much faster than segregation, would tend to suggest that diffusion of the most reactive metal species is not rate limiting.

Chapter 10

Direct Observation of Island Growth: AES Mapping

10-1 Experimental Approach

a) Data Aquisition: Map Generation

The best evidence for the existence of very thin oxide islands to
date, has been the observation of LEED patterns consistent with domains
of NiO concurrent with patterns attributed to chemisorbed oxygen phases
on Ni (see chapter 9). There has however, been no unequivocal imaging of
these islands because the contrast provided by secondary electron emmi-
sion from islands that are approximately 2-3 layers thick, is apparently
insufficient. Furthermore, the island growth reaction proceeds even at
very low pressures of O_2 ($1x10^{-7}$ torr), therefore dosing must proceed in
a UHV chamber where the background pressure during imaging can be held at
$<1x10^{-9}$ torr i.e. the reaction should be halted. A method which can
provide both spatial and chemical information simultaneously in a UHV
chamber is Scanning Auger Mapping.

The PHI 600 SAM used in this thesis is equipped with a hot stage
(see previous chapters) which allows for the collection of Auger spectra
and Maps at an elevated temperature. The need for an elevated tempera-
ture stems from the fact that the probability for homogeneous

nucleation is likely to decrease with increasing temperature and if fewer islands nucleate and grow, the islands present might be large enough to image with the limited spatial resolution of a scanning Auger system.

Holloway and Hudson[90] utilized the relation of Gallon[113] who pointed out that an Auger oxygen signal originating in an oxide of n layers thickness will have an observed intensity[113] of;

$$I_n = I_\infty [1 - (1 - \frac{I_1}{I_\infty})^n] \qquad 10.1)$$

Where I_∞ is the signal from an infinite number of layers and I_1 is the signal from one layer of material. 10.1) holds true if there are uniform layers present, but in the case where there are regions in the sampling field with islands of varying thickness, then the relation of Seah[114] may be more appropriate;

$$I_n^c = I_\infty^c \{1 - \exp^{(-n/n_c^1)}\} \qquad 10.2)$$

where $n_c^1 = \{1 - \exp^{(-1/n_c)}\}^{-1}$ and n_c is usually the IMFP (see chapter 5). However, the fractional coverage is not included in such a model and it is clear that direct quantitation in this regime is likely very difficult and complex. For the purposes of this study, the exact

Figure 30
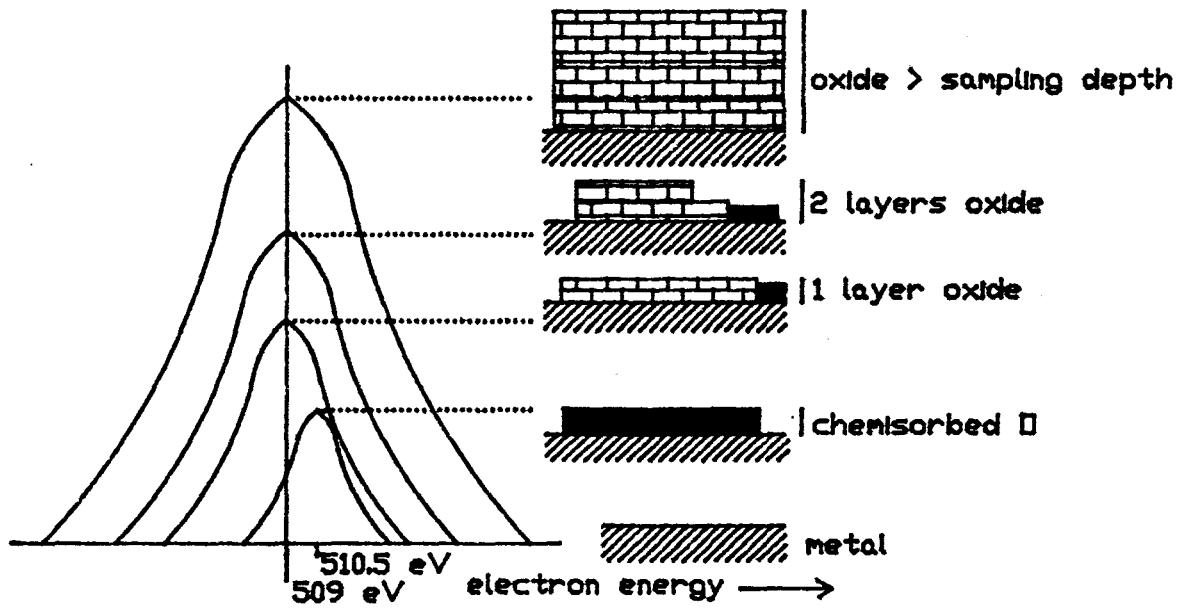
Schematic variation of Auger peak intensity with island thickness

AES   MULT   EL= O 1 SF=6.180, -722.176 DAT=14.00   MOX2   P-C

Figure 31 a: Chemisorbed O Auger peak.

AES   MULT   EL= O 1 SF=9.449, -549.120 DAT=.60   COHI2 P-C

Figure 31 b: Oxide O Auger peak.

intensity correction is not critical, but the idea that the intensity of Auger signal increases in discrete but dwindling steps up to the effective sampling depth, is important (see fig. 30).
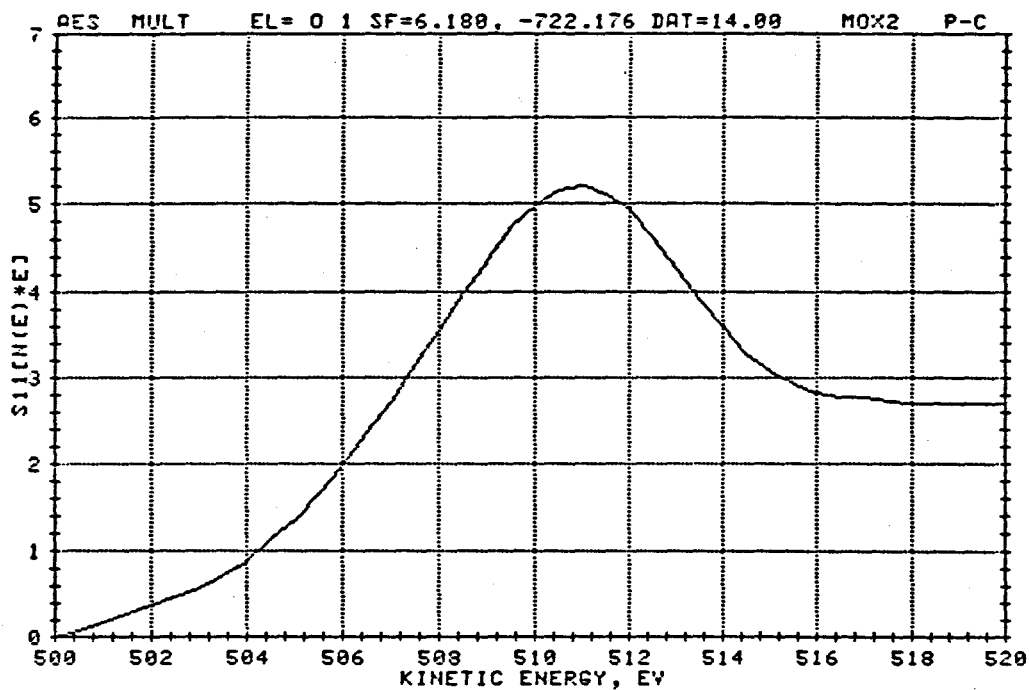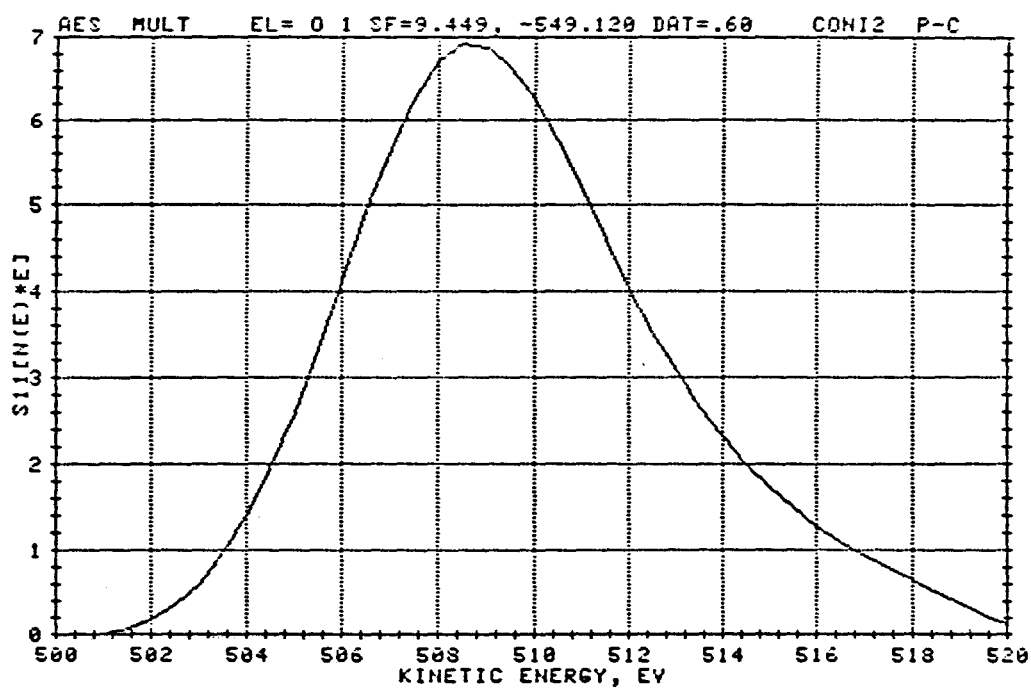
In fig. 30 the Auger peaks are schematic representations only and should not be taken as data, but the fact that the chemisorbed oxygen peak is shifted to higher energy than the oxide is real and is shown in fig. 31 where an oxygen signal from the very early stages (chemisorption) of an exposure experiment is presented with a signal from the latter stages where the sample (pure Cobalt standard) is oxidized. This observed shift is consistent with other work on Ni[90,102,103,105,109-111]. The vertical line in fig. 30 is set at 509 ev which is the peak energy used in producing Auger maps here (Auger maps plot the difference in counts between a defined peak energy and background divided by the background signal).

Given this information then, an Auger map should contain pixels whose intensity is proportional to the concentration of the analyte in the sampled depth and, in the case of islands, proportional to the depth of the island if the island height is less than the sampling depth and there is no analyte in the bulk. Fig. 32 a-f displays maps which were collected from one grain of a polycrystalline 79a/oNi-Co alloy held at 675 K and exposed to oxygen gas at $1x10^{-6}$ torr in a dosewise fashion. Fig 32a is an oxygen map at 0 exposure and the subsequent maps b-f are in chronological order where fig. 32f is after 75 mins. (4500 L). The beam voltage used for all maps was 5 kV and the resolution of the analyzer was set to 1%. The current density of the analysis beam was reduced to a

level that displayed no apparent beam damage for periods of time longer than that required to collect a map (typically 12 min.) since at very high current densities, some darkening of the map field and loss of a small proportion of the Oxygen Auger signal was observed if the beam was allowed to rest for long periods of time on one spot. Map collection was therefore conducted as quickly as possible and the electron beam turned off when not actually collecting data or contaminant checking sweeps. This sequence of photographs gives direct evidence for the existence of oxide islands which grow laterally at least and the next section details the method used to obtain numerical data from the maps.

For all the maps displayed here, a size marker could not be produced on-screen. An approximate scale has one side of a map being 20 microns.

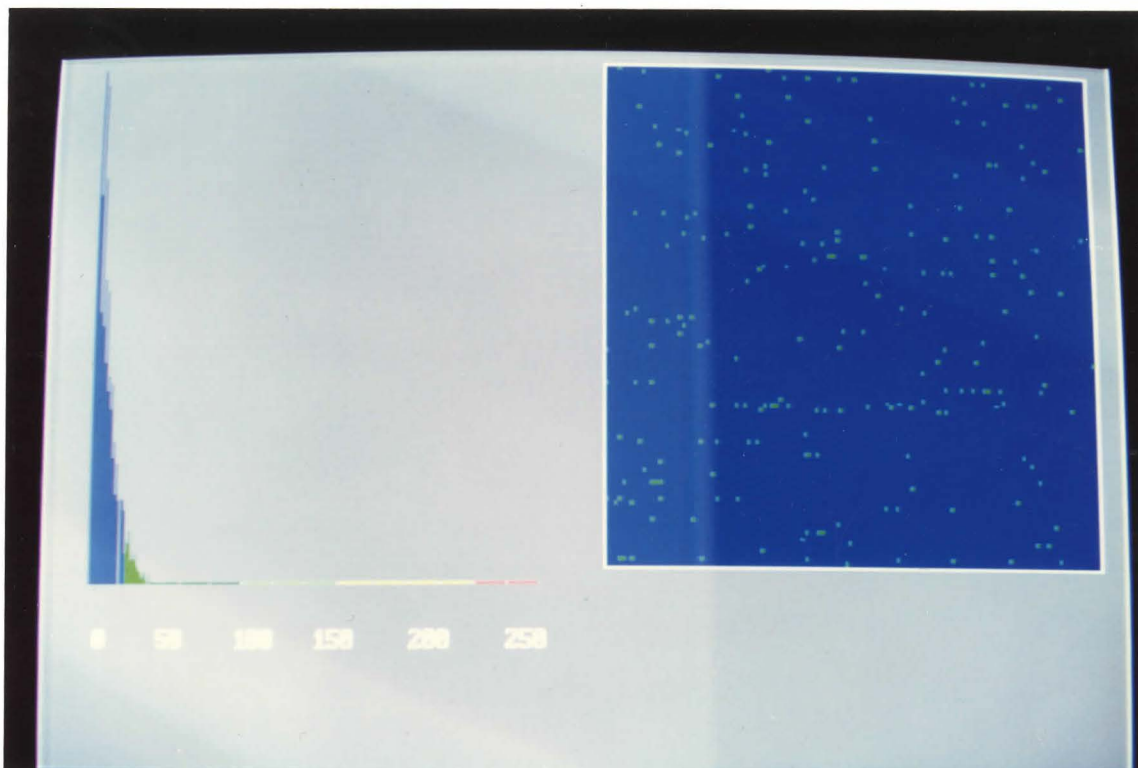---

Figure 32 a: Oxygen map at 0 exposure 675 K

Figure 32 b: Oxygen map at 2 min. 1×10^{-6} torr 675 K.
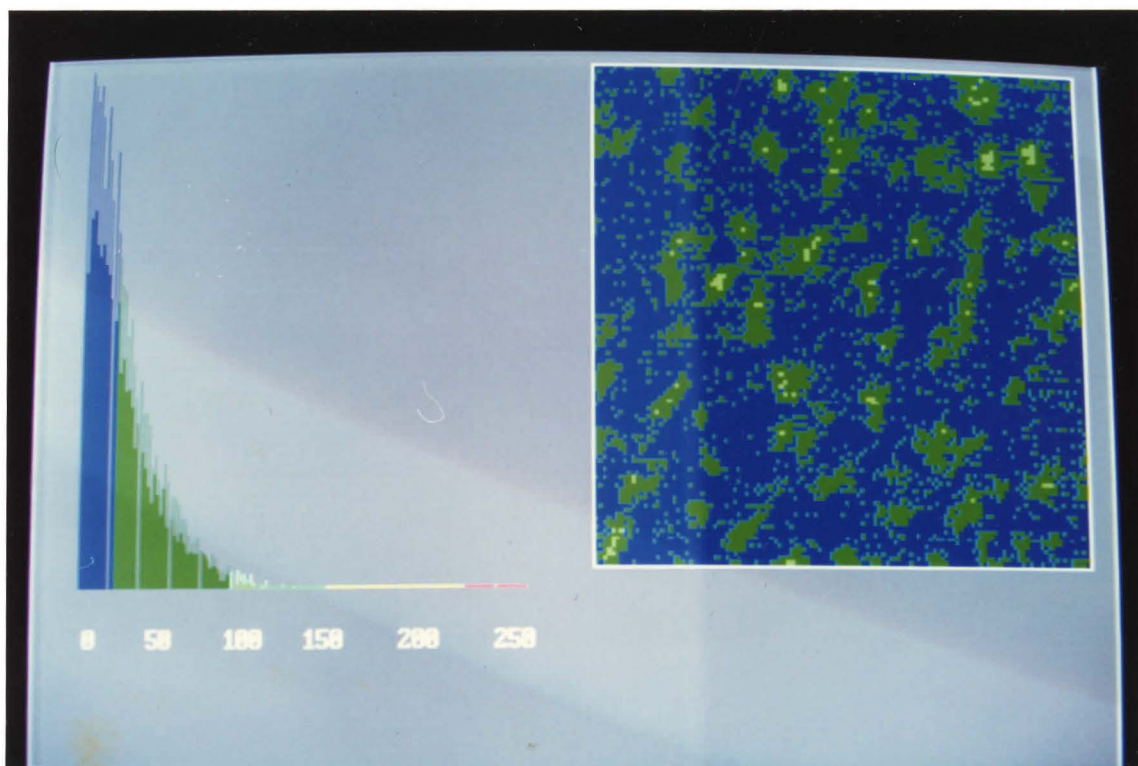
Figure 32 c: Oxygen map at 12 min. 1 x 10^{-6} torr 675 K
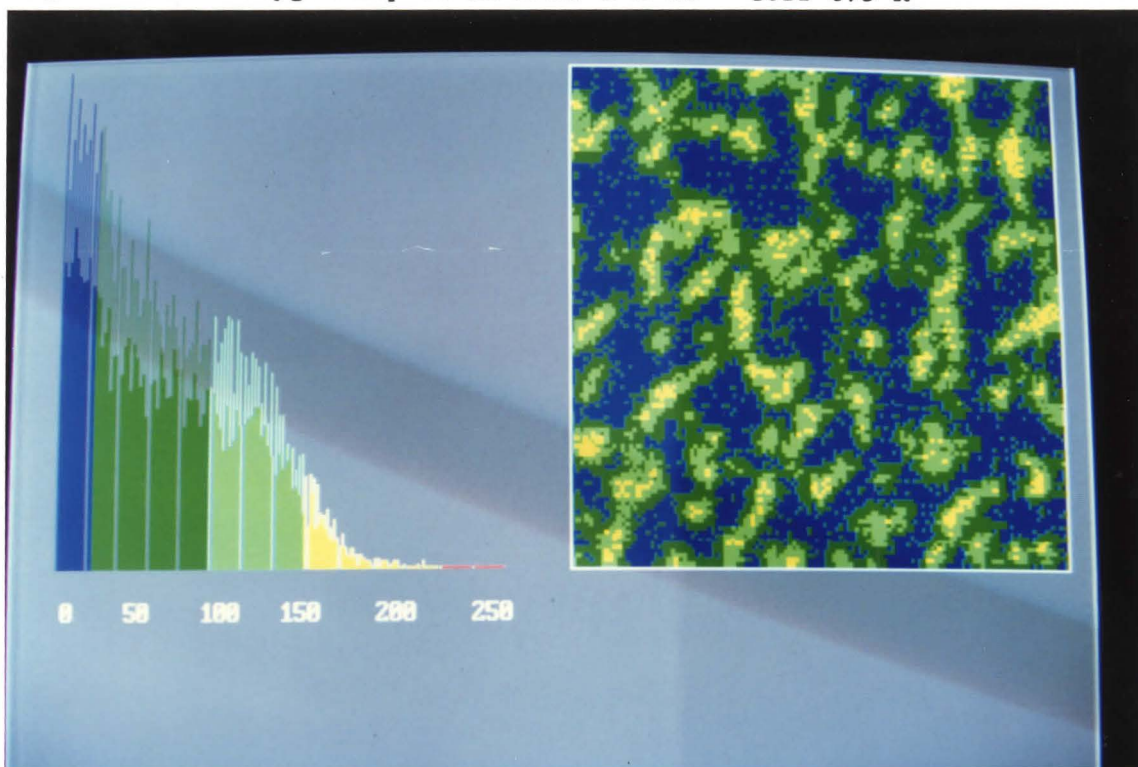

Figure 32 d: Oxygen map at 30 min. 1 x 10^{-6} torr 675 K.
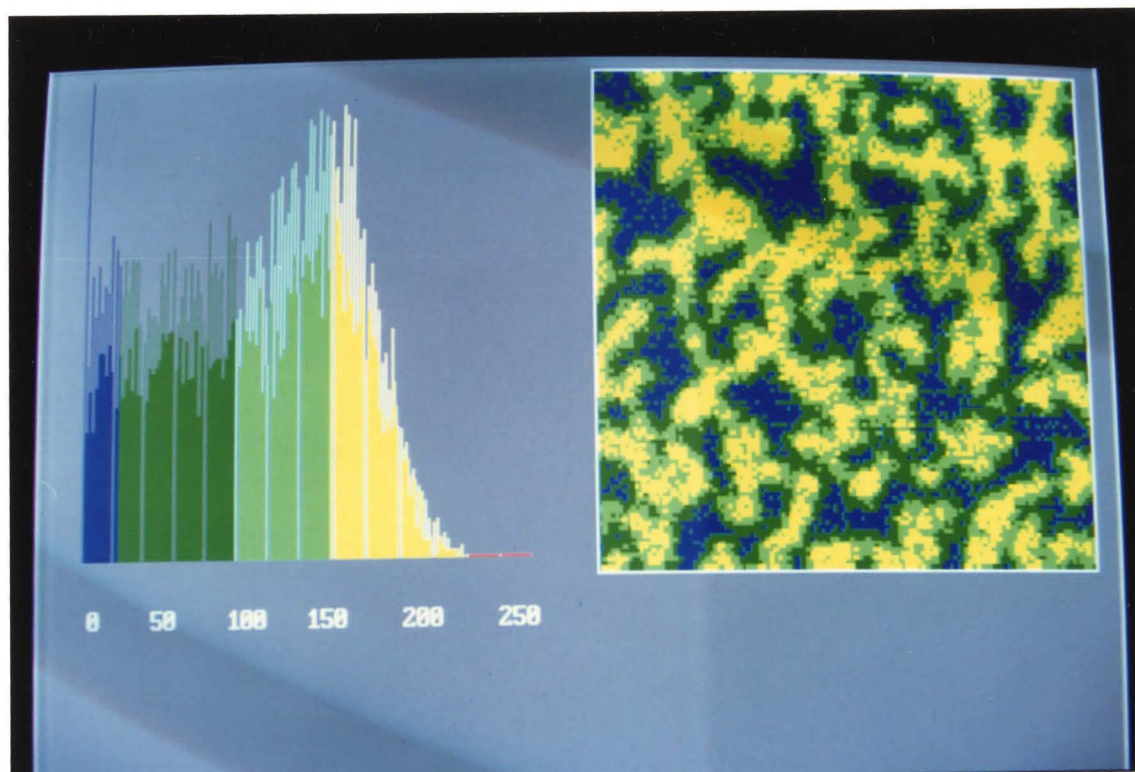
Figure 32 e: Oxygen map at 50 min. 1 x 10^{-6} torr 675 K.
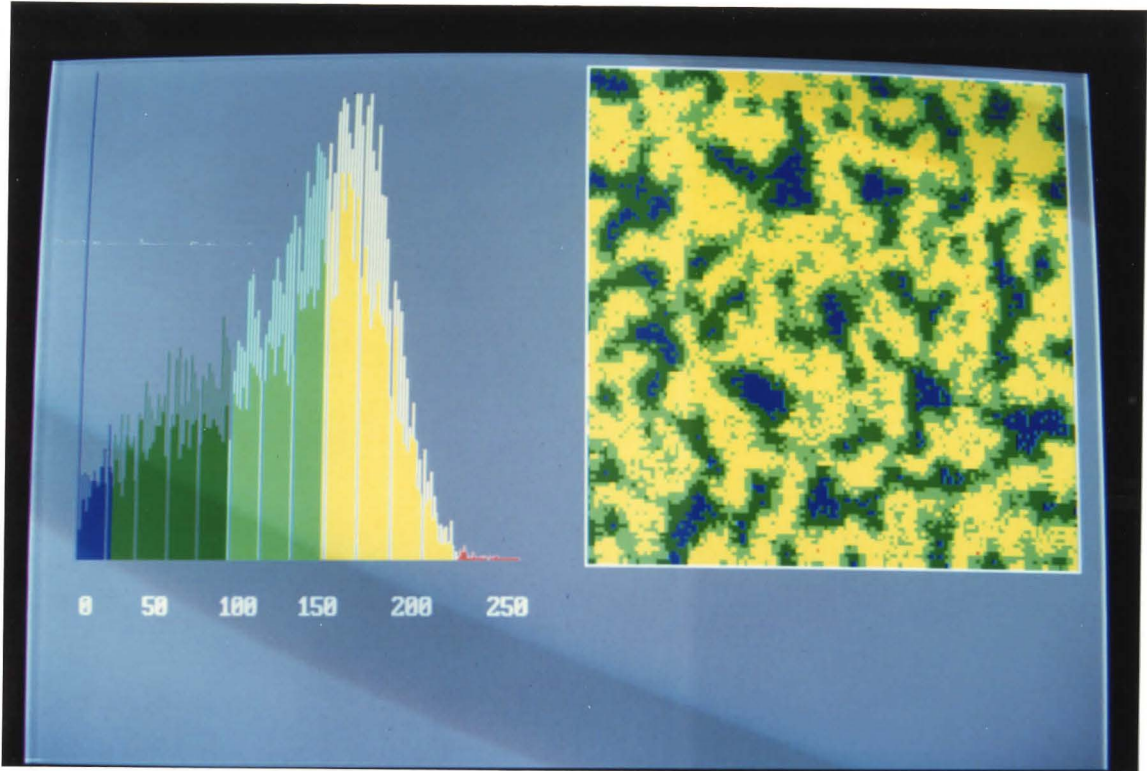
Figure 32 f: Oxygen map at 75 min. 1 x 10^{-6} torr 675 K.
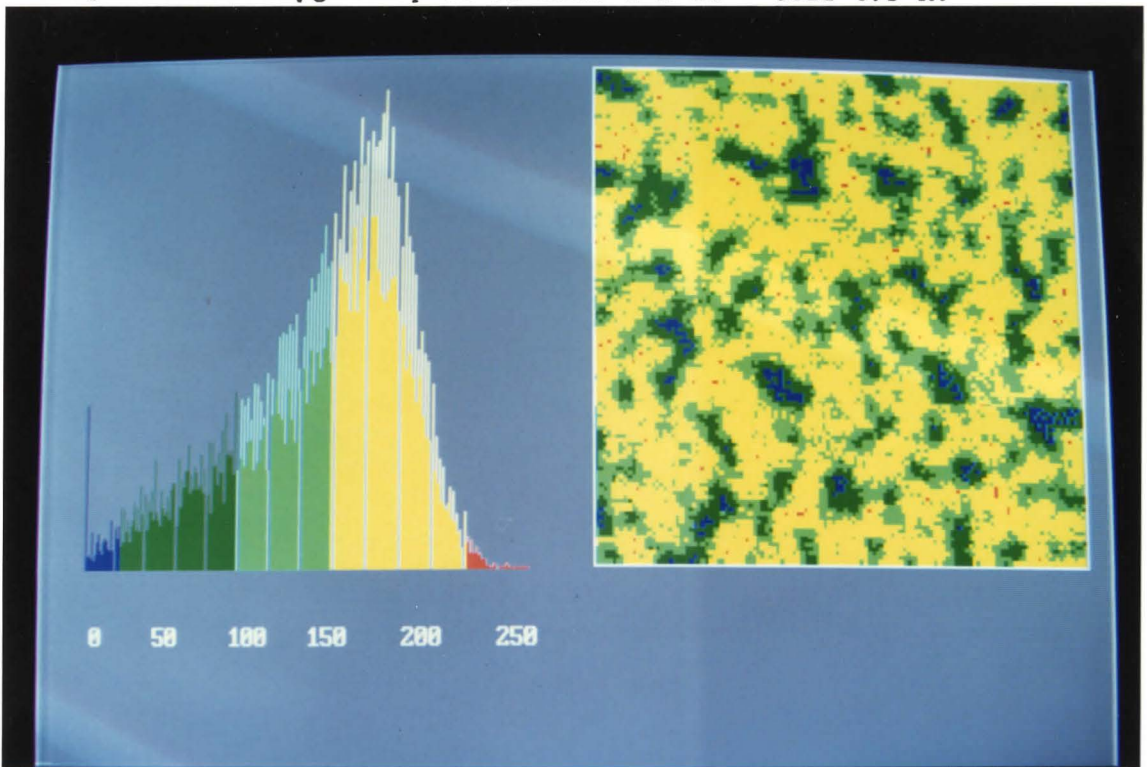
b) Data Handling: Digital Image Processing

With the establishment of the island growth mechanism in general, for this alloy system, the question of which process is limiting, arises out of the development of the model. In order to perform any kinetic experiments, it is necessary to obtain a numerical measure of the coverage at any one time. Towards this end, digital image processing has been employed.

The Auger maps can be reduced, via a computer routine, to a histogram of intensities for all pixels in the analysis window. From the preceeding arguments, peaks should be observed at discrete intensity levels, which correspond to differing island thicknesses. A clean metal will have lowest intensity while a chemisorbed signal should be at an intensity between clean metal and the first layer of oxide both because the positioning of the sampling energy means that only a shoulder of the chemisorbed peak is measured (see fig. 30) and the oxygen content in the sampling region is much smaller for chemisorbed O than for an oxide. One oxide layer will be next highest, followed by subsequent oxide layers up to the sampling depth. Random variation in any of the signals should give the intensity peaks a gaussian-like shape. Figures 32a-f have the corresponding histograms of intensity plotted next to the map. Close inspection of the histograms reveals the presence of up to, but usually less than, 5 heavily overlapped gaussians with peaks at intensity levels of 0, 60, 120, 160 and >220 (difficult to see).

The assignment of the zero level peak is easily made as that corresponding to bare metal (blue). The next peak is assigned as chemisorbed O_2 (dark green) and the following peaks as 1 layer of oxide (light green), 2 layers oxide (yellow) and >2 layers of oxide (red). No peak assignment is made for O_2 ads. for two reasons; i) at the temperatures used in this work (600 K and greater) the mean residence time of a physisorbed species is most likely vanishingly small[104] and ii) the probe electron beam would in all likelihood desorb such a weakly bound species if it existed on the surface at all. By dividing the histogram into 5 contrast levels (colors) which have been selected to bisect the difference between peaks of interest and their next neighbour, the color enhanced images of figs. 32a-f have been produced. This method of separating the histograms is admittedly crude and the preferred method would involve de-convolution but, such a programme was not readily available at the time and is non-trivial to produce. Therefore for the purposes of this study, the method of separating peaks by eye was used.

The data that can be extracted from such digitally enhanced images, results from the fact that the number of pixels in a given map are known, and a computer routine can sum all the pixels of the particular color (layer). The ratio of the number of pixels of a given layer to the total is therefore θ (the fractional coverage) for that layer. Plots of these individual θ's vs exposure (L = $1x10^{-6}$ torr.sec) are given for this series of maps in fig. 33a. The appearance of fig. 33a is at first somewhat confusing since the chemisorbed and 1layer

curves, reach a maximum and then decrease. The reason for this is of course the fact that where there is a signal for a 2layer, there must be
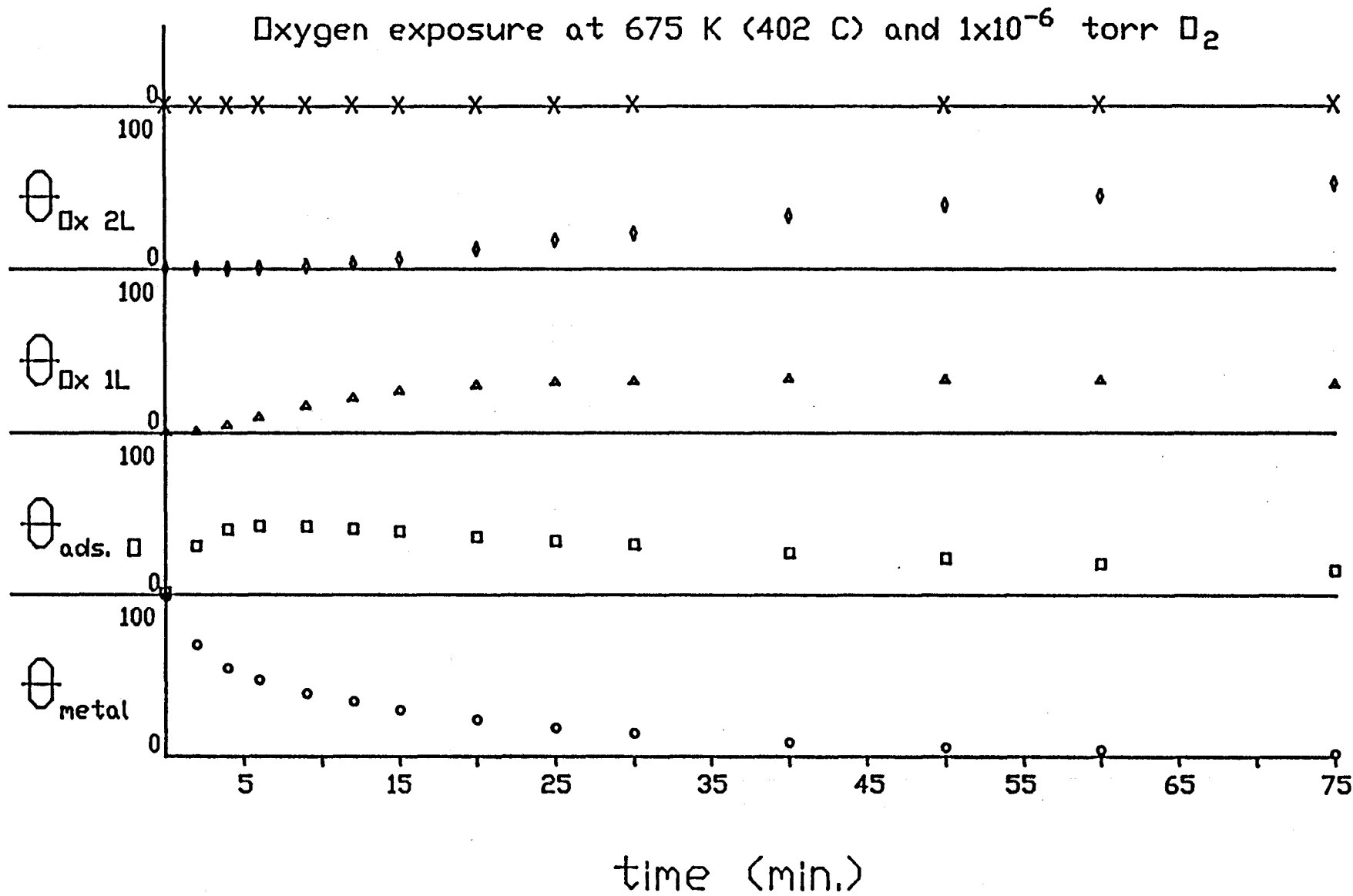
Figure 33 a: Observed fractions of pixels for figs. 32 a-f.

Oxygen exposure at 675 K (402 C) and 1×10^{-6} torr O_2

second layer islands impinge

$\theta_{Ox\ 2L}$

first layer islands impinge

$\theta_{Ox\ 1L}$

$\theta_{ads.\ O}$

θ_{metal}

Exposure (Langmuirs)
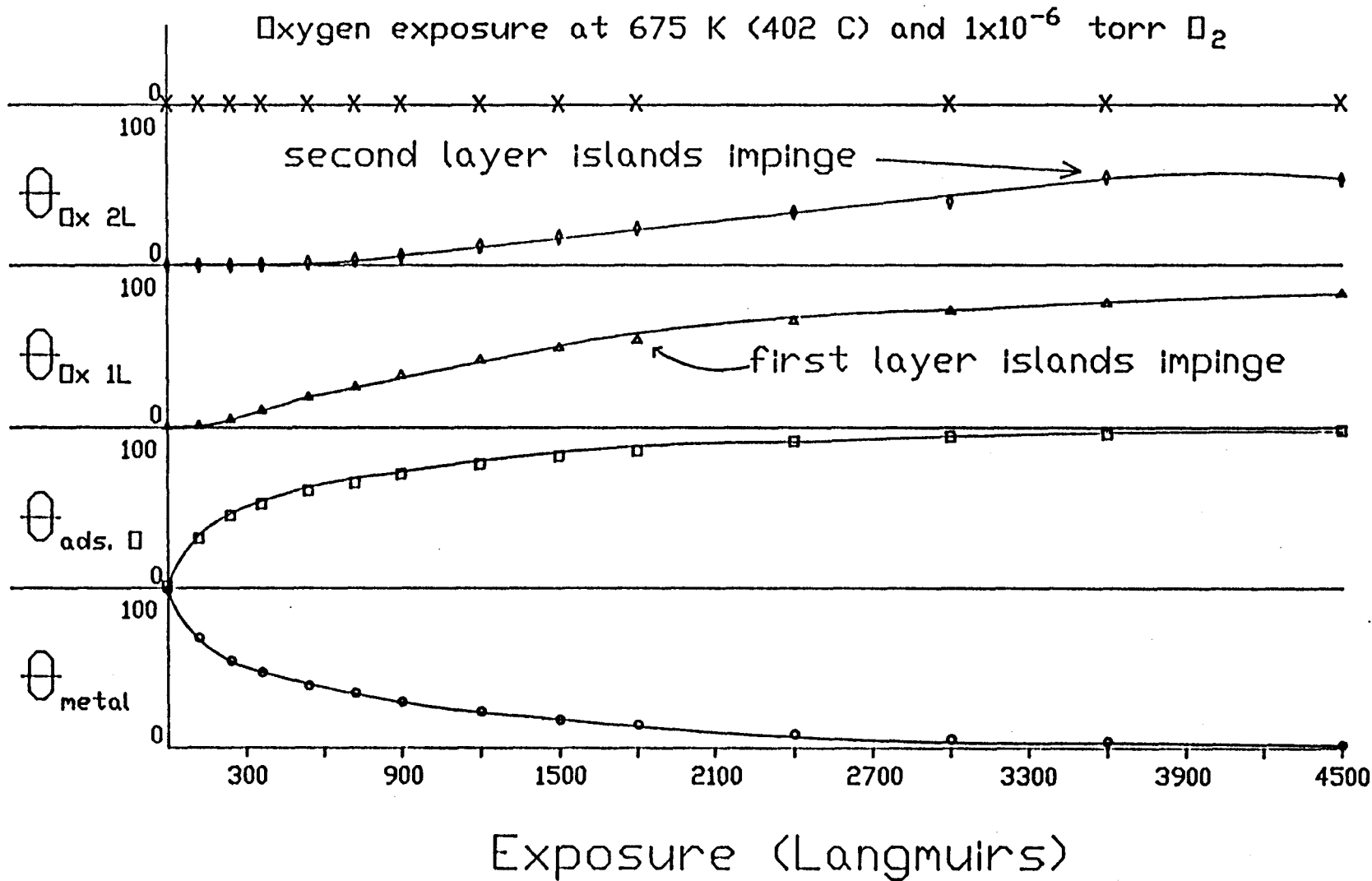
Figure 33 b: Corrected fractional coverages for figs. 32. a-f.

First Oxide layer at 600 K

Percent area vs Exposure time (min.)

- 1×10^{-6} torr (dotted)
- 5×10^{-7} torr (dashed)
- 1×10^{-7} torr (solid)

a 1layer underneath and where a 1layer exists, there must have been chemisorbed O present before etc.. The data in figure 33a must be altered to reflect this fact by adding the fraction of all deeper species to the fraction obtained directly from the map. Figure 33b is a plot of the corrected θ's. The chemisorbed layer curve is just the mirror image of the metal curve and corresponds to the fraction of the surface that is at least covered in chemisorbed O ($\theta_{ads.}$).

10-2 Results and Discussion

Inspection of figures 33b and c (a condensation of other exposure experiments with conditions listed) yields some very important observations regarding the kinetics of the island growth mechanism:

1)The shape of the curves for θ_{metal} and $\theta_{ads.}$ is comparable to the shape of the θ vs. L curves of HH[105] which have been more adequately investigated elsewhere and identified as proceeding via a dissociative Langmuir or a modified dissociative Langmuir type adsorption isotherm (see previous chapter).

2)At least the first oxide layer grows via a three stage process, as indicated by apparent break points on the curves. The proposed interpretation of this observation is that the stages in chronological order are;

i) rapid growth due to nucleation--beyond this bend in the θ_{1Layer} curve, no new islands are observed to nucleate on the maps.

ii) an apparently linear increase in θ probably due to lateral growth limited by the rate of gas impingement close to the edge of the growing islands.

iii) non-linear growth due to the decreasing active area at the perimeter of islands as they impinge on neighbouring islands. The onset of this part of the graph corresponds exactly to the observation of impingement on maps.

3) The rate of growth in the second oxide layer (linear lateral growth) is different from that of the first layer (a distinct nucleation phase was not evident). This leads to the possibility that the geometry (sticking probability) at the edge of a second layer island is different from that at the edge of the first oxide layer.

4) Nucleation occurs at preferred sites both away from and on grain boundaries, which are reproducible from experiment to experiment.

This interpretation of the processes involved in island growth is consistent with the assertions of Brundle[104] and Mitchell et. al.[110,111] who also concluded that the rate limiting step is direct gas impingement at island edges.

With this mechanism and the experimental observation that when nucleation has stopped, θ appears to vary linearly with time, it is

possible to describe the kinetics of the lateral growth of islands prior to island impingement under these conditions. The rate of growth of the oxide islands $d\theta/dt$ can be written as;

$$d\theta/dt = K_i P \qquad 10.3).$$

We notice that the islands in all experiments are not circular as in the Holloway-Hudson model, but long and growing in width. This means that K_i appears not to be a function of θ as might be intuitively thought because the length of the active edges of the islands change so slowly as to allow the "active area" to be thought of as being essentially constant until impingement. An illustrative comparison can be made if a rectangle is imagined to have a long dimension of 10 units and a short dimension of 1 unit. At the beginning, the area is 10 square units and the perimeter length is 22 units. If the short direction is doubled while the long direction remains the same, the new area is 20 square units (an increase of 100%) while the perimeter is now 24 units (an increase of only 9%). Making the assumption that the islands in this experiment behave similarly to the long rectangle i.e. essentially constant active area, the surface coverage of an island layer i at time t after the end of the nucleation phase would then be;

$$\theta_i = k_i P t = k_i L \qquad 10.4)$$

where $P = (2mkT_g)$, L is a Langmuir $Pt = 1x10^{-6}$ torr.sec. and k_i in the simplest possible model is the fraction of gas collisions that successfully incorporate Oxygen into the oxide island and is therefore an activated process;

$$k_i = k_i^{\circ} \exp^{-(E_c)/kT} \qquad 10.5)$$

where E_c is the activation energy of the incorporation process.

Although the evidence from the exposure curves and maps is very strong, a test of the interpretation needed to be made. The simplest test of the interpretation was to conduct a series of experiments where both P and T were independently varied during the reaction and the rate of lateral growth measured. During these experiments it was also possible to test some other aspects of the interpretation.

It has been pointed out that nucleation at these elevated temperatures is likely to occur only at preferred sites such as defects and grain boundaries where the local chemisorbed O density may more easily reach a critical value for nucleation. To check this, maps would need to be obtained in the region of grain boundaries and since the conversion of impinging gas is asserted to be determined by the nature of geometry at the island edges, it is also reasonable to assume that there

Figure 34 a: Very early stage of Oxygen exposure showing the nucleation of islands at grain boundaries and also, to a lesser extent away from the grain boundary and presumably at defects.
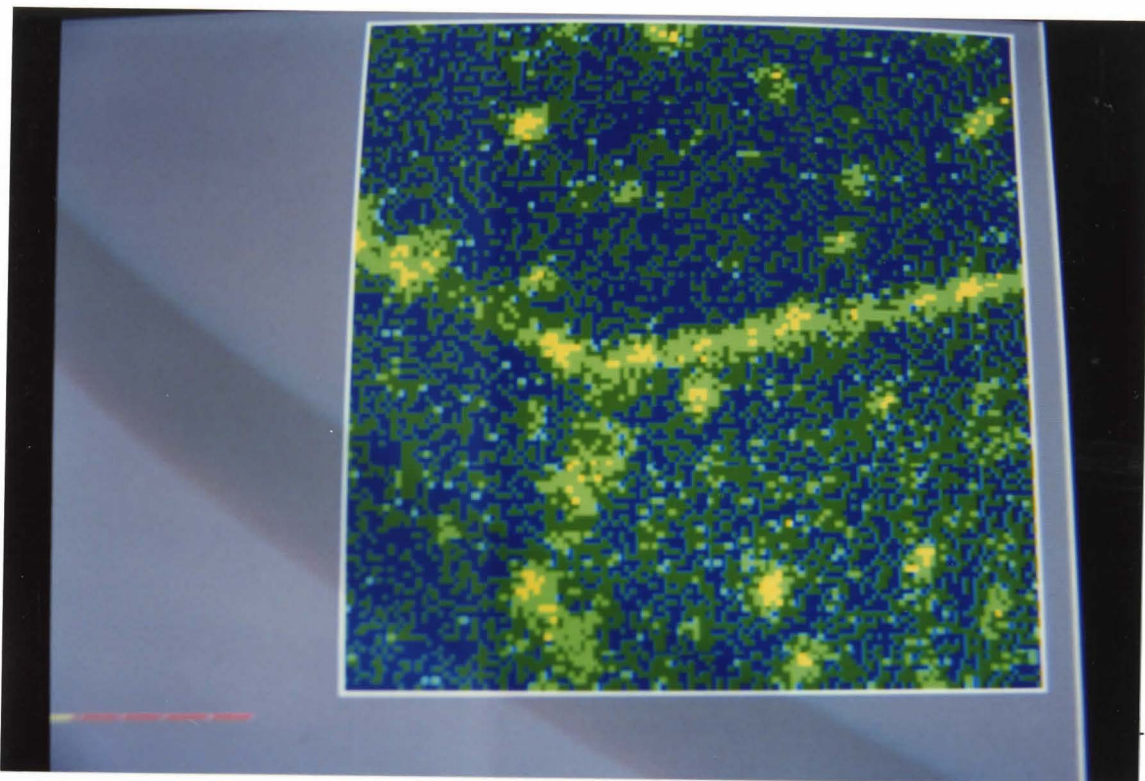
Figure 34 b: Dependence of island growth on crystallographic orientation.
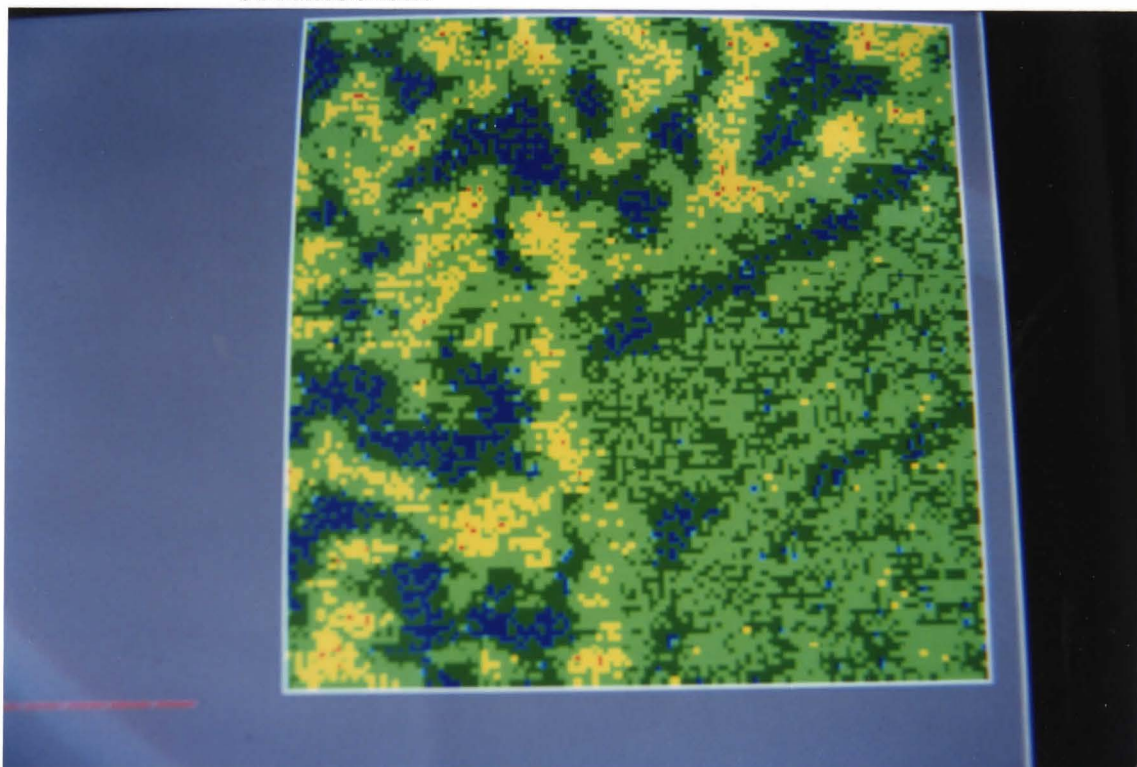
is a crystallographic effect. To check these two points simultaneously, as well as, to get average kinetic data, maps were collected at a triple grain boundary during oxygen exposure P and T experiments.

The question of nucleation site selection is addressed in figure 34a where it is clear that nucleation does occur first at grain boundaries, but also at other sites on the surface where presumably there were defects (SEM images at 5000X did not reveal any obvious defects at the identifiable and repeatably preferred sites for nucleation away from the grain boundary). The question of whether or not there was a crystallographic dependence is illustrated very clearly in fig. 34 b. The lower right hand grain grows the second layer oxide much slower than the other two grains despite the fact that the apparent coverage of chemisorbed Oxygen and the first oxide layer is higher on that grain, than on the others. Unfortunately attempts to determine the orientation of the grains by electron channelling patterns were not successful owing to the small size of the grains and the difficulties associated with this method.

To test for a dependence on pressure, three different pressures were used at a constant temperature and the results are summarized in figs. 35a and b. In figure 35a the coverage of the first layer of oxide vs. exposure is plotted for three different pressures and within experimental error, the rate of lateral growth is dependent only on the total exposure in Langmuirs, consistent with 10.4). The second layer data is less conclusive due to experimental scatter but the conclusion can probably still be made that total exposure is controlling the rate of growth at a fixed temperature.

First Oxide layer growth at 600 K

% area (θ)

Exposure (L)

.... 1×10^{-6} torr
- - - 5×10^{-7} torr
——— 1×10^{-7} torr
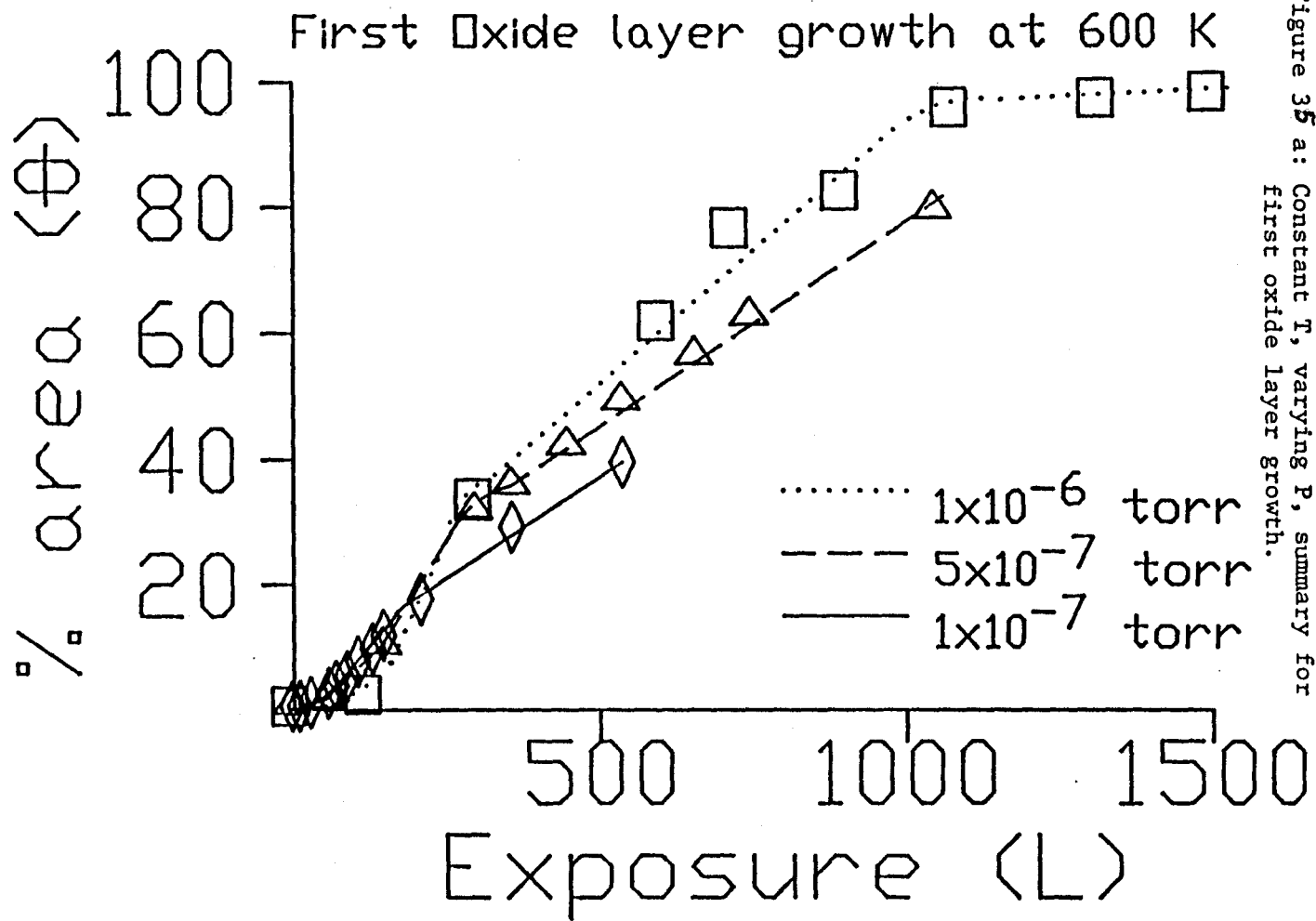
Figure 35 a: Constant T, varying P, summary for first oxide layer growth.
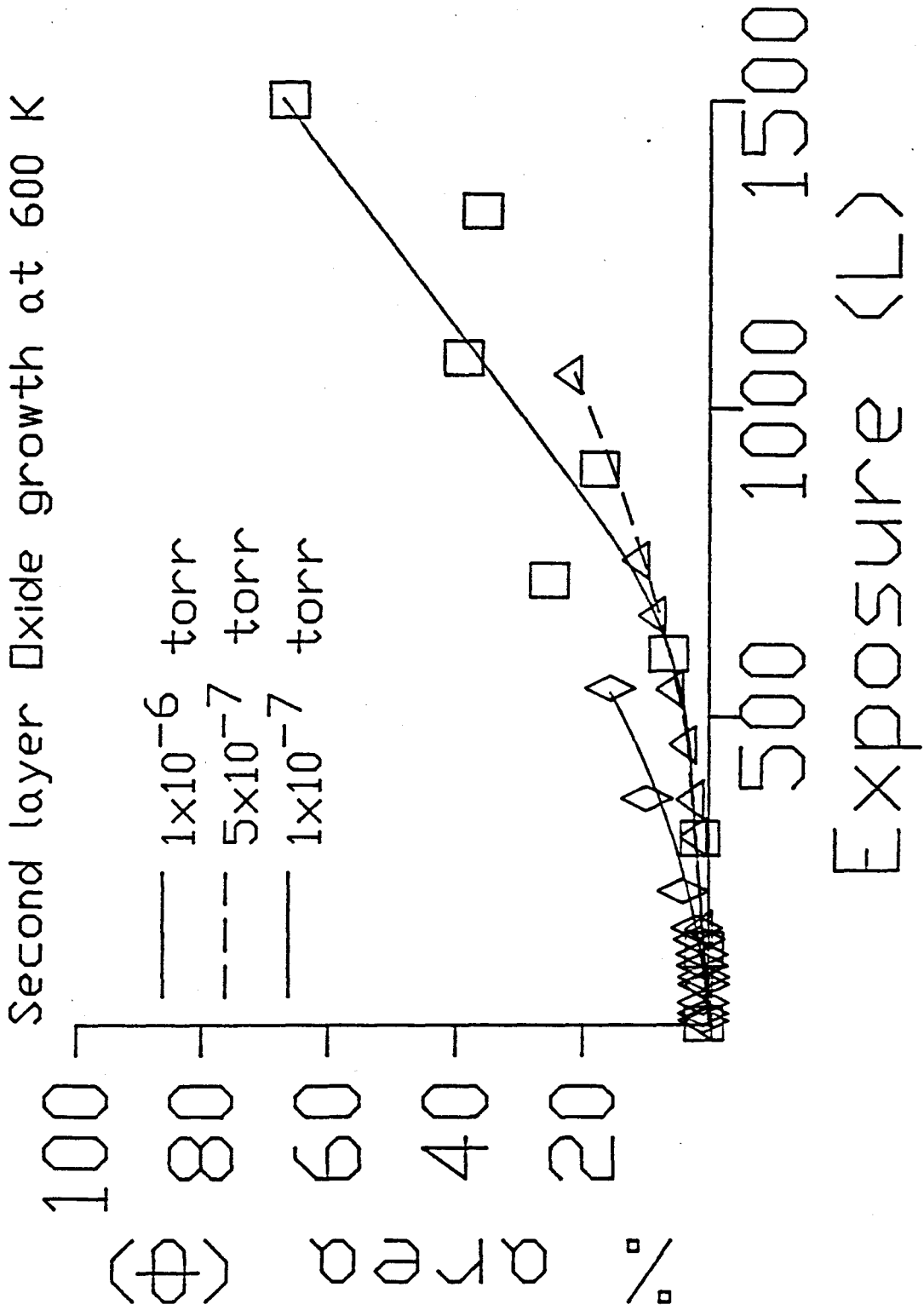
Figure 35 b: Constant T, varying P, summary for second oxide layer growth.

First Oxide layer 1×10^{-6} torr O_2

Percent coverage (θ)

Exposure (L)

— 600 K
---- 650 K
— — 660 K
········ 675 K
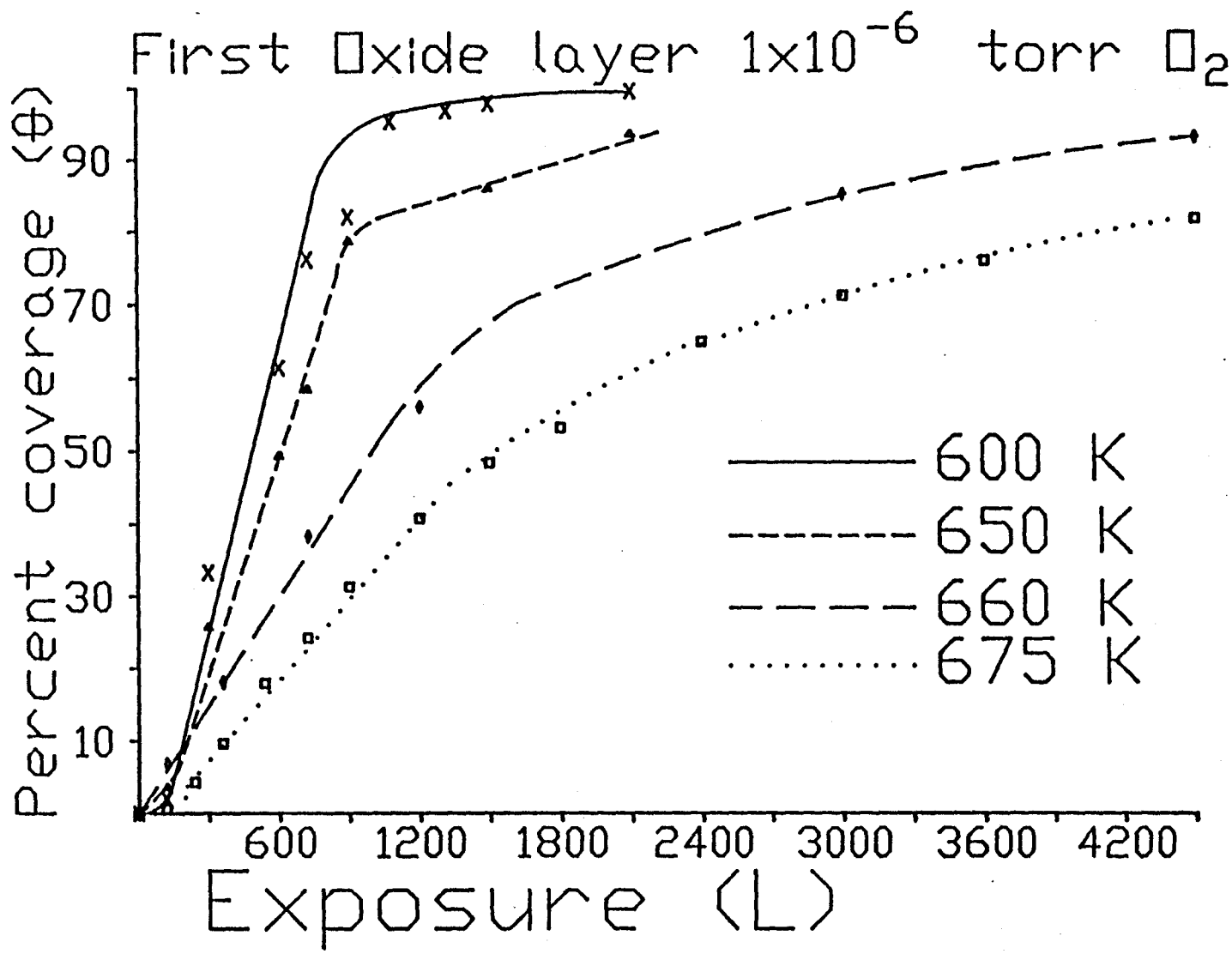
Figure 36 a: Summary of constant P, varying T, for first oxide layer growth.

151

Figure 36 b: Summary of constant P, varying T for second
oxide layer growth.
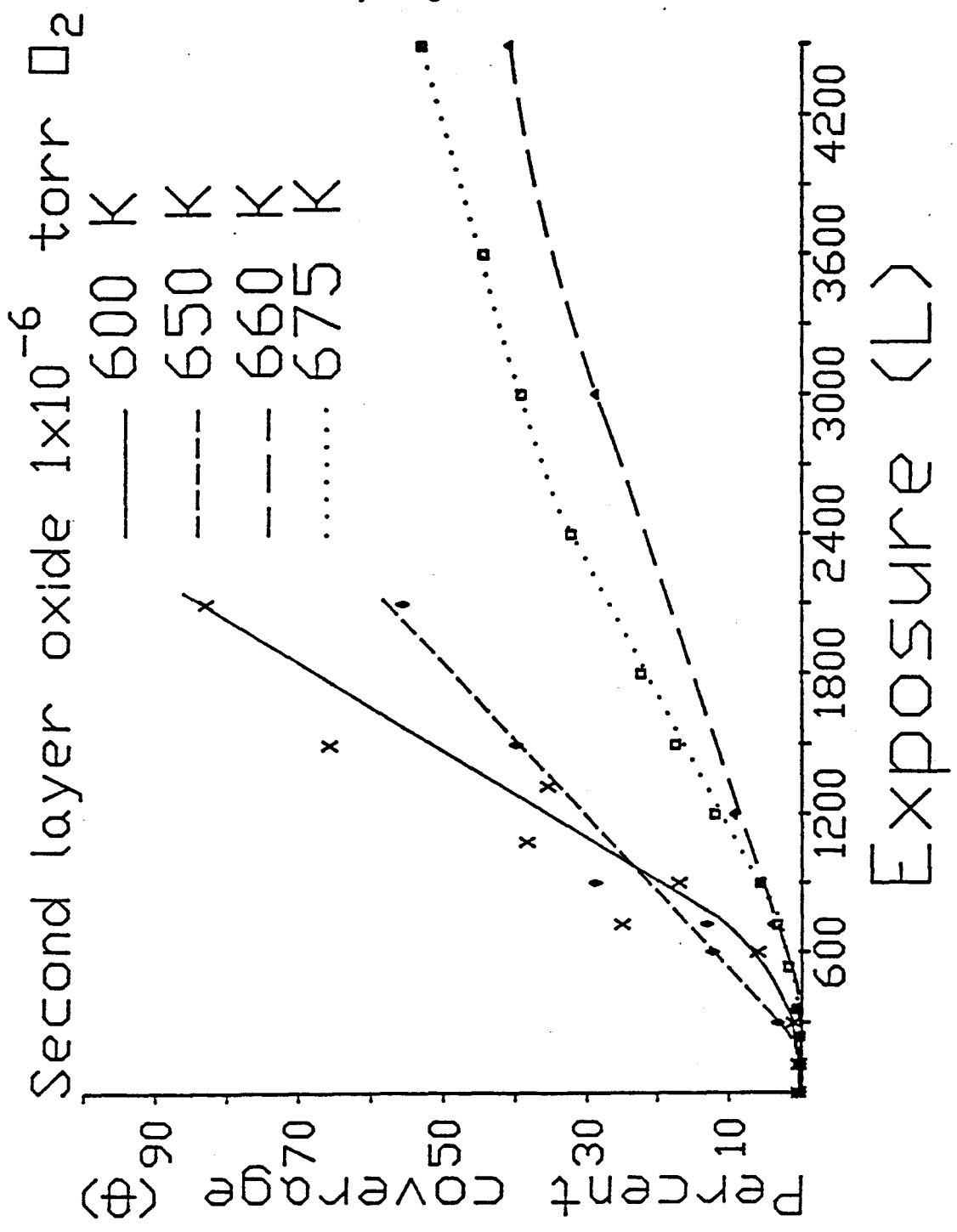
The dependence on temperature study is summarized in figs. 36a and b. In fig. 36a, the rate of the first oxide layer growth is markedly dependent on temperature. It is interesting to note that increasing temperature decreases the rate of growth. This may indicate that in fact there are two processes in competition during the linear growth phase. One process is the incorporation of oxygen, presumably from direct impingement and dissociation, the second process is probably either the bulk dissolution of oxygen or desorption. The observed rate is therefore a net rate such that:

$$k_i = k_c - k_D \qquad 10.6)$$

where k_c is the rate of capture and k_D is the rate of dissolution into the bulk or desorption. If it is assumed that capture is an un-activated process (or one with a very low activation barrier), then E_c (the activation energy of capture) can be assumed to be zero and;

$$k_i = k_i^o \exp^0 - k_D^o \exp^{-E_D/kT} \qquad 10.7)$$

therefore

$$k_i = k_i^o - k_D^o \exp^{E_D/kT} \qquad 10.8)$$

This dissolution into the bulk or desorption would therefore explain why the rate of island growth increases with decreasing temperature.

$$\theta = L(k_i^0 - k_D^0 exp^{E_D/kT}) \qquad 10.9)$$

Experiments have been performed where oxygen exposure has generated islands which were then heated to a greater temperature than the original exposure in vacuum. The background gas was monitored for any signs of evolving O_2 or oxygen containing species with a quadrupole mass spectrometer residual gas analyzer mounted proximal to the sample, but none were observed. This result, although not absolutely conclusive, does not support the notion of gas desorption as the competing process and leaves bulk dissolution as the most likely candidate. From the four curves of fig. 36a, it is also possible to extract the factors k_i^0 and k_D^0 for the various temperatures and an Arrhenius plot may yield a value for the activation energy. This approach is possible, but in light of the fact that there is data available for only four temperatures over a range of 75K, such a determination would be of limited value. This type of experiment may be particularly useful in future studies on single crystal faces.

The second layer oxide also exhibits evidence of increasing growth rate with decreasing temperature, since out of the four curves, three display a trend similar to that for the first oxide layer with only the 660K or 675K being out of the expected order.

The variation of the fractional coverages for the chemisorbed layer with temperature is shown in fig. 37a and as expected, lower temperatures allowed the chemisorption to proceed more rapidly, presumably

since the rate of desorption or bulk dissolution will increase with increasing temperature. The variation of chemisorption with pressure is somewhat less clear here and is presented in fig. 37b. At the highest pressures used in this thesis, saturation at θ = 100% ensues after a certain level of exposure and the total exposure required to saturate, increases with decreasing pressure. The results of further investigation into this is summarized in figs. 38a-e.
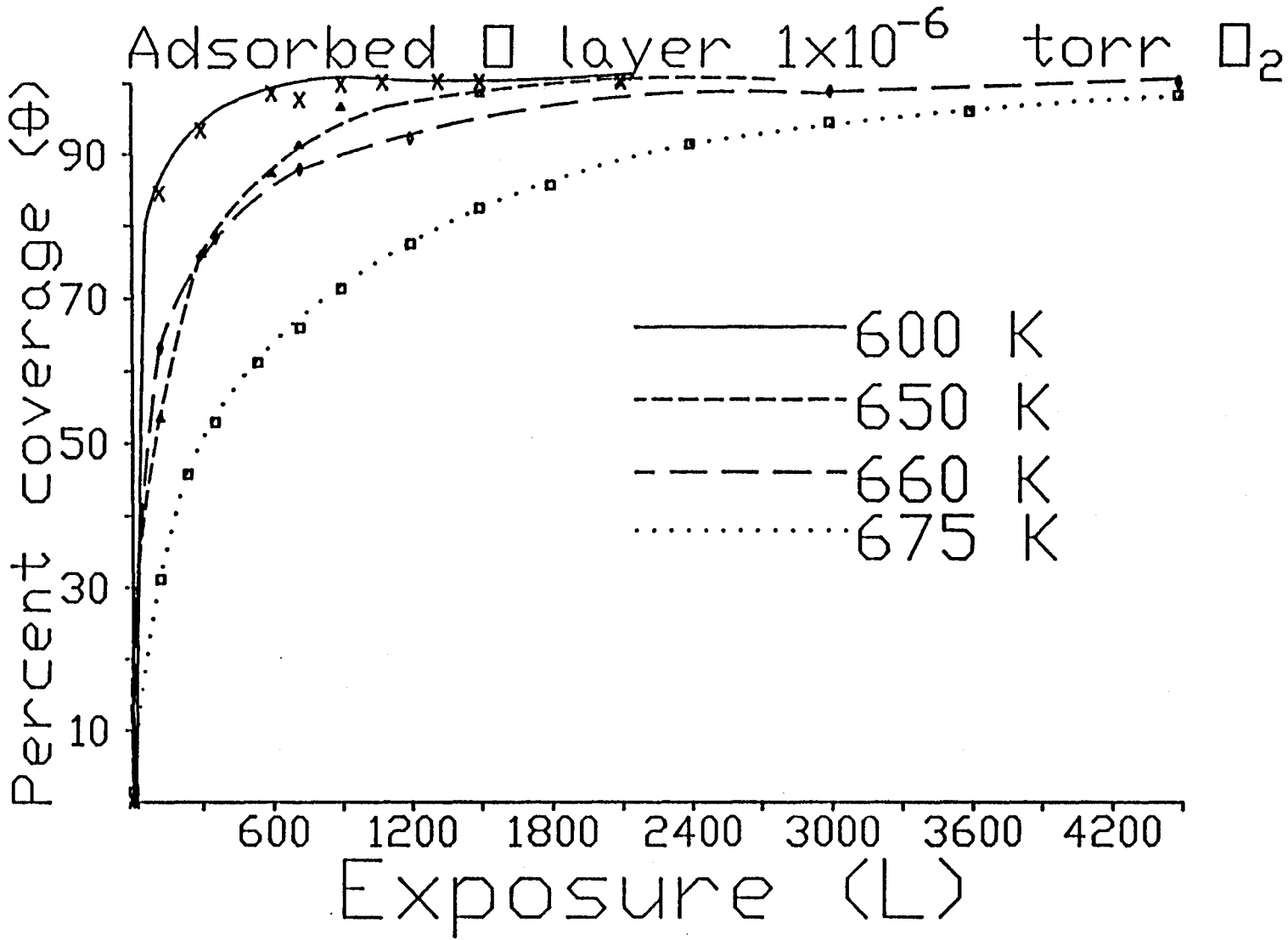
Figure 37 a: Summary of constant P, varying T, for chemisorbed layer.

Figure *37* b: Summary of constant T, varying P, for chemisorbed layer.
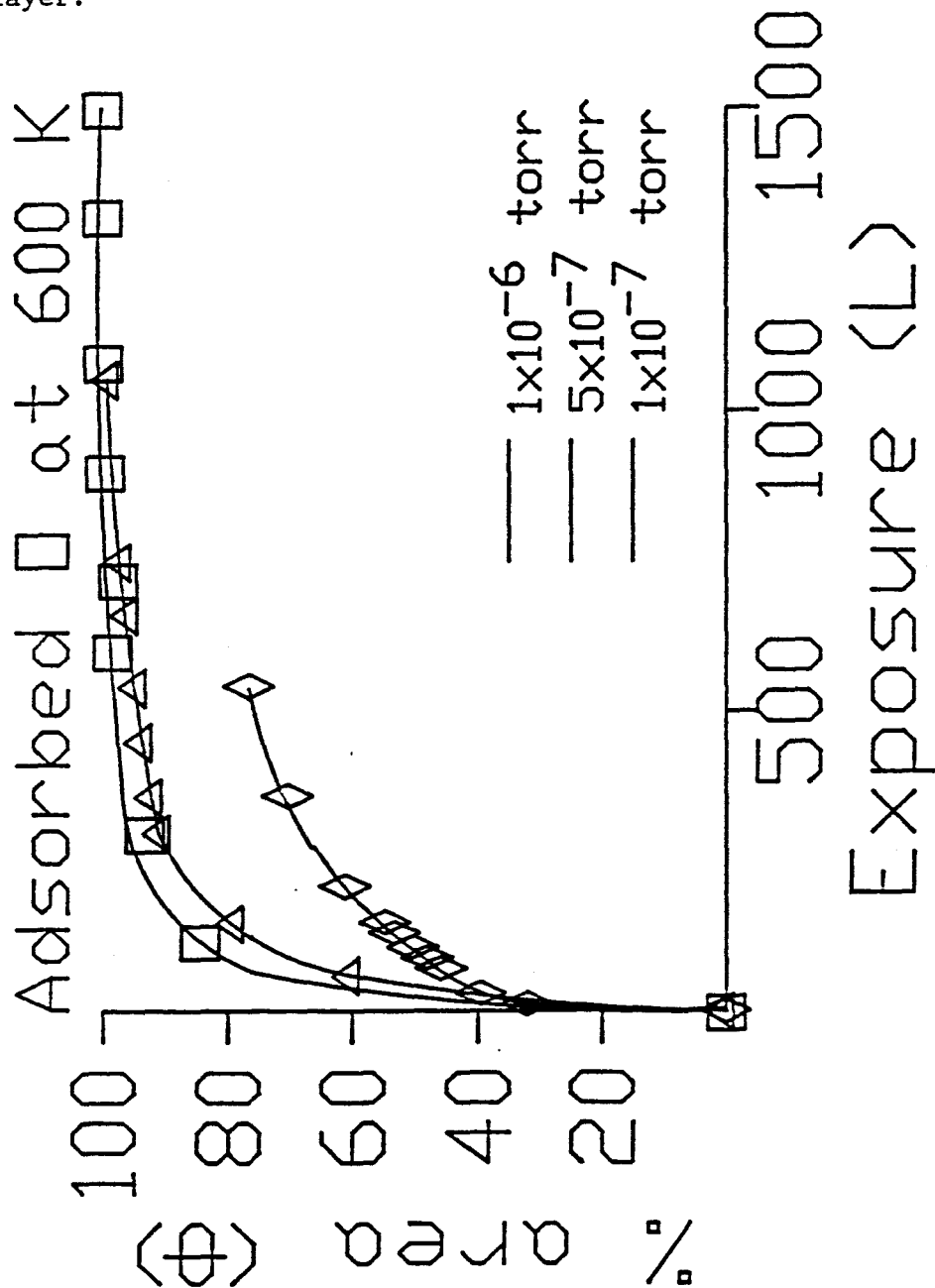
Figure 38 : Varying pressure experiment over wide range.   Establishment
of equilibrium fractional coverages of chemisorbed O?

Fractional coverage vs. exposure (L) at 650 K
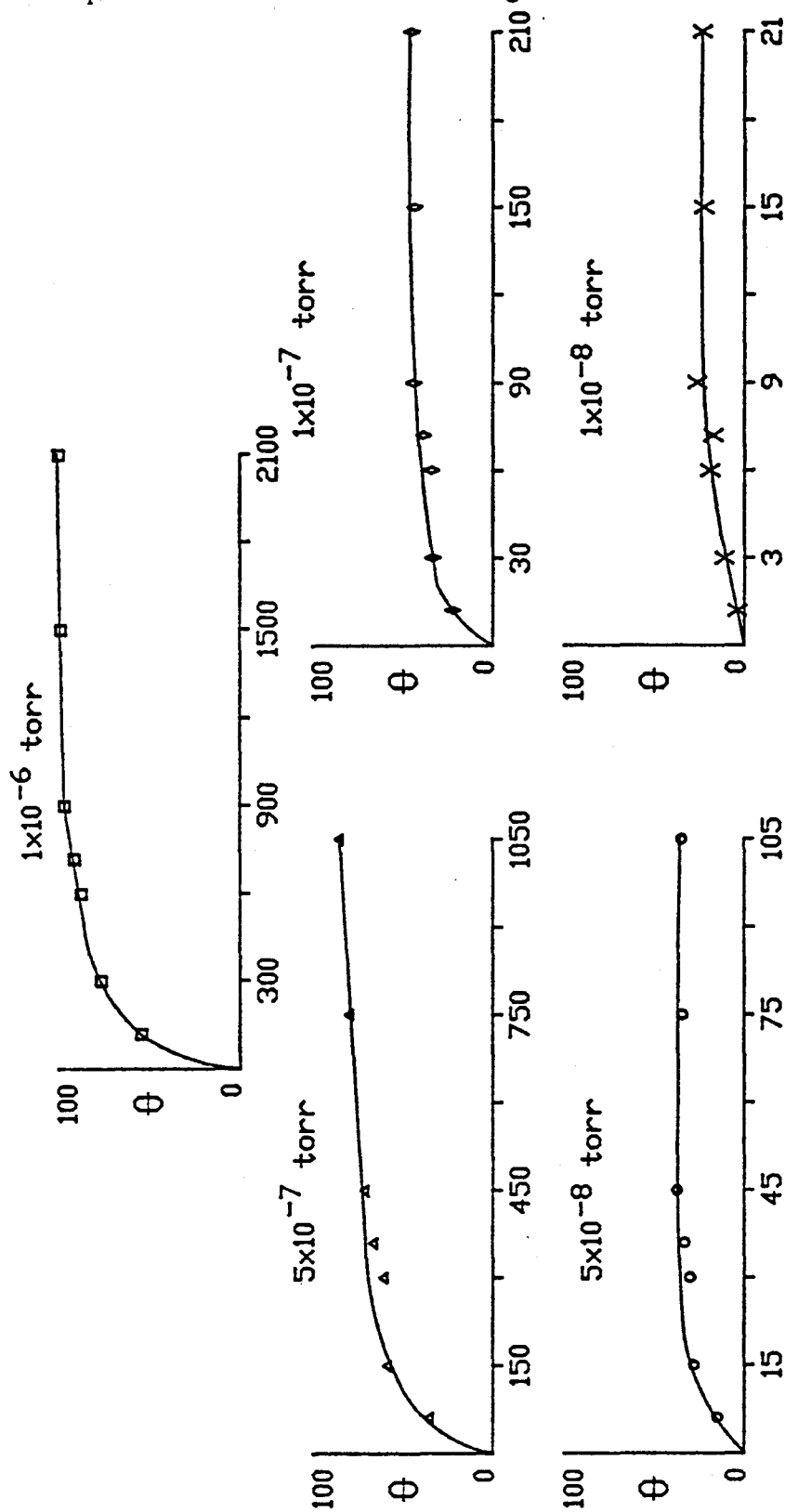
The sequence of graphs in figure 38 indicate that there is some saturation level of chemisorbed oxygen coverage which is pressure dependant. This dependence on pressure may be the result of repulsive interactions between chemisorbed O atoms on the surface. Because chemisorption is dissociative, a surface site which can incorporate both Oxygen atoms would be greatly preferred over a site where significant re-arrangement is required before both atoms can be accomodated. Lower surface collisional rates (pressures) may allow significant re-arrangement of surface adsorbed species in order to minimize repulsive interactions. Such a uniformly distributed surface with most preferred dissociation sites occupied, may establish an equilibrium fractional coverage such that the impingement and dissociation rate, which has been reduced greatly by the saturation of "most preferred" sites, is just balanced by normal thermal desorption. The effect of increasing pressure may be to increase the number of statistically less favourable dissociations at higher O coordinated sites, until a new equilibrium coverage is achieved etc.. From fig. 38 the apparent equilibrium fractional coverages for differing pressures are;

$$1 \times 10^{-6} \text{ torr} \qquad 100\%$$
$$5 \times 10^{-7} \text{ torr} \qquad 100\%$$
$$1 \times 10^{-7} \text{ torr} \qquad 45\%$$
$$5 \times 10^{-8} \text{ torr} \qquad \simeq 33\%$$
$$1 \times 10^{-8} \text{ torr} \qquad \simeq 25\%$$

From the above sequence of data, it is unclear if the equilibrium fractional coverage is a continuous function of pressure or if there are definite stages involved in chemisorption here, as there are in the Ni/O system. Inspection of the above data might suggest that the intuitively satisfying trend of fractional coverages being 1 in 4, 1 in 3, 1 in 2 and 1 in 1 for increasing impingement rates is being obeyed. This interpretation however suffers from the lack of LEED data which might confirm or refute the situation as described. Furthermore, since differing crystal faces are being simultaneously sampled, fractional coverages will not necessarily have a real significance.

The final experimental observation that must be addressed has to do with the effect of this system being an alloy, on the island growth kinetics. As mentioned in chapter 9, the effect of the substrate metal being an alloy must be to introduce another possible rate limiting step, that step being diffusion from the near surface region to the edges of the oxide island where the reaction with Oxygen takes place but that has been discounted here owing to the short distances that the metals must diffuse. It has been mentioned that quantitation on this type of surface would be difficult but, a rough estimate of the general trend in composition of the oxide might be obtained by monitoring the ratio of the highest energy Ni peak to the 654 eV Co peak. For the alloy in question here, the starting (sputtered surface) ratio of these two peaks was Ni:Co = 4.08. After 35 mins exposure at 1×10^{-6} torr the ratio had dropped to 2.14 and after 50 mins. was 2.41 and 60 mins. was 2.43. From this limited data it may be concluded that in the sampling depth of the Auger

electrons, CoO is being preferentially formed. The recent work of Majumdar et.al. 1986[116] on the oxidation of a 20 a/o Ni-Co alloy has indicated that for conditions virtually identical to those employed in this study, a very thin layer of CoO is formed exclusively and Ni remains in the metallic state for exposures of up to 4500L at 773K. The Ni Auger signal which is still visible after this exposure, was thought to originate from beneath a uniform overlayer of oxide but, the results of this study indicate that Ni signal could also have originated in the spaces between islands since the formation of a truly complete overlayer appears to be a very slow process at these conditions. This preference at the surface for Co is most graphically displayed in figs. 39 a-c where fig 39 a is an Oxygen map, fig. 39 b is the corresponding Ni map and fig. 39 c is the Co map. From the maps of fig. 39 a and b, clear and strong negative correlation of oxide islands with Ni is evident. The Co map of fig. 39c shows a definitely weaker negative correlation with oxide, probably due to the fact that the atomic density of Co in CoO is less than that of the alloy.

The question of why the Holloway-Hudson model has been well obeyed in the past remains to be addressed. This present work is not only the first to image very thin islands successfully, but is also the first that has attempted to separate the signals from layers in the islands. All of the previous "Oxygen uptake" data has been extracted from the intensity of Oxygen Auger peaks which presumably originated from electron beams which had diameters larger than the islands being proposed

by the model (100 Å in some estimates, although this will depend criti-
cally on nucleation, which is not entirely understood). It is clear that
that type of experiment will yield only a sum of signals from the various
layers that evidently coexist during this stage of oxidation and have
different growth kinetics. The Holloway-Hudson model relation therefore
provides an adequate fit to the total Auger intensity, but the assertion
that island growth is limited by either lateral diffusion or capture of
an adsorbed O_2 species, is not likely in the temperature-pressure regime
used in this work, and possibly not at other conditions either.
Furthermore, the assumption that islands are circular and that the active
sites are simply proportional to the square root of the area is not
supported.

Figure **39** a: Oxygen map corresponding to Ni map below and Co
map on next page.
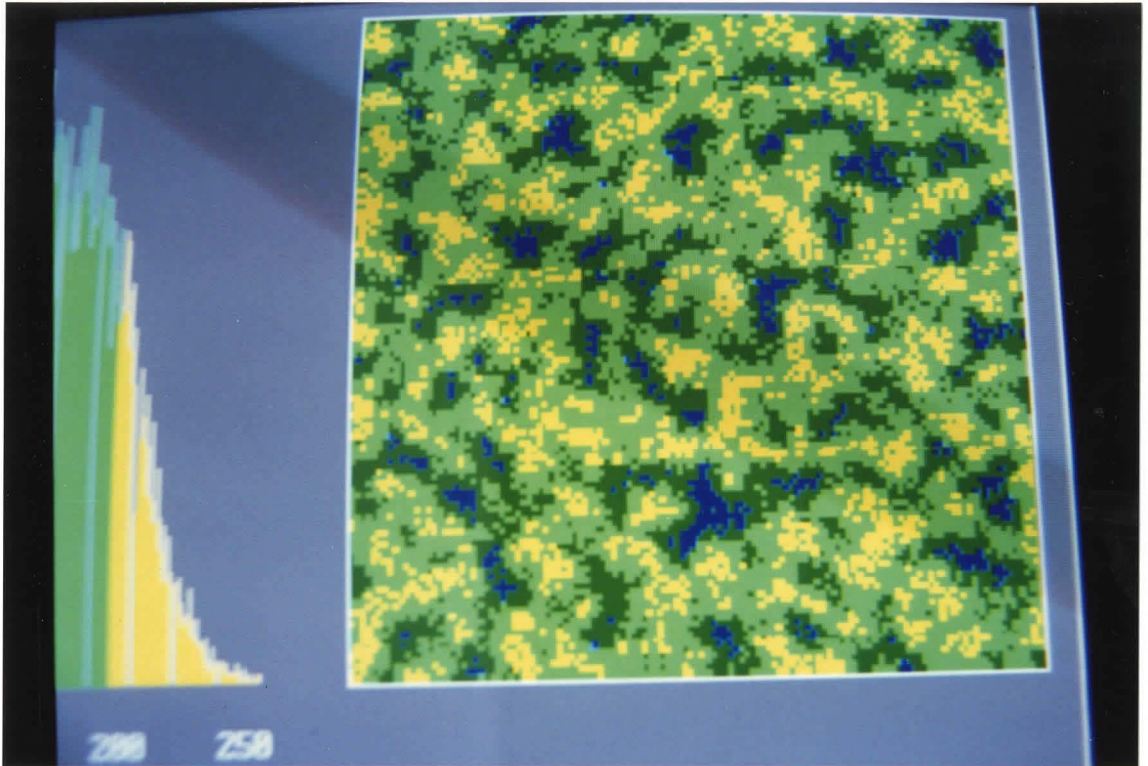
Figure **39** b: Ni map
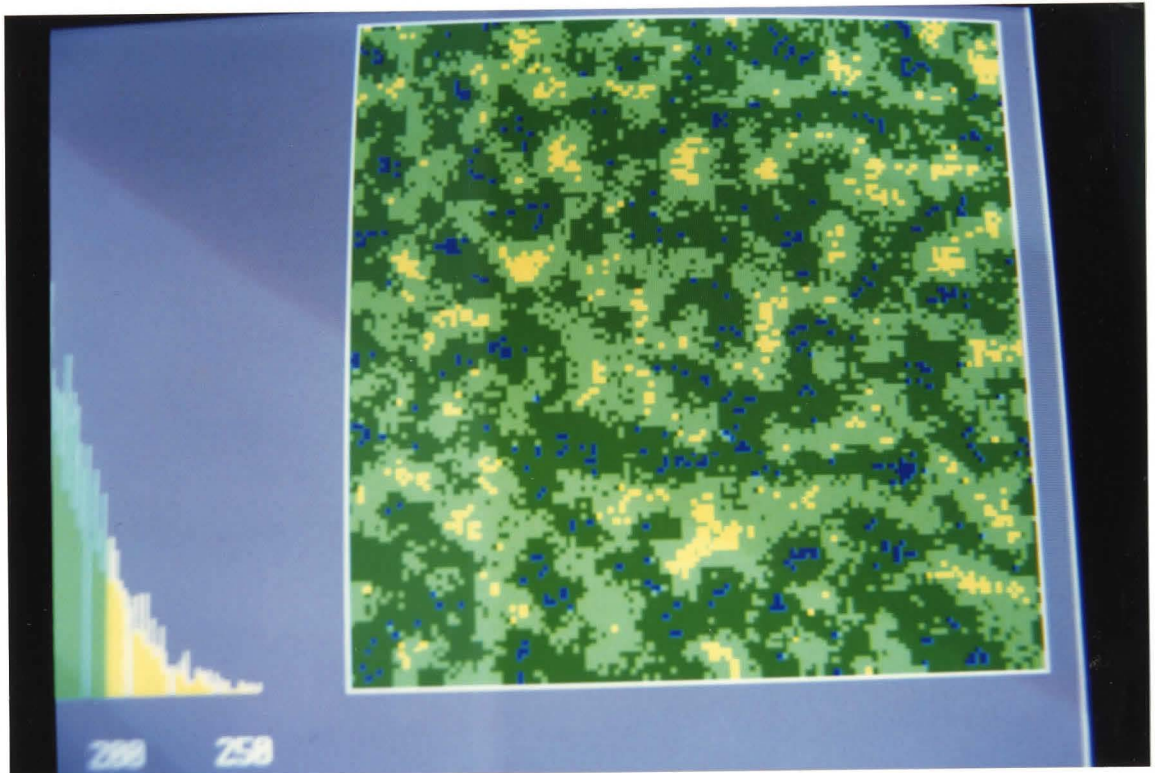
figure 39c
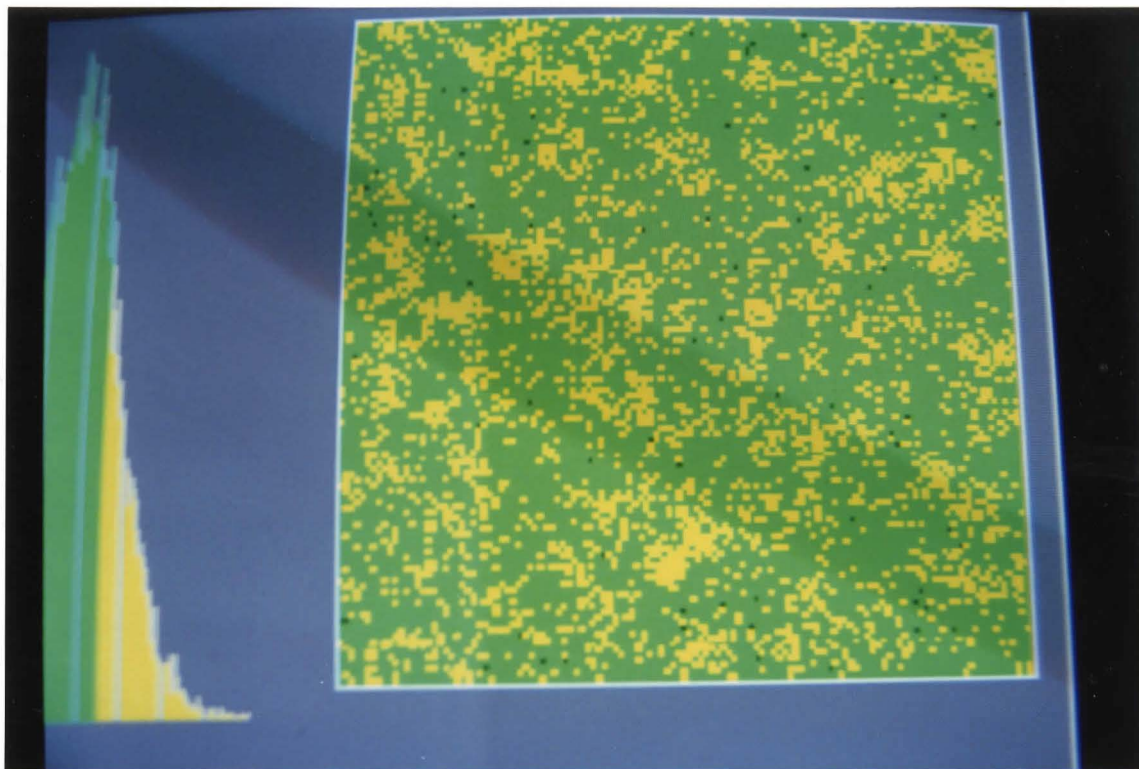
SUMMARY

The results of this investigation into the surface behaviour of Ni-Co alloys have been the following;

1) Ni is preferentially sputtered over the entire range of compositions studied here (14 to 90 a/o Ni).

2) Ni segregates at elevated temperatures over the range of composition from 14 to 90 a/o Ni.

3) The segregation of Ni is only evident in the low energy range of Auger spectra owing to the greater surface sensitivity of those peaks.

4) Computer simulation of Auger spectra using sputtered pure metal standards has permitted quantitation in this system with a claimed fitting accuracy of $\pm$ 0.05 a/o.

5) The temperature dependence of segregation has been measured for the (111) and (210) faces of a 56 a/o Ni alloy as well as for the (111), (100) and (110) faces of a 50 a/o Ni alloy. The temperature dependencies of the simpler faces may be related to the Enthalpy and Entropy of segregation and a Free Energy of segregation may be calculated at a specified temperature for comparison.

6) The early stages of oxidation of these alloys follow kinetics consistent with the nucleation and lateral growth of oxide islands which grow at a rate determined by the rate of gas impingement at island perimeters and substrate temperatures.

^Suggestions for Further Work

Segregation

The evidence of this thesis has suggested that the entropy component of the free energy of segregation plays an unexpectedly important role in surface segregation. The variation of both entropy and enthalpy on specific crystal faces, with composition would make a valuable contribution to the understanding of the segregation process as a whole. It is perhaps unfortunate that the current lack of knowledge about the variation of inelastic mean free paths with crystallographic orientation would preclude further studies on higher index faces but, this may not be a barrier for long and a study of the effects of crystallographic orientation on surface segregation would be interesting.

It has been suggested in the discussion of this thesis that d-band filling plays a very important role in determining segregation behaviour. It would be interesting to see if similar segregation behaviour were observed in a comparable binary alloy system with less than 5 d electrons such as Ti-V where vaporization enthalpies are very similar and the alloy system has a relatively simple phase diagram. Another interesting system to look into would be the Fe-Co system where where predictions based on the difference in vaporization enthalpies opposes segregation driven by differences in d electrons.

Early Stages of Oxidation

Clearly the oxidation experiments in this thesis must be viewed as a preliminary study. The variation of island growth kinetics with temperature and pressure in the early stages of oxidation needs to be examined over much wider ranges for both variables. It is very remarkable that nucleation seems to stop after a very definite phase and does not continue concurrently with growth, whether this is the result of lack of appropriate nucleation sites or some other factor, is an intriguing question. Exactly how do the experiments conducted on copper by Milne and Howie relate to the much thinner oxides observed here? Is it just that in a different regime of temperature and pressure that lateral growth and nucleation can be stopped while vertical growth continues? As these experiments are carried out, more questions will arise but it is certain that varying pressure and temperature experiments with perhaps improved image analysis techniques is the next step. So long and thanks for all the fish.

Index of Symbols[*]

ΔG - change in Gibbs Free energy

ΔH - change in Enthalpy

T- Temperature

ΔS - change in Entropy

X_A^S- the fractional composition of element A at the surface

X_B^b- the fractional composition of element B in the bulk

N_A- number of A atoms in a system

Γ_A- surface excess of A

Λ - area of an interface

α, β - hypothetical phases

c_A^α - concentration of element A in phase α

v_α - volume of phase α

f - Helmholtz free energy

γ - surface tension

μ - chemical potential

F - molar Helmholtz free energy

ΔG_{seg}^o - standard free energy of segregation

Ω - regular solution parameter

Z - atomic coordination number

W - a simplifying parameter = Ω/Z

$\nu_{E,s}$ – Einstein vibrational frequency at the surface

E – energy due to strain

G_m – shear modulus

r_s – radius of a solute atom

K_s – bulk modulus of a solute atom

σ^* – ratio of atomic sizes

μ_m – sheer modulus of a matrix

m,n – parameters in the Leonard-Jones potential

ΔQ_{el} – energy recovered by segregation of a solute

G – shear modulus

b – burgers vector

A_s – molar area of surface

D_A – diffusion coefficient of element A

Q_A – activation energy of diffusion for element A

ϕ_{ij} – interaction potential of atoms i and j

R_{ij} – interatomic distance between i and j

ρ_{ij} – density of an electron gas

Φ_A – electronic work function for Auger electrons

$d\Omega$ – integration parameter representing all space

λ – inelastic mean free path of electrons

I_{Ni} – Auger current due to electrons from Ni atoms

R_B – backscatter yield

Ψ - incident angle for an electron beam

U - ratio of incident beam energy to initial ionization event energy

I' - peak intensity

n_{ws} - elecron density at the edge of a Wigner-Seitz cell

Φ^* - electronegativity

C^* - the surface enrichment factor $= X_A^s X_B^b / X_B^s X_A^b$

d - interplanar spacing

P - gas pressure

θ - fractional surface coverage

η - time from nucleation

τ_p - mean residence time

ν - vibrational frequency

* Not a comprehensive list, most symbol variants and clauses are defined clearly in the accompanying text. Some symbol overlap is inevitable if common useage is be obeyed, but an effort has been made to minimize this.

Appendix 1: Combined Models

A-I Multi-layer Bond Breaking[9]

In this model the difference in bonding energies between bulk atoms and surface atoms is used. In order to fully describe either a bulk atom or a surface atom, 4 layers of atoms are considered in each type of case this model addresses eg. the bulk reference state has compositions $X_1=X_2=X_3=X_4=X_b$ (where the subscripts are for layer number) and the surface has $X_1 \neq X_2=X_3=X_4=X_b$ when only one layer is said to be segregated. In order to understand the following equations it is first necessary to make some definitions;

X_1 = the fraction of A atoms in layer 1

$1-X_1$ = the fraction of B atoms in layer 1

$Z_{1\ell}$ = the number of lateral bonds

$Z_{1\ell}X_1$ = the number of lateral bonds from an A atom in layer 1

$\frac{1}{2}Z_{1\ell}X_1X_1$ = the number of later A-A bonds (the $\frac{1}{2}$ is included to avoid double counting.)

$\frac{1}{2}Z_{1\ell}X_1X_1H_{AA}$ = the enthalpy associated with those bonds

$1.0Z_{1\ell}X_1(1-X_1)H_{AB}$ = the enthalpy associated with A atoms bonding with B atoms

$\frac{1}{2}Z_{1\ell}(1-X_1)(1-X_1)H_{BB}$ = the enthalpy associated with B atoms bound to B atoms.

For the vertical bonds from the first layer to the second.

$Z_{1v}X_1X_2H_{AA}$ = the enthalpy associated with the A-A bonds from layer 1 to layer 2.

$Z_{1v}X_1(1-X_2)H_{AB}$ = the enthalpy associated with the A-B bonds from layer 1 to layer 2.

$Z_{1v}(1-X_1)(X_2)H_{AB}$ = the enthalpy associated with B-A bonds from layer 1 to layer 2.

$Z_{1v}(1-X_1)(1-X_2)H_{BB}$ = the enthalpy associated with the B-B bonds from layer 1 to layer 2.

We then must total all the factors appropriately and subtract the energy

of the reference state and arrive at;

$$\Delta H_{seg.} = Z_{1\ell}[\tfrac{1}{2}X_1^2 H_{AA} + X_1(1-X_1)H_{AB} + \tfrac{1}{2}(1-X_1)^2 H_{BB}$$

$$+ Z_{1v}[X_1 X_2 H_{AA} + X_1(1-X_2)H_{AB} + X_2(1-X_1)H_{AB}$$

$$+ (1-X_1)(1-X_2)H_{BB}] + Z_{1\ell}[\tfrac{1}{2}X_2^2 H_{AA} + X_2(1-X_2)H_{AB}$$

$$+ \tfrac{1}{2}(1-X_2)^2 H_{BB}] + Z_{1v}[X_2 X_3 H_{AA} + X_2(1-X_3)H_{AB}$$

$$+ X_3(1-X_2)H_{AB} + \tfrac{1}{2}(1-X_3)(1-X_2)H_{BB}] + Z_{1\ell}[\tfrac{1}{2}X_3^2 H_{AA}$$

$$+ X_3(1-X_3)H_{AB} + \tfrac{1}{2}(1-X_3)2H_{BB}] + Z_{1v}[X_3 X_4 H_{AA}$$

$$+ X_3(1-X_4)H_{AB} + X_4(1-X_3)H_{AB} + (1-X_3)(1-X_4)H_{BB}$$

$$+ Z_{1\ell}[\tfrac{1}{2}X_4^2 H_{AA} + X_4(1-X_4)H_{AB} + \tfrac{1}{2}(1-X_4)^2 H_{BB}$$

$$+ Z_{1v}[X_4 X_b H_{AA} + X_4(1-X_b)H_{AB} + X_b(1-X_4)H_{AB}$$

$$+ (1-X_4)(1-X_b)H_{BB}] - \{4Z_1(\tfrac{1}{2}X_b^2 H_{AA} + (1-X_b)X_b H_{AB}$$

$$+ (1-X_b)^2 H_{BB} + \tfrac{1}{2}Z_{1v}[X_b^2 H_{AA} + 2X_b(1-X_b)H_{AB}$$

$$+ (1-X_b)^2 H_{BB}]\} \qquad \textbf{A.1)}$$

This equation of course only accounts for the change in enthalpy, entropy must then also be accounted for (configurational only see eqn 2.24);

$$\Delta S_{seg.} = S^s - S^b = -R[X_1 \ln X_1 + (1-X_1)\ln(1-X_1) + X_2 \ln X_2$$

$$+ (1-X_2)\ln(1-X_2) + X_3 \ln X_3 + (1-X_3)\ln(1-X_3)$$

$$+ X_4 \ln X_4 + (1-X_4)\ln(1-X_4)] + 4k[X_b \ln X_b$$

$$+ (1-X_b)\ln(1-X_b)] - (X_4 + X_3 + X_2 + X_1 - 4X_b)$$

$$+ (S_A^\circ - S_B^\circ). \qquad \textbf{A.2)}$$

Thus we may write the free energy expression

$$\Delta G^s = G^s - G^b = \Delta H^s - T\Delta S^s \qquad \text{A.3)}.$$

The total free energy is then defined as;

$$G_T = G^s + G^b \qquad \text{A.4)}$$

and find the compositions which minimize G_T. That is to say we differentiate G_T with respect to composition and find the compositions that satisfy

$$\frac{\delta G_T}{\delta X_1} = \frac{\delta G^s}{\delta X_1} + \frac{\delta G^b}{\delta X_i} = 0 \quad \text{for i = 1 to 4} \quad \text{A.5)}$$

and

$$\frac{\delta G^s}{\delta Xi} - (\mu_A^b - \mu_B^b) = 0 \quad \text{for i = 1 to 4} \quad \text{A.6)}$$

The solutions to these equations are as follows;

$$X_1 = A/(1 + A) \qquad X_2 = X_3 = X_4 = X_b \qquad \text{A.7)}$$

$$A = [X_b/(1-X_b)]\exp^{[(-\Delta H_{sub}Z_{1v})/Z_1 RT]} \qquad \text{A.8)}$$

$$\Delta H_{sub.} \simeq (\Delta H_A^\circ)_{vap.} - (\Delta H_B^\circ)_{vap.} > 0 \qquad \text{A.9).}$$

Note here that only the first monolayer has a composition different from the bulk and it is important to remember that this will only be the case when $H_{AB} = 1/2(H_{AA} + H_{BB})$ i.e. mixing is not accounted for since bonds are assumed to be linear combinations of atomization enthalpies.

There are two major problems with this approach: 1)Bonds at the surface are assumed to be the same as bonds in the bulk. This is not very realistice since the lack of atoms on one side will surely allow surface atoms to relax into the vacuum. 2) Only nearest neighbours are considered when in reality distortion of the bulk matrix structure at the surface will likely affect more than just the nearest neighbours.

The first of these problems was addressed by introducing a relaxation factor (δ) which allowed for changes in the bonds to the surface layer from the underlying layer of atoms that the authors described as "the fractional change in all of the bond enthalpies". The relaxation factor therefore has not only the effect of changing the surface (i.e. lateral) bonds but will also affect the compositon of the second layer. The compositions of the first,second and subsequent layers will therefore be;

$$X_1 = A/(1+A), \quad X_2 = B/(1+B), \quad X_3 = X_4 = X_b \quad A.10)$$

where

$$A = [X_b/(1-X_b)]\exp\left[-\frac{\Delta H_{sub}}{RT} \frac{Z_{1v} - \delta(Z_{1v} + Z_{1\ell})}{Z_1}\right] \quad A.11)$$

and

$$B = [X_b/(1-X_b)]\exp\left[-\frac{\Delta H_{sub}}{RT} \frac{Z_{1v}\delta}{Z_1}\right] \quad A.12).$$

The problem with these relationships would then become the evaluation of δ . Burton and Jura[26] used a Morse potential which can be likened to a Leonard-Jones potential to evaluate δ. Using their values it is found

that the first layer composition changes only very slightly and the major effect is on the second layer.

Up to this point in this treatment of theory only the nearest neighbour interactions have been counted and that is not likely to reflect a real situation. In order to take account of second nearest neighbours Nicholas[27] found that the second nearest neighbour enthalpy can be given as a function of the first nearest neighbour bonds and hence arrive at;

$$Z = Z_1 + \frac{1}{2}Z_2 \qquad Z_1 = Z_{1\ell} + \frac{1}{2}Z_{2\ell} \qquad Z_v = Z_{1v} + \frac{1}{2}Z_{2v} \qquad A.13).$$

Z_2, Z_{2v} and $Z_{2\ell}$ are the number of second nearest neighbours totally, vertically and horizontally respectively. Table A-1 is presented for ease of use in determining these parameters.

Table A-1

First Nearest neighbours	Effective neighbours

FCC

(100)
$Z_{1v} = 4$ $Z_v = 4.5$
$Z_{1\ell} = 4$ $(Z_{1v}/Z_1 = 0.333)$ $Z_\ell = 6$ $(Z_v/Z = 0.3)$
$Z_1 = 12$ $Z = 15$

(110)
$Z_{1v} = 5$ $Z_v = 6$
$Z_{1\ell} = 2$ $Z_{1v}/Z_1 = 0.417$ $Z_\ell = 3$ $Z_v/Z = 0.40$
$Z_1 = 12$ $Z = 15$

(111)
$Z_{1v} = 3$ $Z_v = 4.5$
$Z_{1\ell} = 6$ $Z_{1v}/Z_1 = 0.25$ $Z_\ell = 6$ $Z_v/Z = 0.30$
$Z_1 = 12$ $Z = 15$

BCC

(100)
$Z_{1v} = 4$ $Z_v = 4.5$
$Z_{1\ell} = 0$ $Z_{1v}/Z_1 = 0.5$ $Z_\ell = 2$ $Z_v/Z = 0.409$
$Z_\ell = 12$ $Z = 11$

(110)
$Z_{1v} = 2$ $Z_v = 3$
$Z_{1\ell} = 4$ $Z_{1v}/Z_1 = 0.25$ $Z_\ell = 5$ $Z_v/Z = 0.273$
$Z_1 = 8$ $Z = 11$

(111)
$Z_{1v} = 4$ $Z_v = 5.5$
$Z_{1\ell} = 0$ $Z_{1v}/Z_1 = 0.5$ $Z_\ell = 0$ $Z_v/Z = 0.50$
$Z_1 = 8$ $Z = 11$

If regular solutions are assumed (as opposed to the ideal solutions assumed to exist to this point) one can redefine the enthalpy of the A-B bond as;

$$H_{AB} = \frac{\Omega}{ZN_o} + \frac{1}{2}(H_{AA} + H_{BB}) \quad \text{c.f.eqn 2.26)} \quad \text{A.14)}$$

Here Ω is called the regular solution parameter and is given in Swalin[28] as;

$$\frac{\Omega}{RT} = \frac{\ln \gamma_A}{(1-X_b)^2 Z} = \frac{\ln\gamma_B}{X_B^2 Z} \quad \text{A.15)}$$

where the γ 's are the empirically observed bulk activity coefficients (not to be confused with surface tensions which are regretably also denoted by γ) of pure A and B. The four surface layers are then given by;

a) $0 = 2\Omega(ZX_b - Z_\ell X_1 - Z_v X_2 - \frac{1}{2}Z_v) + \frac{Z_v}{Z} \Delta H_{sub.} + RT \ln \left(\frac{X_1(1-X_b)}{X_b(1-X_1)} \right)$,

b) $0 = 2\Omega(ZX_b - Z_\ell X_2 - Z_v X_1 - Z_v X_3) + RT \ln \left(\frac{X_2(1-X_b)}{X_b(1-X_2)} \right)$,

c) $0 = 2\Omega(ZX_b - Z_\ell X_3 - Z_v X_2 - Z_v X_4) + RT \ln \left(\frac{X_3(1-X_b)}{X_b(1-X_3)} \right)$,   A.16)

d) $0 = 2\Omega(ZX_b - Z_\ell X_4 - Z_v X_3 - Z_v X_b) + RT \ln \left(\frac{X_4(1-X_b)}{X_b(1-X_4)} \right)$,

From these equations Williams and Nason[9] calculated compositions for 4 layers in hypothetical alloys and found variation from the bulk value

down to the fourth layer in some alloys. In general it was found that the smaller the $\Delta H_{sub.}$ the more "mono-layer like" was the segregation.

Again equations A.16a-d) assume linear combination of bond energies and this is corrected by the inclusion of δ, the relaxation parameter to yield equations A.17a-d.

a) $$0 = 2\Omega[ZX_b - (1+\delta)Z_\ell X_1 - (1+\delta)Z_v X_2 + \frac{\delta}{2}Z_\ell + \frac{\delta-1}{2}Z_v] +$$
$$\Delta H_{sub.} \frac{(Z_v - (Z_\ell + Z_v)\delta)}{Z} + RT \ln \left(\frac{X_1(1-X_b)}{X_b(1-X_1)} \right),$$

b) $$0 = 2\Omega[ZX_b - Z_\ell X_2 - (1+\delta)Z_v X_1 - Z_v X_3 + \frac{\delta}{2}Z_v] +$$
$$\Delta H_{sub.} \left(\frac{-\delta Z_v}{Z} \right) + RT \ln \left(\frac{X_3(1-X_b)}{X_b(1-X_2)} \right),$$

c) $$0 = 2\Omega(ZX_b - Z_\ell X_3 - Z_v X_2 - Z_v X_4) + RT \ln \left(\frac{X_3(1-X_b)}{X_b(1-X_3)} \right), \quad \text{A.17)}$$

d) $$0 = 2\Omega(ZX_b - Z_\ell X_4 - Z_v X_3 - Z_v X_4) + RT \ln \left(\frac{X_4(1-X_b)}{X_b(1-X_4)} \right).$$

We then have four models from this approach;

1) Eqn A.11) which assumes only the first monolayer is modified and is only really useful for ideal solutions with linearly combined bond energies.

2) Eqn A.12) which allows a gradient of concentration from layer 1 to bulk composition in layer 3 and does not assume linearly combined bond energies.

3) Eqns A.16a-d that do not assume ideality of solutions, allow for compositional variation from the bulk for up to 4 layers but still assumes linearly combined bond energies.

4) Eqns A.17a-d do not assume ideality, allow compositional variation down to layer 4 and do not assume linearity of bond energies.

All of the above models can be used either with the first nearest neighbours only or first and second nearest neighbours. More recent[29] modifications have basically attempted to include dwindling contributions from further neighbours and/or allowed variations in up to 20 layers but those models basically alter results only very slightly and their success is not certain.

b) Combined Surface Free Energy, Heat of Mixing and Elastic Strain[7] (I)

In this model the basic equation given here as eqn. 2.6) has been re-written such that surface tensions, enthalpy of mixing and elastic strain energy are all part of the definition of the enthalpy and entropy of segregation as follows:

$$\Delta H_a = (\gamma_A - \gamma_B)\Lambda + \omega\{Z_\ell(X_B^{s^2} - X_A^{s^2} + X_A^{b^2} - X_B^{b^2}) + Z_v(X_A^{b^2} - X_B^{b^2})\} \quad \text{A.18)}$$

where γ_A and γ_B are the surface free energies of components A and B respectively, Λ is the surface area per atom, $\omega = H_{AB} - (H_{AA} + H_{BB})/2$ which can be replaced[30] by $\omega = \Delta H_m/ZX_A^b X_B^b$ where Z is the coordination number) and Z_ℓ and Z_v as previously defined. Thus eqn. A.18) may be re-written as;

$$\Delta H_a = (\gamma_A - \gamma_B)\Lambda + (2\Delta H_m/ZX_A^b X_B^b)[Z_\ell(X_A^b - X_A^s) + Z_v(X_A^B - \tfrac{1}{2})]. \quad \text{A.19)}$$

The elastic strain energy term eqn 2.46) is then included to give;

$$\Delta H_a = (\gamma_A - \gamma_B)\Lambda + \frac{2\Delta H_m}{ZX_A^b X_B^b}[Z_1(X_A^b - X_B^b) + Z_v(X_A^b - \tfrac{1}{2})] - \frac{24\pi KGr_o r_1(r_o - r_1)^2}{3Kr_1 + 3Gr_o} \quad \text{A.20)}$$

The authors of this model find it neccessary to include the elastic strain energy term even though they mention that it is mostly insignificant.

Entropy must now be included in the model such that;

$$\Delta S_a = (S_A - S_B)\Lambda + \frac{2\Delta S_m}{ZX_A^b X_B^b}[Z_\ell(X_A^b - X_B^s) + Z_v(X_A^b - \tfrac{1}{2})] + \frac{d}{dT}\frac{24\pi KGr_o r_1(r_o - r_1)^2}{3Kr_1 + 4Gr_o}$$
$$\text{A.21)}$$

where S_A and S_B are the surface free entropies of the pure components. It is interesting to note that including the entropy term in the free

energy calculation only seems important in dilute solutions with large solute atoms eg Ni(Au) and actually loses predictive power when the reverse situation Au(Ni) is encountered. That is to say that the entropy seems only significant when elastic strain is expected to play a major role in segregation.

c) Combined Surface Free Energy, Enthalpy of Mixing and Strain (II)

Miedema and coworkers[8,31,32] constructed equations relating surface energies to heats of vaporization and electron density of states at the boundary or an atomic cell. Using the results from ref 32) they begin with the simple segregation eqn.;

$$c_1^A/c_b^A = \exp^{[\Delta H_{sol}^A - \Delta H_{vap}^A + \Delta H_{vap}^B)/3RT]} \quad A.22)$$

where c_1^A is the ratio of concentrations of solute (A vs. B) in the first atomic layer and c_b^A is the bulk composition ratio. ΔH_{sol}^A is the partial molar heat of solution of metal A in metal B. The 3 in the exponent term arises from the now usual 1/3 of bonds missing on an FCC (111) face. This equation is simple and easy to use but it suffers from the lack of consideration of differing surface area for different atoms. The use of surface energies was therefore preferred by this author;

$$c_1^A/c_b^A = \exp^{[(\gamma_B^S - \gamma_A^S)a/RT}} \quad A.23)$$

where a is an average molar surface area. Even this was not satisfactory however because the solution enthalpy was not included and an average molar surface area is only truly applicable in a random surface and must be weighted by bulk compos;tion which clearly does not exist in a segregated surface. The solution was to combine eqns A.22) and A.23) to arrive at;

$$c_1^A/c_b^A = \exp^{[f(\Delta H_{sol} - g(\gamma_A^{s,\,\circ} - \gamma_B^{s,\,\circ})V_A^{2/3})/3RT]} \quad A.24).$$

Here f is a relaxation factor empirically determined to be 0.71 for transition metals, g is a constant equal to 4.0×10^8 (see ref 33), V_A is the molar volume. The factors $\gamma_A^{s,\,\circ}$ and $\gamma_B^{s,\,\circ}$ are surface tensions calculated by;

$$\gamma^{s,\,\circ} = n_{ws}^{5/3}(\Phi^* - 0.6)^2 \quad A.25)$$

This equation was arrived at in ref 34 and has excellent correlation with available experimental data. Φ^* is the electronegativity of the atom and n_{ws} is an electron density at the boundary of a Wigner–Seitz cell[32]. Ref 8 contains a compilation of all the necessary data to calculate surface compositions using eqn A.24).

If an alloy is thought to have a significant size mismatch then some correction must be made. This model acknowledges the relations set forth by Eshelby[19,20] in eqn 2.40) but disagrees with the idea that 50% of the bulk strain energy is recovered at the surface and suggests that

25% is more realistic in light of expected significant relaxation. They therefore assume Poissons ratio to be 0.3 for all metals and obtain;

$$\ln(C_1^A/C_b^A)_{size} = 0.42 \ \bar{K}\bar{V}_m \delta^2/RT \quad A.26)$$

where

$$\delta = (V_A^{1/3} - V_b^{1/3})/\bar{V}_m^{1/3} \quad A.27).$$

Eqn. A.26) should be thought of as an add on term for eqn. A.24) in natural log form.

Next and last, the problem of surface entropy was addressed and it was decided that entropy should be temperature independent and only be significantly different for atoms having different volumes. The add on term for surface entropy would then be;

$$\ln(C_1^A/C_b^A)_{\substack{surf. \\ entr.}} = - \ 0.8[1 - (V_B/V_A)^{2/3}] \quad A.28)$$

The full formal segregation equation proposed by Miedema et. al. in natural log form would be;

A.29)

$$\ln \frac{C_1^A}{C_b^A} = \{f\Delta H_{sol}^A - g(\gamma_A^{s,°} - \gamma_B^{s,°})V_A^{2/3}/3RT\}+\{0.42\bar{K}\bar{V}_m\delta^2/RT\}-\{0.8[1-V_B/V_A]^{2/3}$$

| mixing | surface tension | strain | entropy |

Eqn A.29) should be used with some thought however, since the last two terms may not be significant in many cases.

d) Linearly Combined Bond Breaking (or Surface Tension) and Strain

This particular model proposed by Abraham et.al.[2,6,23] has been very attractive to researchers in the field of surface science, because of it s ease of use. This model assumes that the driving force for segregation is the linear sum of the simplistic bond breaking eqn 2.7) and the more complex of Eshelby's[20] elastic contribution equations eqn 2.40).

$$\Delta G_a = \Delta Q_\varepsilon + \Delta Q_{el} \qquad A.30)$$

The difference in bond strength equation is re-written such that;

$$\Delta Q_\varepsilon = \Delta z \varepsilon_{AA} (\varepsilon^* - 1) \qquad A.31)$$

where ε^* is the ratio of bond strengths of solute and solvent atoms $\varepsilon_{AA}/\varepsilon_{BB}$. This equation assumes that the component $\Delta \varepsilon_m$, the mixing enthalpy, is zero in the case of an ideal solution and ε_{AA} is the bond enthalpy of element A and ε_{BB} is the bond enthalpy of element B. The elastic strain component of the total driving force is given in eqn 2.40) and when included the entrire expression for ΔG_a would then be

$$\Delta G_a = \frac{1}{2} \Delta Z \varepsilon_{AA} (\varepsilon^* - 1) - \frac{16}{3} \pi r_A^3 (\sigma^* - 1)^2 \qquad A.32)$$

which can be simplified to;

$$\Delta G_a / \varepsilon_{AA} = C_\varepsilon (\varepsilon^* - 1) - C_{el} (\sigma^* - 1)^2 \qquad A.33)$$

with C_ε and C_{el} becoming constants once ΔZ has been decided on (i.e. wether you use 12:6 or 8:4 in the m:n equation 2.42)) and the solvent has been identified. Eqn A.33) is now very attractive since a researcher does not need to know any enthalpies of solution or entropies (entropy is assumed to be zero--see proof offered in the previous section on entropy). One only needs to know the easily obtainable G_{AA} and G_{BB}, r_A and r_B. If surface free energies are thought to be more important than bond enthalpies a simple substitution of γ^* for ε^* is used such that γ^* is the ratio of pure metal surface tensions and one arrives at;

$$\Delta G_a / \varepsilon_{AA} = C_\varepsilon (\gamma^* - 1) - C_{el} (\sigma^* - 1)^2 \quad \text{A.34)}$$

From these equations we again note that the component with lower $\Delta H_{sub.} \simeq \varepsilon_{AA}$ or ε_{BB} will segregate if only bond breaking is considered and if elastic strain alone is considered then systems with $\sigma^* < 1$ will have no segregation and if $\sigma^* > 1$ the solute segregates. In the combined model i.e. eqn A.34) if $\Delta G_a / \varepsilon_{AA} < 0$ the solute segregates, if $\Delta G_a / \varepsilon_{AA} > 0$ the solvent segregates and if $\Delta G_a / \varepsilon_{AA} = 0$ there is no segregation.

One further modification to the model can be made if the surface in the model is allowed to relax as a real system would in fact relax. This modification is certainly understandable but it would only be significant in systems where elastic strain is the dominant driving force for segregation and that is a rare case as has been mentioned in the section on elastic strain in chapter 2.

References

1) M.J. Kelley, Prog. in Surf. Sci. $\underline{11}$ 139 (1981)

2) F.F. Abrahams and C.R. Brundle, J. Vac. Sci. and Tech. $\underline{18}$ 508 (1981)

3) The Collected Works of J. Willard Gibbs, vol.1 Longmans (1928)

4) Properties of Crystal Surfaces, J.M. Blakely, Permagon (1973) pp38-45

5) Surface Tension and Adsorption, R. DeFay, Wiley (1966)

6) F.F. Abrahams, N. Tsai and G.M. Pound, Scripta Met. $\underline{13}$ 307 (1979)

7) P. Wynblatt and R.C. Ku, Surf. Sci. $\underline{65}$ 511 (1977)

8) A.R. Miedema, Z. Metkde. $\underline{69}$ 455 (1978)

9) F.L. Williams and D. Nason, Surf. Sci. $\underline{45}$ 377 (1974)

10) V. Kumar, D. Kumar and S.K. Joshi, Phys. Rev. $\underline{B19}$ 1955 (1979)

11) V.S. Sundaram and P. Wynblatt, Surf. Sci. $\underline{52}$ 569 (1975)

12) S.H. Overbury, P.A. Bertrand and G.A. Somerjai,
    Chem. Rev. $\underline{75}$ 547 (1975)

13) M.P. Seah and C. Lea, Phil. Mag. $\underline{31}$ 627 (1975)

14) K. Hoshino, J. Phys. Soc. of Japan $\underline{50}$ 577 (1981)

15) A.R. Miedema, P.F. de Chatel and F.R. de Boer, Physica $\underline{100B}$ 1 (1980)

16) M.J. Kelley, J. Catalysis $\underline{57}$ 113 (1979)

17) M.J. Kelley, P. Gilmour and D.G. Swartzfager,
    J. Vac. Sci. Tech. $\underline{17}$ 634 (1980)

18) J. Friedel, Adv. Phys. $\underline{3}$ 446 (1954)

19) J.D. Eshelby, Adv. Sol. State Phys. $\underline{3}$ 79 (1956)

20) Progress in Solid Mechanics, J.D. Eshelby, North Holland (1961)

21) K. Fuchs, Proc. R. Soc. Lon. $\underline{A153}$ 622 (1936)

22) Interfacial Segregation, W.C. Johnson, Amer. Soc. for Metals (1977)

23) F.F.Abrahams, N. Tsai and G.M. Pound, J. Cat. $\underline{50}$ 200 (1977)

24) M.P. Seah, J. Catalysis $\underline{57}$, 450 (1979)

25) D.F. Ollis, J. Catalysis $\underline{59}$, 430 (1979)

26) J.J. Burton and G. Jura, J. Phys. Chem. 71 1937 (1967)

27) J.F. Nicholas, Australian J. Phys. 21, 21 (1968)

28) Thermodynamics of Solids, R.A. Swalin, Wiley (1962)

29) V. Kumar Phys. Rev. B 23, 3756 (1981)

30) Thermodynamics of Solids, R.A. Swalin, Wiley (1972)

31) A.R. Miedema and R. Boom, Z. Metallkunde 69, 183 (1978)

32) R. Boom, F.R. deBoer and A.R. Miedema,
    J. Less Common Metals 46, 271 (1978)

33) R. Boom, F.R. deBoer and A.R. Miedema,
    J. Less Comon Metals 41, 237 (1976)

34) D.G. Swartzfager and M.J. Kelley, Phys. Lett. 76A, 86 (1980)

35) A.D. LeClair, J. Nuc. Mat. 69-70, 70 (1978)

36) Tracer Diffusion in Metals and Oxides, John Askill Ed.,
    Plenum Data Corp. (1970)

37) J. Kerker and J.L. Moran-Lopez, Phys. Rev. B 15, 638 (1977)

38) V.S. Sundarum and P. Wynblatt, Surf. Sci. 52, 569 (1975)

39) R.G. Donelly and T.S. King, Surf. Sci. 74, 89 (1978)

40) S.M. Foiles, Phys. Rev. B 32, 7685 (1985)

41) M.S. Daw and M.I. Baskes, Phys. Rev. B 29, 6443 (1984)

42) J.R. Chelikowsky, Surf. Sci. 139, L197 (1984)

43) L. Brewer and G.M. Rosenblatt, Adv. High Temp. Chem. 2, 1 (1969)

44) Constitution of Binary Alloys, M. Hansen Ed., McGraw-Hill (1958)

45) H. Goretzki, A. Muhlratzer and J. Nickl,
    Proc. 7th Vac. Cong. and 3rd Itl. Conf. on Sol. Surfs. (1977)

46) V.T. Cherepin, M.A. Vasilev and O.A. Yakubtsov,
    Phys. Stat. Sol. A53 K207 (1979)

47) E.S. Shpiro, Y. Rudnyi, O.P. Tkachenko, G.V. Antoshin,
    B.B. Dyushenbina and K.M. Minachev,
    Izvestiya Akademii Nauk USSR 11, 2246 (1981)

48) A. Tanaka, M. Takemori and T. Homma,
    J. Elec. Spec. and Rel. Phen. 32, 277 (1983)

49) <u>Tracer Diffusion in Metals and Oxides</u>, John Askill Ed., Plenum (1970)

50) <u>Effects of X-Ray Diffraction</u> B.D. Cullity, Addison-Wesley Pub. (1967)

51) <u>Crystal Orientation Manual</u>, E.A. Wood, Columbia Univ. Press (1963)

52) P.R. Underhill, K.A. Ellison and W.W. Smeltzer
J. Vac. Sci. Tech. A $\underline{4}$ 1944, (1986)

53) David R. Penn, J. Elec. Spec. and Rel. Phen. $\underline{9}$ 29, (1976)

54) David R. Penn, Phys. Rev. B $\underline{35}$ 382, (1987)

55) C.J. Powell, Surf. Sci. $\underline{44}$ 29 (1974)

56) M.P. Seah and W.A. Dench, Surface and Interface Analysis $\underline{1}$ 2, (1979)

57) P.T. Dawson and N.A. Burke, J. Elec. Spec. and Rel. Phen.
$\underline{31}$ 355, (1983)

58) W. Reuter in <u>Proceedings of the 6$\underline{^{th}}$ International Conference on X-ray Optics and Microanalysis</u> G. Shinoda, K. Kohra and T. Ichinokawa Eds. University of Tokyo Press (1972) p. 121

59) S. Ichimura, R. Shimizu and J.P. Landeron, Surf. Sci. $\underline{124}$ L49, (1983)

60) S. Ichimura and R. Shimizu, Surf. Sci. $\underline{112}$ 386, (1981)

61) S. Ichimura, R. Shimizu and I. Ikuta Surf. Sci. $\underline{115}$ 259 (1982)

62) P.R. Underhill, Surface and Interface Analysis $\underline{8}$ 61 (1986)

63) L.S. DeBernardez, J. Ferron, E.C. Goldberg and R.S. Buitrago,
Surf. Sci. $\underline{139}$ 541, (1984)

64) <u>Ion Bombardment of Solids</u>, G. Carter and J.S. Colligan
American Elsevier (1968)

65) W.L. Patterson and G.A. Shim, J. Vac. Sci. Tech. $\underline{4}$ 343, (1967)

66) P.T. Dawson and S.A. Petrone, J. Vac. Sci. $\underline{18}$ 529, (1981)

67) P.H. Holloway and S.K. Hofmeister, Surface and Interface Analysis
$\underline{4}$ 181, (1982)

68) H.H. Anderson, B. Stenum, T. Sorenson and H.J. Whitlow,
Nucl. Inst. and Methods $\underline{209/210}$ 487, (1983)

69) D.G. Swartzfager, S.B. Ziemecki and M.J.Kelley
J. Vac. Sci. Tech $\underline{19}$ 185, (1981)

70) M. Oku, K. Hirokawa, H. Kimura and S. Suzuki,
Surface and Interface Analysis $\underline{8}$ 67, (1986)

71) P.M. Hall and J.M. Morabito, Surf. Sci. 83 391, (1979)

72) P.R. Underhill, Surface and Interface Analysis 8 21, (1986)

73) Ion Bombardment of Solids G. Carter and J.S. Colligan Eds.
American Elsevier (1968)

74) L. Brewer and G.M. Rosenblatt, Adv. High Temp. Chem 2 1, (1969)

75) C.M. Chan, S.L.Cinningham, M.A. Van Hove and W.H. Weinberg,
Surf. Sci. 67 1, (1977)

76) F. Jona, Surf. Sci. 68 204, (1977)

77) J.E. Demuth, P.M. Marcus and D.W. Jepsen,
Phys. Rev. B 11 1460, (1975)

78) P.R. Underhill private communication

79) A.L. Allred and E.G. Rochow, J. Inorg. Nucl. Chem. 5 264, (1958)

80) J.C. Slater, Phys. Rev. 36 57, (1930)

81) G.V. Sampsonov and A.N. Krasnov,
Fiziko-Khimicheskaya Mekhanika Materiolov 2 485, (1966)

82) P. Lambin and J.P. Gaspard, J. Phys. F 10 2413, (1980)

83) J.L. Moran-Lopez, G. Kerker and K.H. Bennemann,
J. Phys. F 5 1277, (1975)

84) F. Brouers, M. Cyrot and F. Cyrot-Lackmann,
Phys. Rev. B 7 4370, (1973)

85) J.L. Moran-Lopez, G. Kerker and K.H. Benneman,
Surf. Sci. 57 540, (1976)

86) M.L. Shek, P.M. Stefan, D.L. Weissmann-Wonocur, B.B. Pate, I. Lindau
and W.E. Spicer, J. Vac. Sci. Tech. 18 533 (1981)

87) M.L. Shek, P.M. Stefan, D.L. Weissmann-Wonocur, B.B. Pate, I. Lindau
and W.E. Spicer, Suf. Sci. Lett. 115 L86 (1982)

88) P. Lmabin and J.P. Gaspar, J. Phys. F 10 2413, (1980)

89) F.P. Fehlner and N.F. Mott, Oxidation of Metals 2 52, (1970)

90) P.H. Holloway and J.B. Hudson, Surf. Sci. 43 141, (1974)

91) P.H. Holloway and J.B. Hudson, Surf. Sci. 43 123, (1974)

92) C.R. Brundle, Chem. Phys. Lett. 31 423, (1975)

93) H. Hopster and C.R. Brundle, J. Vac. Sci. Tech. 16 548, (1979)

94) K.H. Muller, P. Beckmann, M. Schemmer and A. Benninghoven,
    Surf. Sci. $\underline{80}$ 325, (1979) (see also Appl. Phys. $\underline{16}$ 367, (1978))

95) L.K. Verheij, J.A. Van Der Berg and P.G. Armour,
    Surf. Sci. $\underline{84}$ 408, (1979)

96) D.F. Mitchell, P.B. Sewell and M. Cohen, Surf. Sci. $\underline{61}$ 355, (1976)

97) D.E. Taylor and R.L. Park, Surf. Sci. Lett. $\underline{125}$ L73, (1983)

98) J.E. Demuth and T.N. Rhodin, Surf. Sci. $\underline{45}$ 249, (1974)

99) A.R. Kortan and R.L. Park, Phys. Rev. B $\underline{23}$ 6340, (1981)

100) W.A. Johnson and R.F. Mehl,
     Trans. Am. Inst. Mining and Met. Engrs, $\underline{135}$ 416, (1939)

101) M. Avrami, J. Chem. Phys. $\underline{9}$ 177, (1941)

102) P.H. Holoway and R.A. Outlaw, J. Vac. Sci. Tech. $\underline{20}$ 671, (1982)

103) P.H. Holloway and J.B. Hudson, J. Vac. Sci. Tech. $\underline{12}$ 647, (1975)

104) C.R. Brundle, J. Vac. Sci. Tech. $\underline{A3}$ 1468, (1985)

105) P.H. Holloway, J. Vac. Sci. Tech. $\underline{18}$ 653, (1981)

106) J.A. Van Der Berg, L.K. Verheij and D.G. Armour,
     Surf. Sci. $\underline{91}$ 218, (1980)

107) R.G. Smeenk, R.M. Tromp, J.F. Van Der Veen and F.W. Saris,
     Surf. Sci. $\underline{95}$ 156, (1980)

108) C. Bendorf, B. Egert, C. Nobl, H. Serdel and F. Thieme,
     Surf. Sci. $\underline{92}$ 636, (1980)

109) P.R. Norton, R.L. Tapping and J.W. Goodale, Surf. Sci. $\underline{65}$ 13, (1977)

110) D.F. Mitchell, P.B. Sewell and M. Cohen, Surf. Sci. $\underline{61}$ 355, (1976)

111) D.F. Mitchell, P.B. Sewell and M. Cohen, Surf. Sci. $\underline{69}$ 310, (1977)

112) J. Benard, F. Gronlund, J. Ondar and M. Duret,
     Z. Elektrochem $\underline{63}$ 799, (1959)

113) G.C. Allen and P.M. Tucker, Surf. Sci. $\underline{102}$ 207, (1981)

114) T.E. Gallon, Surf. Sci. $\underline{17}$ 489, (1969)

115) M.P. Seah, Surf. Sci. $\underline{32}$ 703, (1972)

116) D. Majumndar, R.G. Spahn and J.S. Gau, J. Elect. Soc. $\underline{134}$, 1825
     (1987)